Exceptional Event Demonstration for Ozone Exceedances in Clark County, Nevada – September 2, 2020

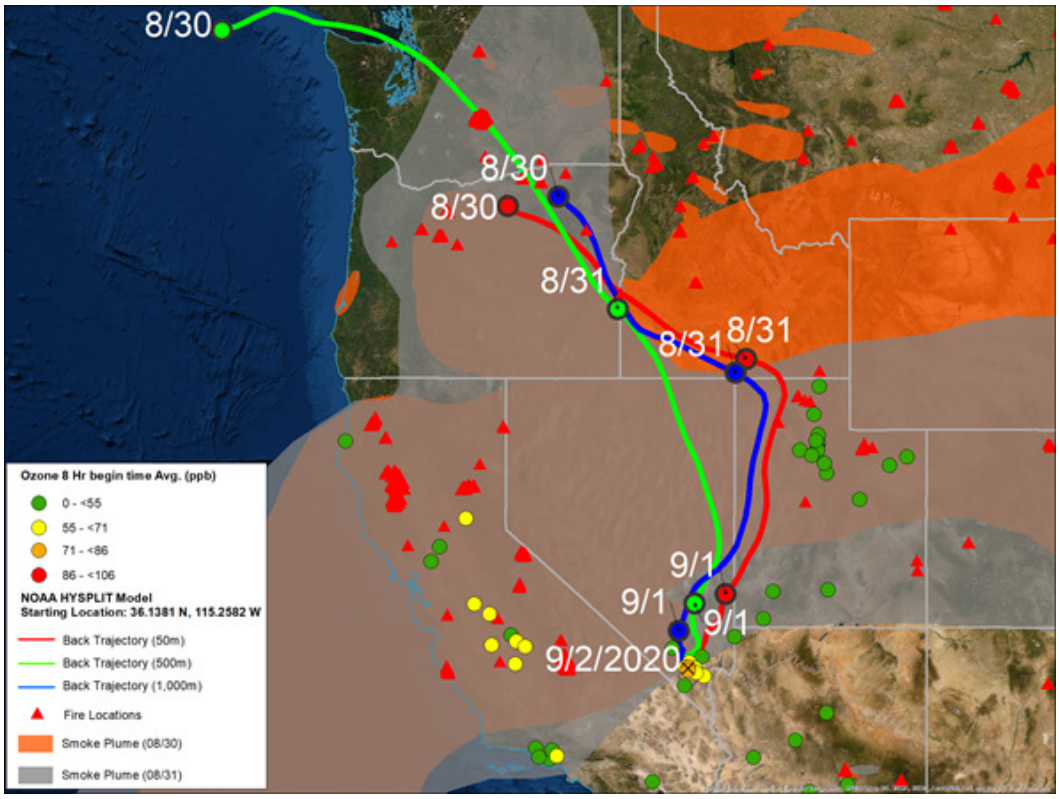

Final Report Prepared for

U.S. EPA Region 9
San Francisco, CA

July 2021

STi | Sonoma Technology

This document contains blank pages to accommodate two-sided printing.

Exceptional Event Demonstration for Ozone Exceedances in Clark County, Nevada – September 2, 2020

Prepared by

Steve Brown, PhD
Crystal McClure, PhD
Cari Gostic
David Miller, PhD
Nathan Pavlovic
Charles Scarborough

Sonoma Technology
1450 N. McDowell Blvd., Suite 200
Petaluma, CA 94954
Ph 707.665.9900 | F 707.665.9800
sonomatech.com

Prepared for

Clark County Department of Environment and Sustainability
Division of Air Quality
4701 W. Russell Road, Suite 200
Las Vegas, NV 89118
Ph 702.455.3206
www.clarkcountynv.gov

Final Report

STI-920053-7477

July 1, 2021

Cover graphic illustrates 72-hour HYSPLIT back trajectories with smoke from downtown Las Vegas, ending on September 2, 2020. See Section 3.1.3 for more information.

Contents

Figures

Tables

Executive Summary

On September 2, 2020, Clark County experienced an atypical, county-wide episode of elevated ambient ozone concentrations. During this episode, the 2015 8-hr ozone National Ambient Air Quality Standards (NAAQS) thresholds were exceeded at the Paul Meyer and Walter Johnson monitoring sites. The exceedances at both sites could lead to an ozone nonattainment designation for the Clark County area. Air trajectory analysis, statistical analysis, and matching day analysis shows that this ozone exceedance was influenced by wildfire smoke that was transported to Clark County from large wildfires burning throughout the western United States in California and Oregon; Table 1-5 in Section 1 provides a breakdown of analyses and associated sections in this document that demonstrate evidence of transport and influence. The U.S. Environmental Protection Agency's (EPA) Exceptional Event Rule (U.S. Environmental Protection Agency, 2016) allows air agencies to omit air quality data from the design value calculation if it can be demonstrated that the measurement in question was caused by an exceptional event. This report describes analyses that help to establish a clear causal relationship between wildfire smoke and the September 2, 2020, ozone exceedance at the Paul Meyer and Walter Johnson monitoring sites.

In this report, we show that (1) smoke was transported from wildfires in California and Oregon to the surface in the Clark County area in the days and hours leading up to the exceedance and on the day of the exceedance; (2) wildfire smoke impacted the typical diurnal profiles of ground-level pollution measurements—including NO_x, CO, and $PM_{2.5}$—in the Clark County area before the exceedance date and on the exceedance date; (3) levoglucosan, a tracer of wildfire combustion, was present and elevated at the surface in the Clark County area on September 2; (4) meteorological regression modeling and similar meteorological day analysis show that ozone concentrations on September 2 were unusually high in the historical record given the meteorological conditions; and, (5) extensive media coverage alerted Clark County residents of smoke impacts on September 2. Sources of evidence used in these analyses include (1) air quality monitor data to show that supporting pollutant trends at the surface were influenced by wildfire smoke; (2) air trajectory analysis to show transport of smoke-laden air to the Clark County area; (3) meteorological regression modeling; and (4) meteorologically similar day analysis.

EPA guidance for exceptional event demonstrations (U.S. Environmental Protection Agency, 2016) provides a three-tiered approach; depending on the complexity of the event, increasingly involved information may be required to demonstrate a causal relationship between wildfire smoke and an exceedance. Here, we provide the results of analyses conducted to address Tier 1, Tier 2, and Tier 3 exceptional event demonstration requirements.

These analyses show that smoke was transported from large wildfires throughout the western United States, including California and Oregon, to the Clark County in the days and hours leading up to the exceedance date and on the exceedance date. Combined with additional evidence, such as

meteorological regression modeling and meteorologically similar day analysis, our results demonstrate there were smoke impacts on ozone concentrations in Clark County on September 2, 2020.

1. Overview

1.1 Introduction

The 2020 wildfire season in California was unprecedented, with five of the six largest wildfires in the state's history occurring in August or September (https://www.fire.ca.gov/media/11416/top20_acres.pdf). Smoke emissions from rapidly growing wildfires in California and Oregon affected downwind areas and reached Clark County on September 2, 2020. On this date, 2 of the 14 ozone (O_3) monitoring locations around Clark County recorded an exceedance of the 2015 National Ambient Air Quality Standard (NAAQS) for 8-hour ozone (0.070 ppm).

Emissions from wildfires can affect concentrations of ozone downwind by direct transport of both ozone and precursor gases (i.e., nitrogen oxides [NO_x] and volatile organic compounds [VOCs]). Each mechanism can enhance the overall ozone concentration and/or the amount of ozone that is produced. For example, in an area where NO_x concentrations are high, such as an urban area like Las Vegas, Nevada, the transport of VOCs from wildfire emissions can enhance ozone production, potentially driving concentrations above the ozone standard. According to U.S. Environmental Protection Agency's (EPA) exceptional event (EE) guidance (U.S. Environmental Protection Agency, 2016), EEs, such as wildfires that affect ozone concentrations can be subject to exclusion from calculations of NAAQS attainment if a clear causal relationship is established between a specific event and the monitoring exceedance.

This report describes the clear causal relationship between the large complex fires in California and Oregon and the exceedance of the maximum daily 8-hour ozone average (MDA8) at the two monitoring sites in Clark County on September 2, 2020. We correlate the following fires with enhanced ozone concentrations in Clark County: White River Fire (OR), Lionshead Fire (OR), Slink Fire (CA), SQF Lightning Complex (CA), Dolan Fire (CA), North Complex (CA), SCU Lightning (CA), August Complex (CA), and Red Salmon Complex (CA) (more details provided in Section 3.2.1). We suggest that these fires contributed ozone and ozone precursors Clark County, which enhanced ozone concentrations and caused an exceedance of the NAAQS. The evidence in this report includes all three tiers of analysis required by EPA's EE guidance: for Tier 1, ground and satellite-based measurement of smoke emissions, transport of smoke from the fires in California and Oregon to Clark County, and media coverage of the smoke event in Clark County; for Tier 2, emission versus distance analysis, ground and satellite analysis of smoke-related pollutants, and comparison of event and non-event concentrations; and for Tier 3, vertical column analyses, meteorologically similar day analyses, and statistical Generalized Additive Modeling (GAM) of the event. The wildfires that affected ozone concentrations in Clark County could not be reasonably controlled or prevented because they were naturally caused and are unlikely to recur. Table 1-1 lists the sites affected during the September 2 event, as well as their locations and MDA8 ozone concentrations.

Table 1-1. September 2, 2020, EE information. All monitoring sites in Clark County that exceeded the 2015 NAAQS standard on September 2, 2020, are listed along with AQS Site Codes, location information, and MDA8 ozone concentrations.

AQS Site Code	Site Name	Latitude (degrees N)	Longitude (degrees W)	MDA8 O_3 Concentration (ppb)
320030043	Paul Meyer	36.106	-115.253	73
320030071	Walter Johnson	36.170	-115.263	75

Concurrent with this document, Clark County is submitting documentation for other ozone EEs in 2018 and 2020 that were caused by wildfires and stratospheric intrusions. These events are mentioned throughout this report and are referred to as "proposed 2018 and 2020 exceptional events," recognizing that discussion with EPA is still pending. All proposed EEs for Clark County in 2018 and 2020 are listed in Tables 1-2 and 1-3. Wherever possible, we calculated statistics to provide context that both include and exclude the proposed EEs from 2018 and 2020.

Table 1-2. Proposed Clark County 2018 EEs. For each site and date combination where the 2015 NAAQS standard was exceeded, the MDA8 ozone concentration is shown in parts per billion (ppb). Blank cells indicate that there was no exceedance on that site/date combination.

Date	Paul Meyer	Walter Johnson	Green Valley	Jerome Mack	Joe Neal	Palo Verde	Jean	Indian Springs	Apex	Boulder City
6/19/2018	72	72	77	75						
6/20/2018	71	74			72					
6/23/2018	72	76	75	72	72	71	77	73		
6/27/2018	75	76	78	76	72	72	81	78	74	72
7/14/2018	72		78	78						
7/15/2018		71	73	73	78					
7/16/2018	75	79	71	73	80	75				
7/17/2018	74	77				74				
7/25/2018	71	72	72							
7/26/2018	72	75	77	77					71	
7/27/2018	72	74			76					
7/30/2018			73	72						
7/31/2018		73			73					
8/6/2018	79	77	74	71	76	72			74	
8/7/2018	73	74	72	71	74				71	

Table 1-3. Proposed Clark County 2020 EEs. For each site and date combination where the 2015 NAAQS standard was exceeded, the MDA8 ozone concentration is shown in ppb. Blank cells indicate that there was no exceedance on that site/date combination.

Date	Walter Johnson	Paul Meyer	Joe Neal	Jerome Mack	Green Valley	Boulder City	Jean	Indian Springs	Apex
5/6/2020	78	77	76	73	72		75		76
5/9/2020	71	74							
5/28/2020	71	76							
6/22/2020	73	74	78						
6/26/2020		73							
8/3/2020	82	78	81		72	72	73	71	
8/7/2020	71		72					72	
8/18/2020	82	79	78						
8/19/2020	74	74	73		71				
8/20/2020			71						
8/21/2020		71							
9/2/2020	75	73							
9/26/2020	71		75						

1.2 Exceptional Event Rule Summary

The "EPA Guidance on the Preparation of Exceptional Events Demonstration for Wildfire Events that May Influence Ozone Concentrations" (U.S. Environmental Protection Agency, 2016) describes a three-tier analysis approach to determine a "clear causal relationship" for EEs demonstrations from an air agency. A summary of analysis requirements for each tier is listed in Table 1-4 and in the list below.

- Tier 1 analyses are used when ozone exceedances are clearly influenced by a wildfire in areas of typically low ozone concentrations, are associated with ozone concentrations higher than non-event-related values, or occur outside of an area's usual ozone season.
- Tier 2 analyses are appropriate for wildfire emissions cases where the impacts of the wildfire on ozone levels are less clear and require more supportive documentation than Tier 1 analyses.
- If a more complicated relationship between the wildfire and the ozone exceedance is observed, Tier 3 analyses with additional supportive documentation—such as statistical modeling of the ozone event, vertical profile analysis of smoke in the column, and meteorological analysis—should be used.

In this work, we conduct all the recommended Tier 1, Tier 2, and Tier 3 analyses.

Table 1-4. Tier 1, 2, and 3 EE analysis requirements for evaluating wildfire impacts on ozone exceedances.

Tier	Requirements
1	• Comparison of fire-influenced exceedance with historical concentrations • Key factor: Evidence that fire and monitor meet one of the following criteria: — Seasonality differs from typical season, or — Ozone concentrations are 5-10 ppb higher than non-event-related concentrations • Evidence of transport of fire emissions to monitor: — Trajectories of fire emissions (reaching ground level) — Satellite images and supporting evidence from surface measurements — Media coverage and photographic evidence of smoke
2	• All Tier 1 requirements • Key Factor #1: Fire emissions and distance of fires • Key Factor #2: Comparison of the event-related ozone concentration with non-event-related high ozone concentrations (high percentile rank over five years/seasons) — Annual and seasonal comparison • Evidence that fire emissions affected the monitor (at least one of the following): — Visibility impacts — Changes in supporting measurements — Satellite enhancements of fire-related species (i.e., NO_x, carbon monoxide (CO), aerosol optical depth (AOD), etc.) — Fire-related enhancement ratios and/or tracer species — Differences in spatial/temporal patterns
3	• All Tier 2 requirements • Evidence of fire emissions effects on monitor: — Multiple analyses from those listed for Tier 2 • Evidence of fire emissions transport to the monitor: — Trajectory or satellite plume analysis, and — Additional discussion of meteorological conditions • Additional evidence such as: — Comparison to ozone concentrations on matching (meteorologically similar) days — Statistical regression modeling — Photochemical modeling of smoke contributions to ozone concentrations

1.3 Demonstration Outline

As discussed in Section 1.2, the "clear causal relationship" analyses involve comparing the exceedance ozone concentrations to historical values, providing evidence that the event and monitors meet the tier's key factors and of the transport of wildfire emissions to the monitors, and additional analyses such as ground-level measurements and various forms of modeling based on the complexity of the event. Table 1-5 summarizes the key factors and additional supporting evidence of the tiered approach and shows the corresponding sections in this report for each analysis.

Table 1-5. Locations of Tier 1, 2, and 3 elements in this report.

Tier	Element	Section of This Report (Analysis Type)
Tier 1	Key Factor: seasonality differs from typical season and/or ozone concentrations are 5-10 ppb higher than non-event-related concentrations	Section 3.1.1 (comparison of event with historical data)
	Evidence of fire emissions transport to monitor	Sections 3.1.2 (maps of ozone, $PM_{2.5}$ fire, smoke, visible satellite imagery), 3.1.3 (HYSPLIT trajectories)
	Media coverage and photographic evidence of smoke	Section 3.1.4 (Media coverage and Images)
Tier 2	Key Factor #1: fire emissions and distance of fires	Section 3.2.1 (Q/d analysis)
	Key Factor #2: comparison of event concentrations with non-event-related high ozone concentrations	Section 3.2.2 (comparison of event concentrations with non-event concentrations)
	Evidence that the fire emissions affected the monitor	Sections 3.2.3 (visibility impacts, satellite NO_x (and other pollutant) enhancements), 3.2.4 (changes in supporting measurements, differences in spatial/temporal patterns, and tracer measurements)
Tier 3	Evidence of fire emissions transport to the monitor	Section 3.3.1 (trajectory or satellite plume analysis, additional discussion of meteorological conditions, comparison to ozone concentrations on matching [meteorologically similar] days)
	Meteorologically similar matching day analysis	Section 3.3.2 (methodology and analysis for meteorologically similar days)
	Additional evidence	Section 3.3.3 (statistical regression modeling)

Tier 1 analyses are shown in Section 3.1. The key factor of Tier 1 analyses is the ozone concentration's uniqueness when compared to the typical seasonality and/or levels of ozone exceedance. The EPA guidance suggests providing a time series plot of 12 months of ozone concentrations overlaying more than five years of monitored data and describing how typical seasonality differs from ozone in the demonstration (U.S. Environmental Protection Agency, 2016). In addition, trajectory analysis, produced by the Hybrid Single-Particle Lagrangian Integrated Trajectory (HYSPLIT) model, together with satellite plume imagery and ground-level measurements of plume components (e.g., $PM_{2.5}$, CO, or organic and elemental carbon) should be used to provide evidence of the transport of wildfire emissions to the monitoring sites. We demonstrate the Tier 1 analysis results for the September 2, 2020, event in Section 3.1. We address the key factors in Section 3.1.1, provide evidence of wildfire smoke transport to the Clark County monitoring sites in Sections 3.1.2 and 3.1.3, and discuss the media coverage and show ground images in Section 3.1.4.

Tier 2 analyses are shown in Section 3.2. The two key factors for Tier 2 analyses are (1) fire emissions and distance of fires to the impacted monitoring sites and (2) comparison of event-related ozone concentrations with non-event-related high ozone values. We address the first factor in Section 3.2.1 by determining the emissions divided by distance (Q/d) relationship, and address the second factor in Section 3.2.2 by comparing the five-year percentiles and yearly rank-order analysis of ozone concentrations. The Tier 2 analyses also require evidence of wildfire smoke transport to affected monitoring sites; we provide this evidence in Section 3.2.3 through satellite measurements of pollutant concentrations. In Section 3.2.4, we discuss supporting pollutant trends and diurnal patterns of $PM_{2.5}$, CO, NO_x, and total non-methane organic carbon (TNMOC) compared with ozone concentrations and wildfire tracer measurements. The Tier 2 analyses are included in this demonstration for completeness and to inform the Tier 3 analyses but, alone, are not expected to clearly demonstrate a relationship between the wildfire emissions and the monitored exceedances (see Section 3.2). We performed Tier 3 analyses to provide clear causal weight of evidence of this relationship.

Tier 3 analyses are shown in Section 3.3. We investigated total column information and event-related meteorological conditions (Section 3.3.1) and developed a Generalized Additive Statistical Model (GAM) to estimate the wildfire's contribution to ozone concentrations (Section 3.3.2).

Following the EPA's EE guidance, we performed Tier 1, Tier 2, and Tier 3 analyses to show the "clear causal relationship" between the large complex fires in California and Oregon and the exceedance event in Clark County on September 2, 2020. Focusing on the characterization of the meteorology, smoke, transport, and air quality on the days leading up to the event, we conducted the following specific analyses (results of these analyses are presented in Section 3):

- Developed time series plots that show the September 2 ozone concentrations at each affected monitoring site in historical context for 2020 and the past five years.
- Compiled maps of (1) ozone and $PM_{2.5}$ concentrations in the area, (2) smoke plumes, and (3) fire locations from satellite data

- Showed the transport patterns via HYSPLIT modeling and identified where the back trajectory air mass intersected with smoke plumes or passed over or near fires
- Discussed media coverage of the September 2 event and showed ground images
- Quantified total fire emissions and calculated emissions/distance ratio (Q/d) for the fire
- Performed statistical analysis to compare event ozone concentrations to non-event concentrations
- Provided maps showing satellite retrievals of NO_x, AOD, and CO
- Developed plots to show diurnal patterns of ozone and supporting pollutants such as $PM_{2.5}$, CO, NO_x, and TNMOC
- Examined wildfire tracer species and their background concentrations versus event concentrations
- Assessed vertical transport of smoke using satellite-observed aerosol vertical profiles and ceilometer mixing height retrievals
- Created a GAM model of MDA8 ozone concentrations to assess the enhancement of ozone concentrations due to wildfire influence

1.4 Conceptual Model

The conceptual model for the exceptional event that led to the ozone exceedances at the Paul Meyer and Walter Johnson sites on September 2, 2020, is outlined in Table 1-5. Table 1-5 provides the analysis techniques performed and evidence for each Tier. This establishes a weight of evidence for the clear causal relationship between the wildfire emissions in Oregon and California and the September 2 exceptional ozone event. We assert that wildfire emissions from Oregon and California fires from August 30 through September 1 led to enhanced ozone concentrations in Clark County on September 2 and the MDA8 ozone exceedances at the Paul Meyer and Walter Johnson sites. In support of this assertion, the key points of evidence for the conceptual model are summarized below.

1. The September 2 ozone exceedance occurred during a typical ozone season, but event concentrations at the Paul Meyer and Walter Johnson exceedance sites were significantly higher than non-event concentrations. Ozone concentrations at both exceedance sites showed a high percentile rank when compared with the past six years and ozone seasons.
2. HMS smoke and fire detections and CALIPSO aerosol vertical profiles show a consistent picture of wildfire smoke upwind of Clark County on August 30 through September 1. The White River and Lionshead Fires in Oregon on August 30 and 31 show plumes extending across Oregon, Nevada, and Idaho at 3-5 km altitude that were then transported southeastward. Multiple large complex fires in California (August Complex, Red Salmon Complex, North Complex, SQF Lightning Complex, Slink Fire, Dolan Fire, and SCU Complex)

contributed to smoke that blanketed the western U.S. on August 30 and 31. The Slink Fire and SQF Lightning Complex in California on August 31 and September 1 exhibited smoke plumes across California that were transported eastward into Clark County.

3. Back and forward trajectories from the near-surface boundary layer at the exceedance sites at the time of maximum ozone concentration show consistent transport patterns passing over the HMS smoke and aerosol vertical profile observed plumes originating from the Oregon and California fires. The combination of (1) trajectories intersecting fire locations or their associated smoke plumes and (2) a deep mixed layer over Clark County favoring vertical mixing demonstrate that wildfire emissions were transported to the surface in Clark County by September 1, 2020, the day prior to the exceedance event.
4. Meteorological conditions on September 2 did not favor enhanced local ozone production when compared with meteorologically similar ozone season days. Average MDA8 ozone across similar days was well below the ozone NAAQS and 10 ppb lower than the September 2 ozone exceedances.
5. GAM model predictions of MDA8 ozone on September 2 are all well below the 70-ppb ozone NAAQS for each EE-affected site. Using the 75^{th}-95^{th} quantile of positive residuals (observed MDA8 ozone minus GAM-predicted MDA8 ozone) we find a minimum wildfire effect on ozone of 4-12 ppb in Clark County from an atypical source; in this case, large fires in California and Oregon.
6. Persistent surface enhancements of $PM_{2.5}$ concentrations with typical PM_{10}:$PM_{2.5}$ ratios on the day prior to the exceedance event, and enhancement of the wildfire tracer levoglucosan above background ozone season levels, indicate the presence of wildfire emissions of ozone precursors at the surface in Clark County coincident with the wildfire plume arrival on September 1.

2. Historical and Non-Event Model

2.1 Regional Description

Clark County is located in the southern portion of Nevada and borders California and Arizona. It includes the City of Las Vegas, one of the fastest growing metropolitan areas in the United States with a population of approximately 2 million (U.S. Census Bureau, 2010). Las Vegas is located in a 1,600 km^2 desert valley basin at 500 to 900 m above sea level (Langford et al., 2015). It is surrounded by the Spring Mountains to the west (3,000 m elevation) and the Sheep Mountain Range to the north (2,500 m elevation). Three mountain ranges comprise the southern end of the valley. The valley floor slopes downward from west to east, which influences surface wind, temperature, precipitation, and runoff patterns. The Cajon Pass and I-15 corridor to the west is an important atmospheric transport pathway from the Los Angeles Basin into the Las Vegas Valley (Langford et al., 2015). **Figures 2-1 and 2-2** show the topography of Clark County and surrounding areas.

The Las Vegas Valley climatology features abundant sunshine and hot summertime temperatures (average summer month high temperatures of 34-40°C). Because of the mountain barriers to moisture inflow, the region experiences dry conditions year-round (~107 mm annual precipitation, 22% of which occurs during the summer monsoon season in July through September). The urban heat island effect in Las Vegas during summer causes large temperature gradients within the valley, with generally cooler temperatures on the eastern side. During the summer season, monsoon moisture brings high humidity and thunderstorms to the region, typically in July and August (National Weather Service Forecast Office, 2020). Winds in the Las Vegas basin generally come from the southwest during spring and summer (Los Angeles is upwind), and from the northwest in the fall and winter, with air transported between the neighboring mountain ranges and along the valley.

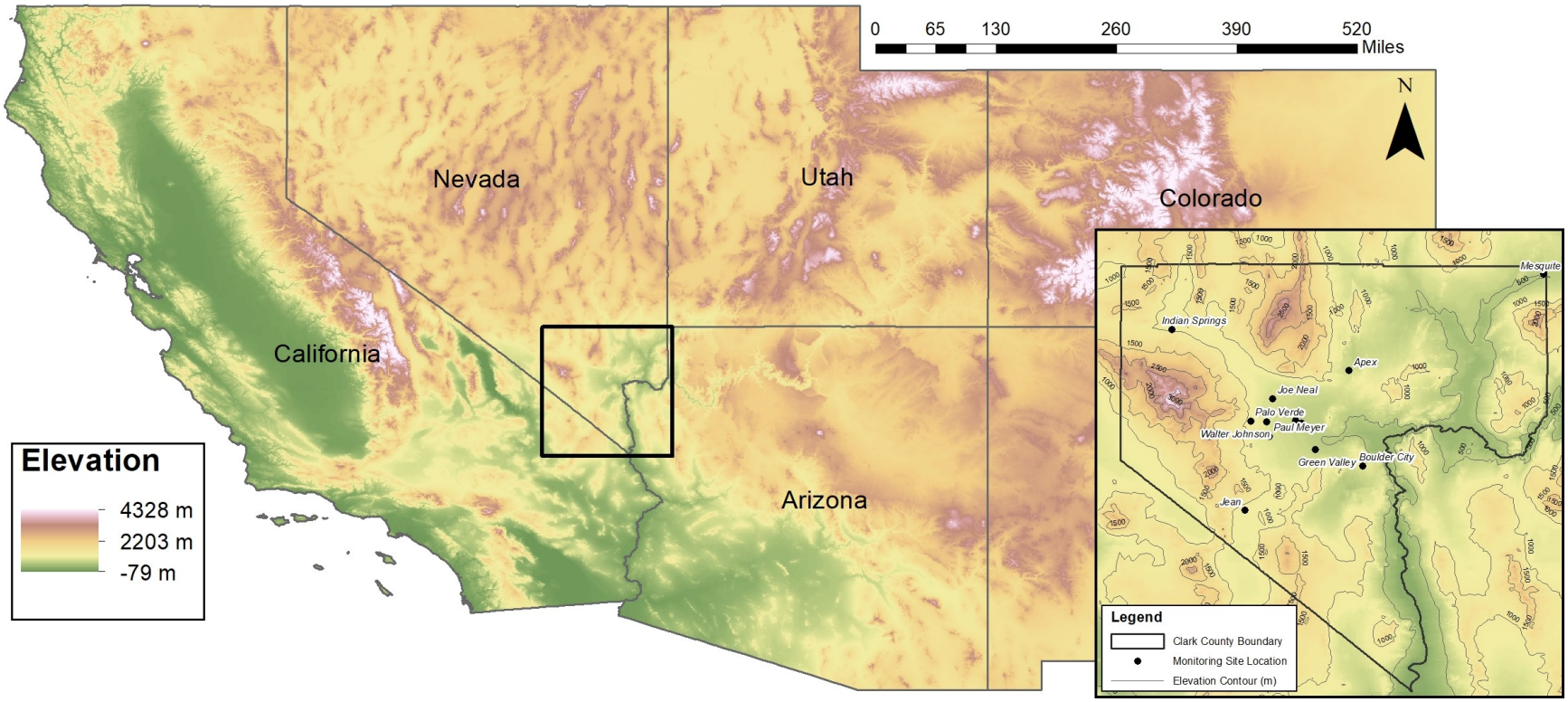

Figure 2-1. Regional topography around Clark County, with an inset showing county boundaries and the air quality monitoring sites analyzed in this report.

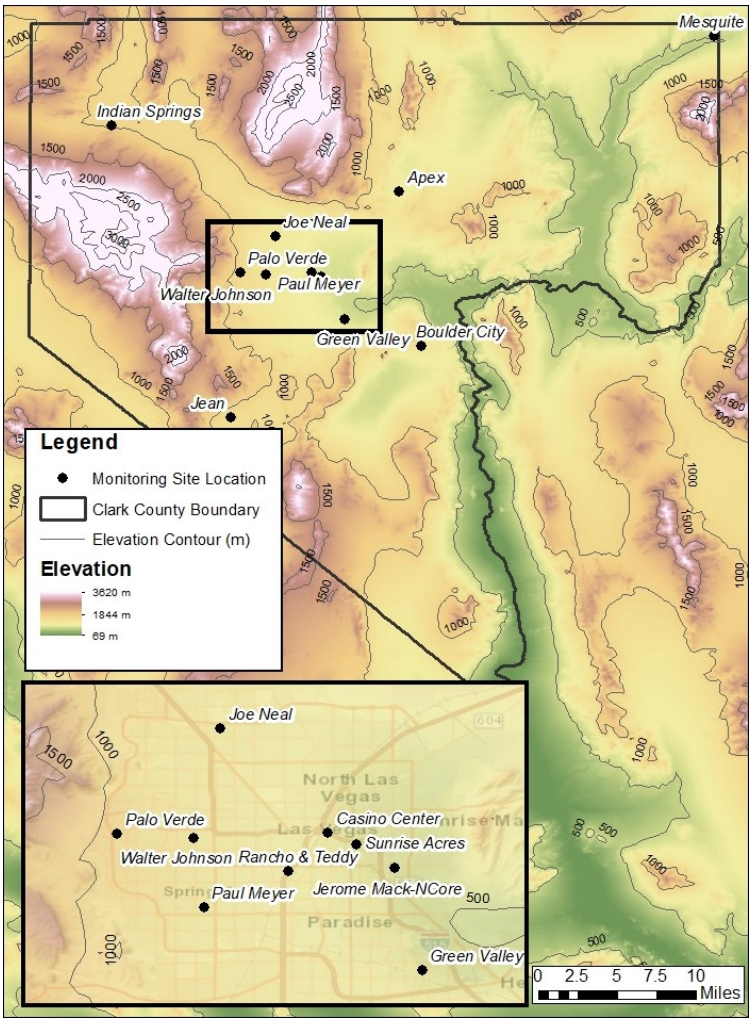

Figure 2-2. Clark County topography, with an inset showing all air quality monitoring sites in the Clark County area.

2.2 Overview of Monitoring Network

The Clark County Department of Environment and Sustainability, Division of Air Quality (DAQ) operated 14 ambient air monitoring sites in the region during 2020 (Figure 2-2). These sites measure hourly ozone (O_3), particulate matter ($PM_{2.5}$, PM_{10}), nitrogen oxides (NO_x), TNMOC, and carbon monoxide (CO) concentrations along with meteorological parameters. Table 2-1 presents monitoring data across time and space for criteria pollutants and surface meteorological parameters (barometric pressure, temperature, wind speed and direction), as well as mixing height. We examined ozone and other criteria pollutants at 11 sites around Clark County to investigate the high ozone event observed on September 2, 2020. DAQ's ambient air monitoring network meets the monitoring

requirements for criteria pollutants pursuant to Title 40, Part 58, of the Code of Federal Regulations (CFR), Appendix D (U.S. Environmental Protection Agency, 2008). Data are quality-assured in accordance with 40 CFR 58 and submitted to the EPA's Air Quality System (AQS). The spatial distribution of monitoring sites characterizes the regional air quality in Las Vegas, as well as air quality upwind and downwind of the urban valley region (Figure 2-2). The Jean monitoring site along the I-15 corridor is generally upwind such that it captures atmospheric transport into the region and is least impacted by local sources (Figure 2-2).

Table 2-1. Clark County monitoring site data. The available date ranges of all parameters and monitoring sites used in this report for Clark County, Nevada, are shown. Casino Center and RT are near-road sites that are not used for the exceptional event analysis.

Site	AQS Sitecode	O_3	$PM_{2.5}$	CO	NO	NO_2	TNMOC	Temp.	Wind Speed	Wind Direction	Barom. Pressure	Mixing Height
Apex	320030022	2014-2020						2014-2020	2014-2020	2014-2020		
Boulder City	320030601	2014-2020									2014-2016	
Casino Center	320031502							2014-2020	2016-2020	2016-2020		
Green Valley	320030298	2015-2020	2014-2020	2020				2016-2020	2014-2020	2014-2020	2014-2016	
Indian Springs	320037772	2014-2020										
Jean	320031019	2014-2020	2014-2020					2014-2020	2014-2020	2014-2020	2014-2016	
Jerome Mack	320030540	2014-2020	2014-2020	2015-2020[1,2]	2015-2020	2015-2020	2020	2014-2020	2014-2020	2014-2020	2014-2020	2020
Joe Neal	320030075	2020	2018-2020	2019-2020		2015-2020		2014-2020	2014-2020	2014-2020	2014-2016	
Mesquite	320030023	2014-2020						2014-2020	2014-2020	2014-2020		
Palo Verde	320030073	2014-2020	2020					2014-2020	2014-2020	2014-2020	2014-2016	
Paul Meyer	320030043	2014-2020	2017-2020					2014-2020	2014-2020	2014-2020	2014-2016	
RT	320031501							2015-2020	2015-2020	2015-2020	2014-2016	
Sunrise Acres	320030561			2020				2014-2020	2014-2020	2014-2020	2014-2016	
Walter Johnson	320030071	2014-2020	2020					2015-2020	2015-2020	2015-2020	2014-2016	

[1] CO data invalid at Jerome Mack on Sep. 2, 2020

[2] CO data invalid at Jerome Mack Apr. 28, 2020 – May 20, 2020

2.3 Characteristics of Non-Event Historical O_3 Formation

During the ozone season (April–September) in Clark County, Nevada, ozone concentrations are typically influenced by local formation, transport into the region, and, on occasion, by EEs such as wildfires and stratospheric intrusions. Southwesterly winds transport emissions from upwind source regions (e.g., Los Angeles Basin, Mojave Desert, Asia), and southerly transport dominates later in the season due to the summer monsoon (Langford et al., 2015; Zhang et al., 2020). Local precursor emissions in Clark County include mobile NO_x and VOCs sources, coal and natural-gas fueled power generation NO_x sources, and biogenic VOC emissions. Based on 2017 Las Vegas emission inventories, on a typical ozone season weekday there are 98 tons of NO_x emissions per day and 238 tons of VOC emissions per day (Clark County Department of Environment and Sustainability, 2020). On-road mobile sources comprise 40% of NO_x emissions and total mobile emissions comprise 88% of total NO_x emissions during the ozone season. In contrast, 52% of VOC emissions originate from biogenic sources within Clark County. Local emissions and/or precursors transported into the region contribute to ozone formation within Clark County (Langford et al., 2015; Clark County Department of Air Quality, 2019).

In this demonstration, we discuss the impacts of wildfire smoke on ozone concentrations in Clark County on September 2, 2020. In order to fully discern these effects, we examine the historical ozone record for all affected sites (Table 1-1). *Non-event days* refer to all days other than the September 2 event. Because percentile rankings are sensitive to including the relatively large number of potential EE days during 2018 and 2020, we also provide statistics *excluding potential EE days* (i.e., without including the 2018 and 2020 potential EE days as defined in Tables 1-2 and 1-3 in Section 1). The 8-hour ozone design value (DV) is the three-year running average of the fourth-highest maximum daily 8-hour (MDA8) ozone concentration (U.S. Environmental Protection Agency, 2015). Within Clark County, Las Vegas is classified a marginal nonattainment region with a 73 ppb ozone DV for 2017-2019 (U.S. Environmental Protection Agency, 2020).

Ozone EE days were identified as days with significant wildfire or stratospheric intrusion influence in addition to an MDA8 concentration greater than 70 ppb. By this criterion, we identified 15 possible EE days in 2018,13 possible EE days in 2020, and none in 2019.

The September 2, 2020, EE occurred late in the ozone season under hot, dry air, upper-level high pressure, and surface low-pressure meteorological conditions favoring subsidence and vertical mixing of wildfire smoke-influenced ozone and precursors to ground level (see Section 3.3.1-2). Compared with a non-event conceptual model of local precursor emissions contributing to ozone formation at ground level under similar conditions, the September 2 conditions indicate additional transport of wildfire-influenced air parcels via northerly winds aloft.

Figures 2-3 through 2-6 depict the six-year historical record and seasonality of MDA8 ozone concentrations at each monitoring site, along with the 99th percentile and NAAQS standard ozone concentrations. September 2 ranks in the top 1% for daily maximum ozone concentration in the six-

year historical record at the two EE affected monitoring sites (Paul Meyer and Walter Johnson). Figure 2-7 depicts a two-week diurnal cycle of 1-hour ozone concentrations beginning one week before the September 2 event and ending one week after. On September 2, daily maximum 1-hour ozone concentrations were the highest during this two-week period at four of the 11 monitoring sites shown, including both of the EE affected sites (Paul Meyer and Walter Johnson).

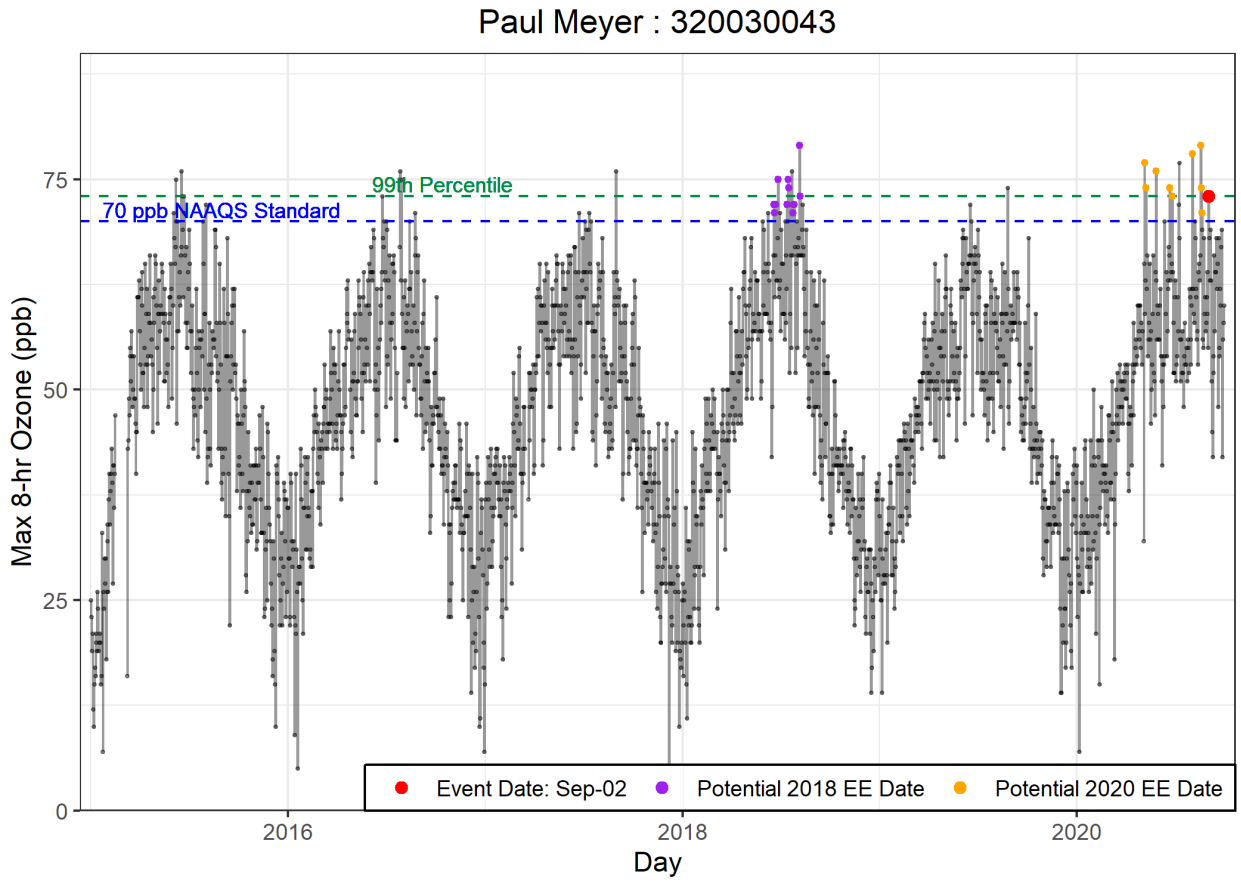

Figure 2-3. Time series of 2015-2020 ozone concentrations at Paul Meyer.

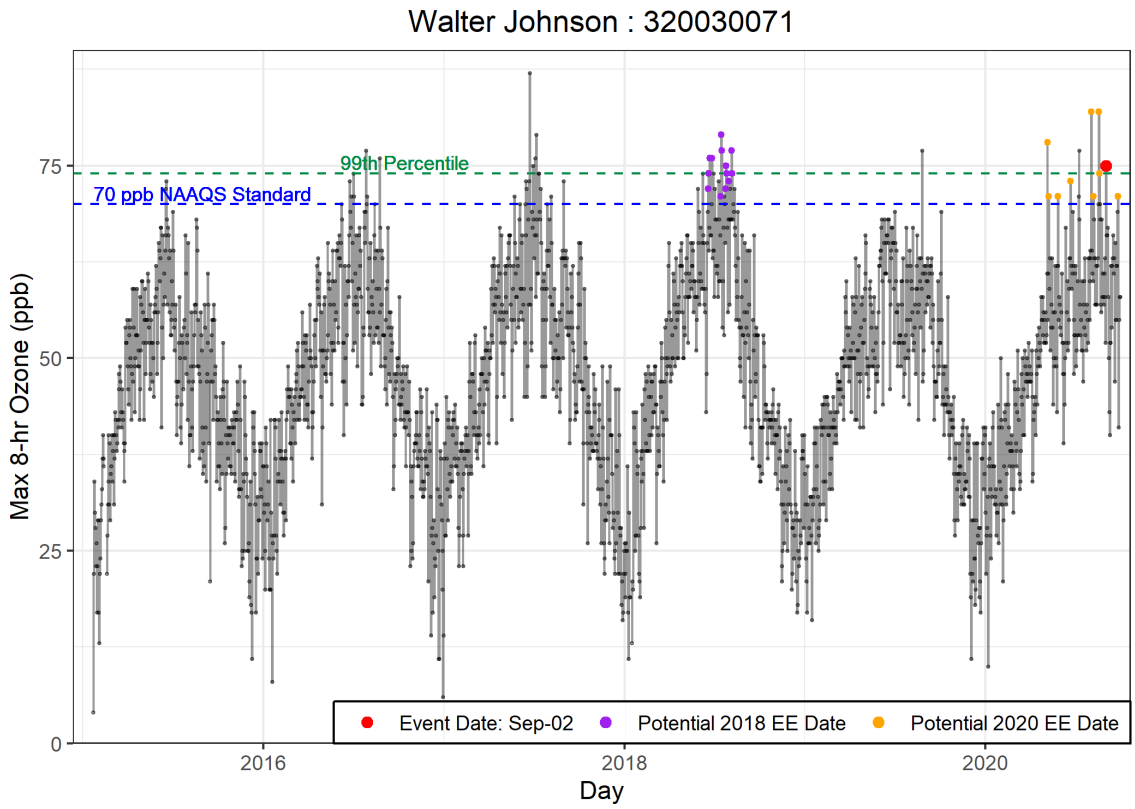

Figure 2-4. Time series of 2015-2020 ozone concentrations at Walter Johnson.

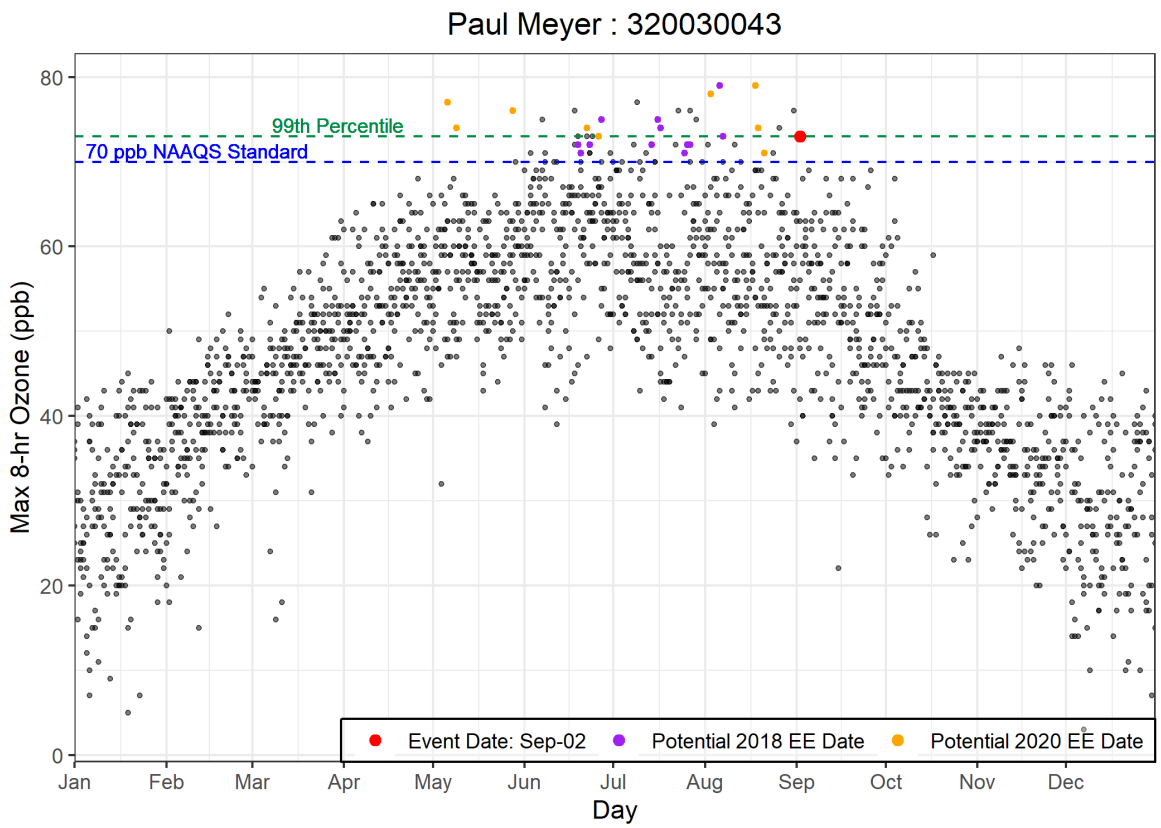

Figure 2-5. Seasonality of 2015-2020 ozone concentrations from Paul Meyer.

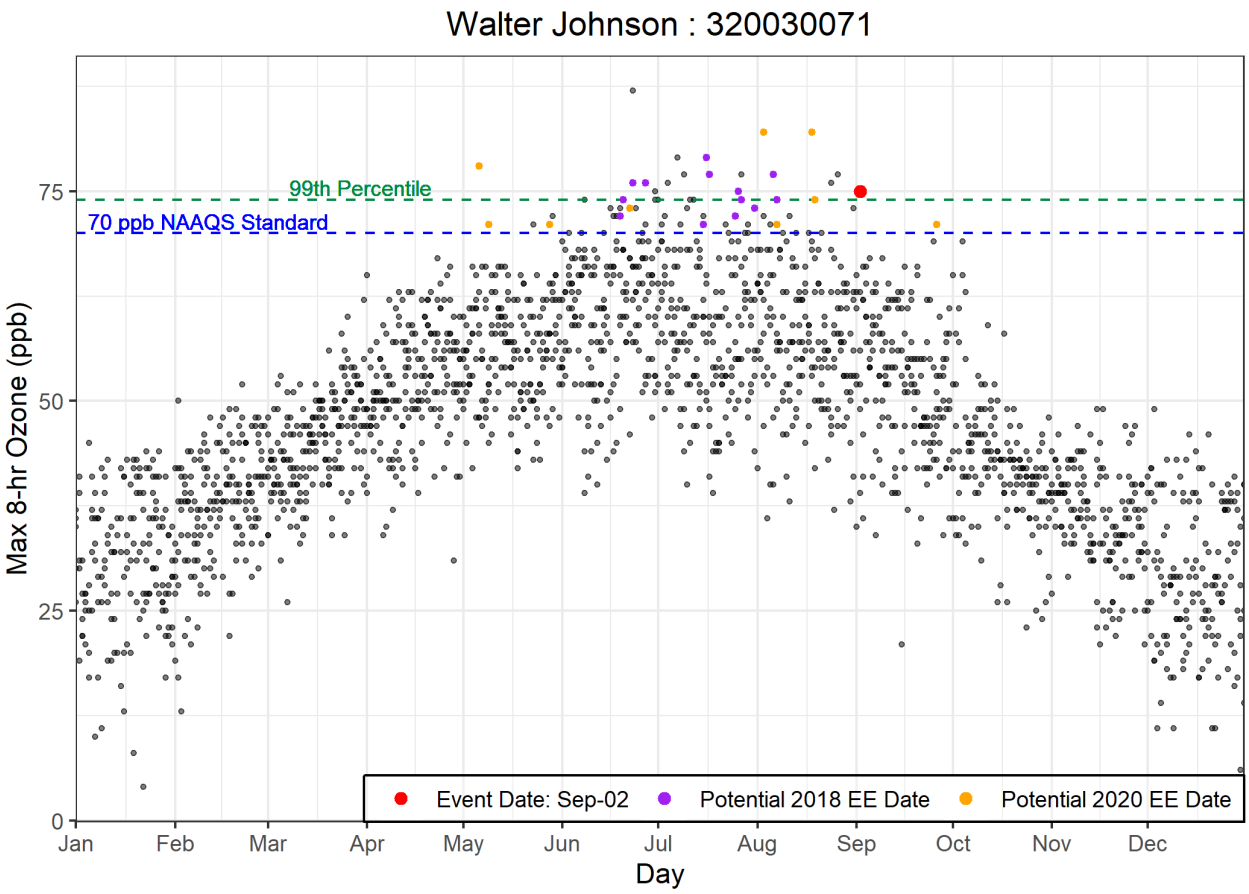

Figure 2-6. Seasonality of 2015-2020 ozone concentrations from Walter Johnson.

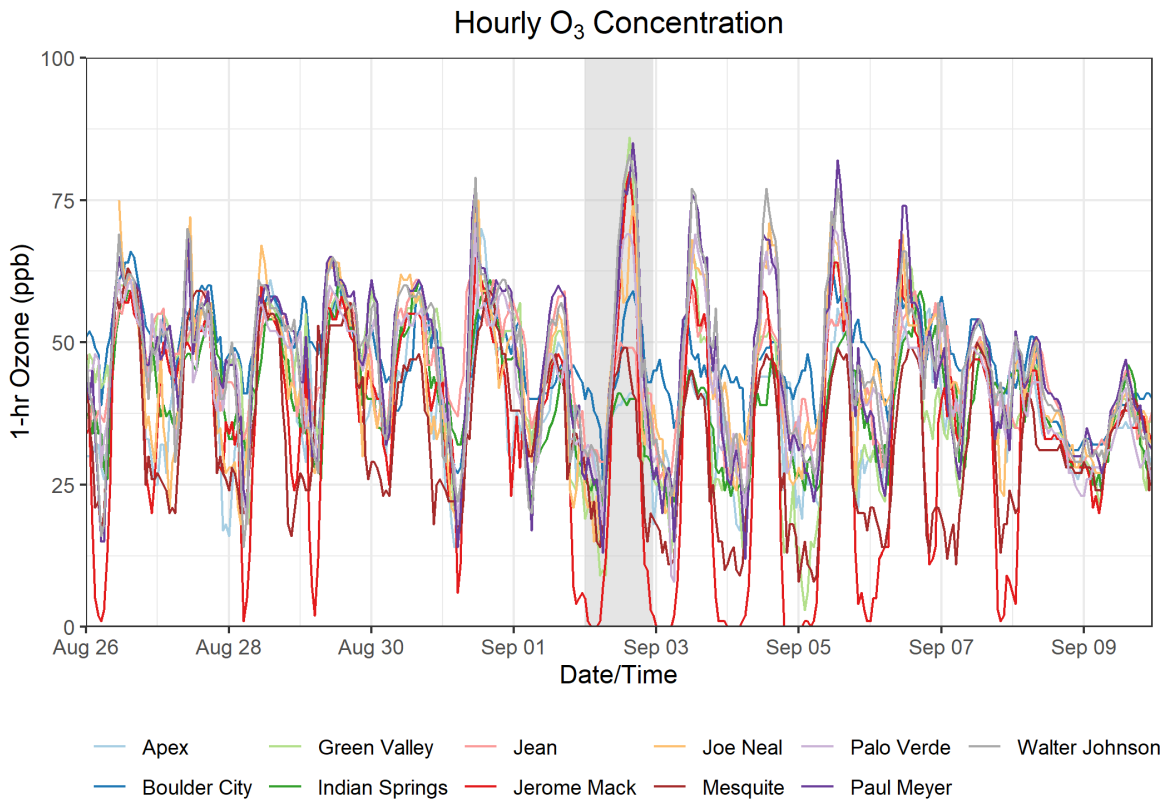

Figure 2-7. Ozone time series at all monitoring sites. Time series of hourly ozone concentrations at monitoring sites in Clark County for one week before and after the September 2 event are shown. September 2, 2020, is shaded for reference.

3. Clear Causal Relationship Analyses

3.1 Tier 1 Analyses

3.1.1 Comparison of Event with Historical Data

To address the Tier 1 EE criterion of comparison with historical ozone, we compared the September 2 EE ozone concentrations at each site with the 2020 ozone record, focusing mainly on the ozone season when highest ozone concentrations occur. **Figures 3-1 and 3-2** depict the 2020 daily maximum ozone record at each monitoring site, along with the 99th percentile of previous 5-year MDA8 ozone and NAAQS criteria ozone concentrations. September 2 ranks in the top 1% for daily maximum ozone concentration during 2020 at the Walter Johnson and Paul Meyer sites. When compared with daily ozone rankings on September 2 over the six-year ozone record (Figures 2-5 and 2-6), the 2020 ozone concentration ranks as the highest, indicating that September 2, 2020, was an extreme event.

The September 2, 2020, ozone exceedance occurred during a typical ozone season, but September 2 MDA8 ozone concentrations were the second highest compared with daily ozone concentrations excluding potential EE days (Figures 3-1 and 3-2). The MDA8 ozone concentration on September 2 was >10 ppb above the mean or median ozone concentrations for the historical ozone season non-event days at all EE affected sites (**Table 3-1**). However, the MDA8 ozone concentrations at EE affected sites were < 5 ppb above the 95th percentile of ozone during historical ozone season non-event days (Table 3-1). Because September 2 is during the normal ozone season and MDA8 ozone concentrations at EE affected sites could not be clearly distinguished from the 95th percentile ozone concentration during the non-event historical ozone season, the September 2, 2020, event does not satisfy the key factor for a Tier 1 EE. Tier 2 comparison of the event-related ozone concentrations with non-event-related high ozone concentrations (>99th percentile over five years or top four highest daily ozone measurements) are described in Section 3.2.2.

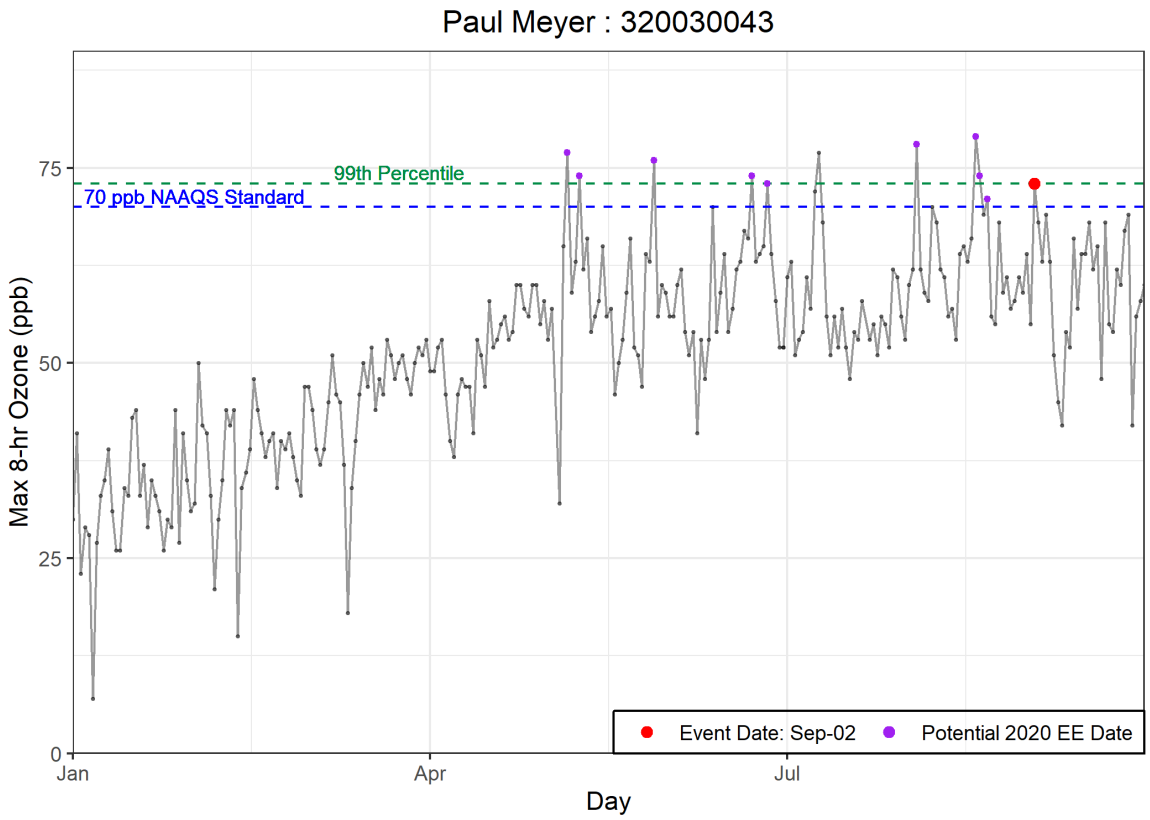

Figure 3-1. Time series of 2020 MDA8 ozone concentrations from Paul Meyer.

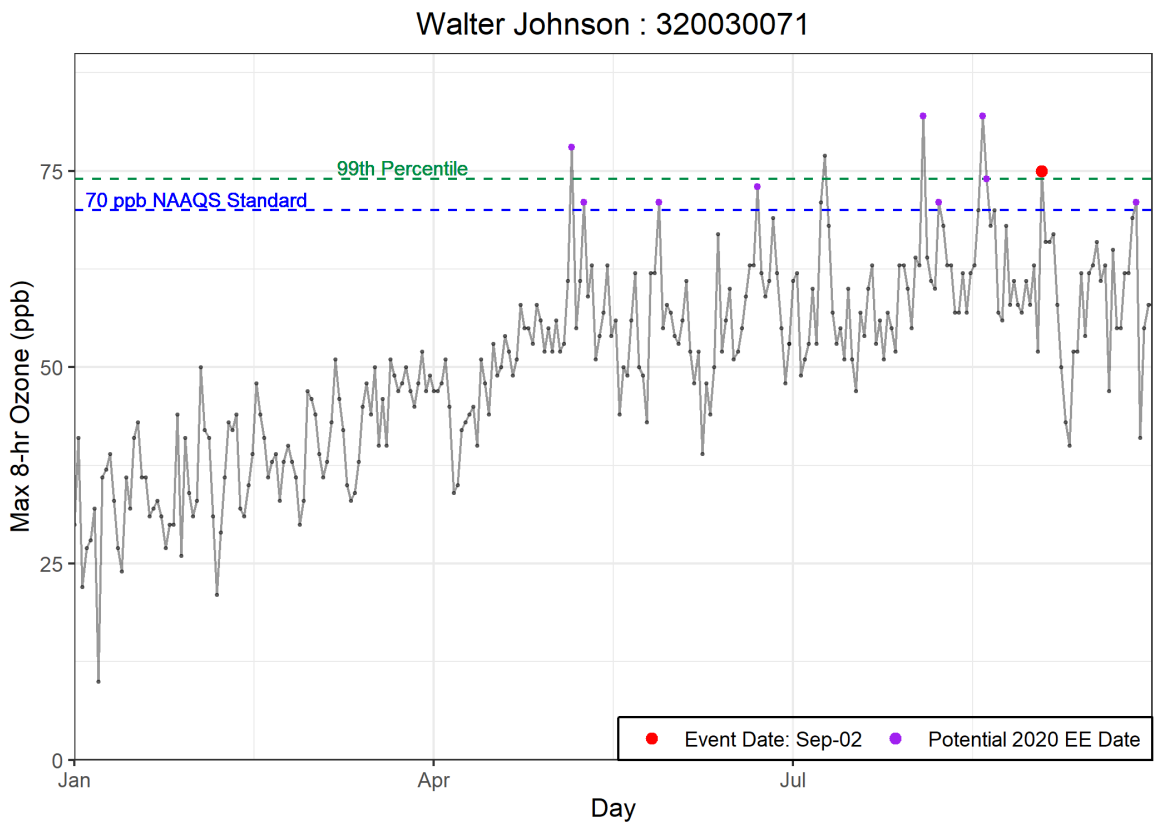

Figure 3-2. Time series of 2020 MDA8 ozone concentrations from Walter Johnson.

Table 3-1. Ozone season non-event comparison. September 2, 2020, MDA8 ozone concentrations for each affected site are shown in the top row. Five-year (2015-2019) average MDA8 ozone statistics for May through September ozone season are shown for each affected site around Clark County to compare with the event ozone concentrations.

	Paul Meyer 320030043	Walter Johnson 320030071
Sep. 2	73	75
Mean	57	57
Median	58	57
Mode	58	57
St. Dev	8	9
Minimum	22	21
95 %ile	70	71
99 %ile	76	77
Maximum	79	87
Range	57	66
Count	911	917

3.1.2 Ozone, Fire, and Smoke Maps

3.1.2.1 O_3 and $PM_{2.5}$ Maps

We produced maps of ozone Air Quality Index (AQI), $PM_{2.5}$ AQI, active fire and smoke detections from satellites, and visible satellite imagery that show the transport of smoke to Las Vegas from fires in the Pacific Northwest and California on September 2, 2020. These maps also show that high ozone concentrations corresponding with the presence of wildfire smoke occurred across multiple states.

From August 30 through September 2, 2020, moderate and unhealthy ground-level ozone concentrations (indicated by the yellow, orange, and red areas) were detected in the western United States (Figure 3-3), especially in California and southern Nevada. High ozone concentrations (i.e., the orange and red areas) were seen in regions across California consistently over the 4-day period. On the day proceeding the event, areas of high ozone concentrations appeared in Oregon. On September 2, high ozone covered Clark County in southern Nevada.

A similar pattern of pollutant distribution over the western United States is also seen in the AQI plots for $PM_{2.5}$ (Figure 3-4). High concentrations of $PM_{2.5}$ were observed across California over the 4-day

period, transporting towards Nevada and covering Las Vegas in elevated concentrations. Starting September 1, areas of elevated $PM_{2.5}$ concentrations were observed in the Pacific Northwest. Those areas grew larger on the day of the event, corresponding to fire locations in Oregon (including the White River and Lionshead Fires).

According to EPA guidance (U.S. Environmental Protection Agency, 2016), "if plume arrival at a given location coincides with elevation of wildfire plume components (such as $PM_{2.5}$, CO or organic and elemental carbon), those two pieces of evidence combined can show that smoke was transported from the event location to the monitor with the enhanced ozone concentration." Sections 3.1.2 through 3.2.4 of this report show that the September 2, 2020, enhanced ozone and $PM_{2.5}$ concentrations observed in the aforementioned regions in the western United States—including Clark County, Nevada— corresponded with the arrival of a smoke plume from the Pacific Northwest fires (especially the White River and Lionshead Fires in Oregon) and large complex California fires.

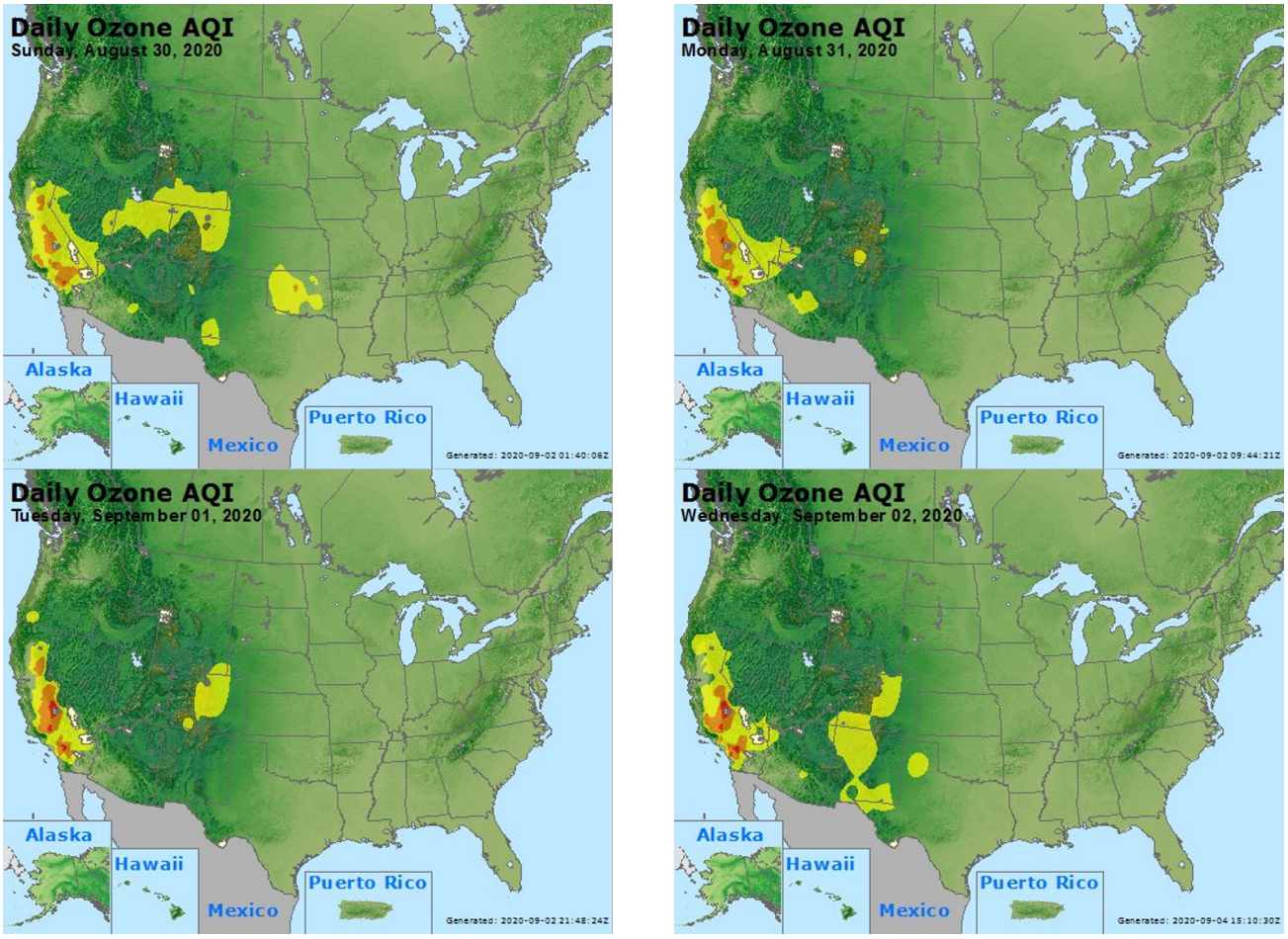

Figure 3-3. Daily ozone AQI for the three days before the September 2 event and the day of the event.

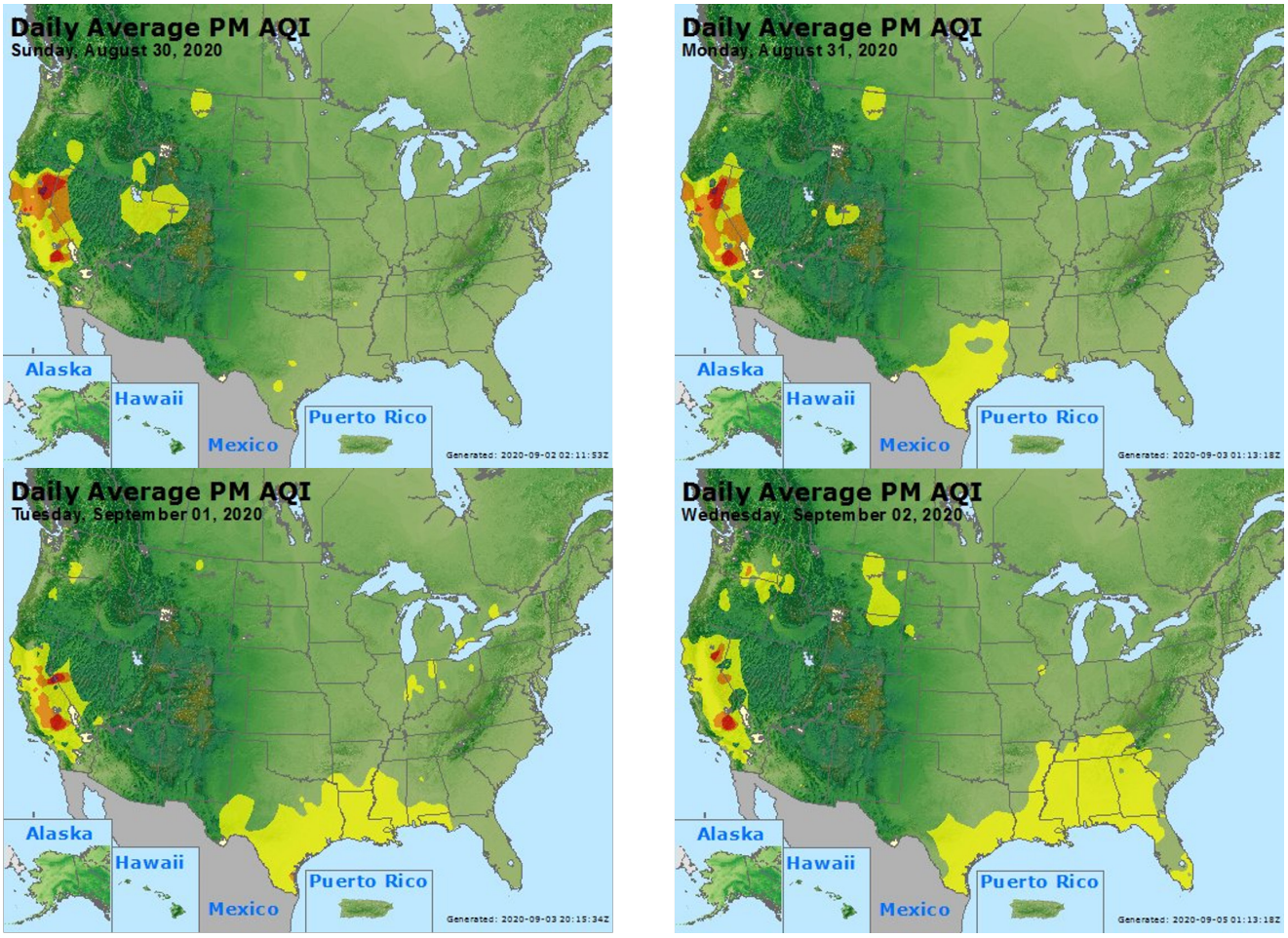

Figure 3-4. Daily $PM_{2.5}$ AQI for the three days before the September 2 event and the day of the event.

3.1.2.2 HMS Fire Detection Maps

According to EPA's guidance for Tier 1 analysis requirements (U.S. Environmental Protection Agency, 2016), the National Oceanic and Atmospheric Administration (NOAA) Hazard Mapping System (HMS) Fire and Smoke Product can be used to demonstrate the transport of fire emissions to the impacted monitors. The HMS Fire and Smoke Product consists of

1. A daily fire detection product derived from three satellite data products[1] to spatially and temporally map fire locations at 1 km grid resolution, and
2. A daily smoke product derived from visible satellite imagery[2] that consists of polygons showing regions impacted by smoke.

[1] The HMS fire detection product is developed using data from the Moderate Resolution Imaging Spectroradiometer (MODIS), Geostationary Operational Environmental Satellite system (GOES), Advanced Very High Resolution Radiometer (AVHRR) and Visible Infrared Imaging Radiometer Suite (VIIRS) satellite instruments.
[2] The HMS smoke product is derived from GOES-EAST and GOES-WEST visible satellite imagery.

The HMS smoke plume data is based on measurements from several environmental satellites and is reviewed by trained NOAA analysts to identify cases where smoke is dispersed by transport. One can download real-time HMS fire detection and smoke products, and a six-month archive of the products from the NOAA Satellite and Information Service website (ospo.noaa.gov/Products/land/hms.html).

Figure 3-5 shows the HMS smoke plume and fire detection data across the U.S. for August 30 to September 2, 2020, highlighting the long-ranging effects of the fires in California and Oregon. Figure 3-6 shows zoomed-in HMS smoke and fire detections over the northwestern United States, including California and the Pacific Northwest where the wildfires burned (including the White River Fire and the Lionshead Fire in Oregon), during the same period. As the daily plots indicate, there was concentrated fire activity in the Pacific Northwest, in central and northern California, and in the central and southern United States. Although Nevada was almost clear of fires, its surrounding states were burning with a significant number of large fires, especially in California and Oregon. Substantial smoke plumes from both the Pacific Northwest fires and California ones swept across the country horizontally, joined by the plumes from fires burning in central states, reaching east towards Ohio during the first two days (August 30 to August 31). During September 1 and September 2 (day of the event), although the majority of the smoke covering the western and central United States had dissipated, concentrated plumes still formed from the Pacific Northwest fires (especially the White River Fire and the Lionshead Fire in Oregon) and the California fires. This is consistent with the increased ozone and $PM_{2.5}$ concentrations observed in those regions, as shown above in the AQI plots (Figures 3-3 and 3-4).

The HMS smoke plume data for the days leading up to September 2 were obtained and combined with HYSPLIT back trajectories on high ozone concentration days to identify intersections and assess potential smoke impacts (Section 3.1.3). The following sections provide further evidence of smoke transport, based on HYSPLIT trajectories and satellite data, that traveled from the Pacific Northwest fires (especially the White River Fire and the Lionshead Fire in Oregon) and California fires to the Clark County area.

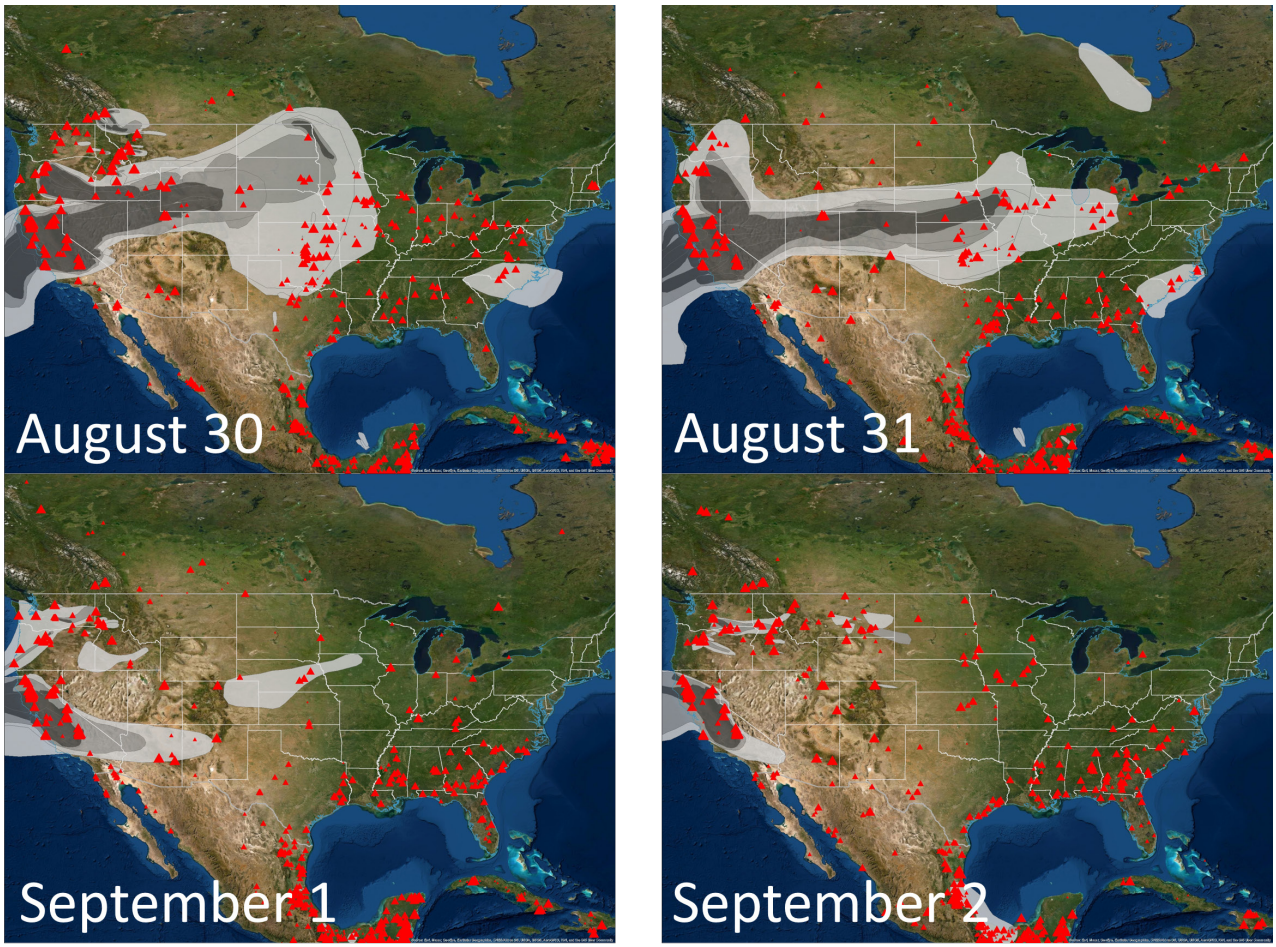

Figure 3-5. Daily HMS Smoke for the three days before the September 2 event and the day of the event.

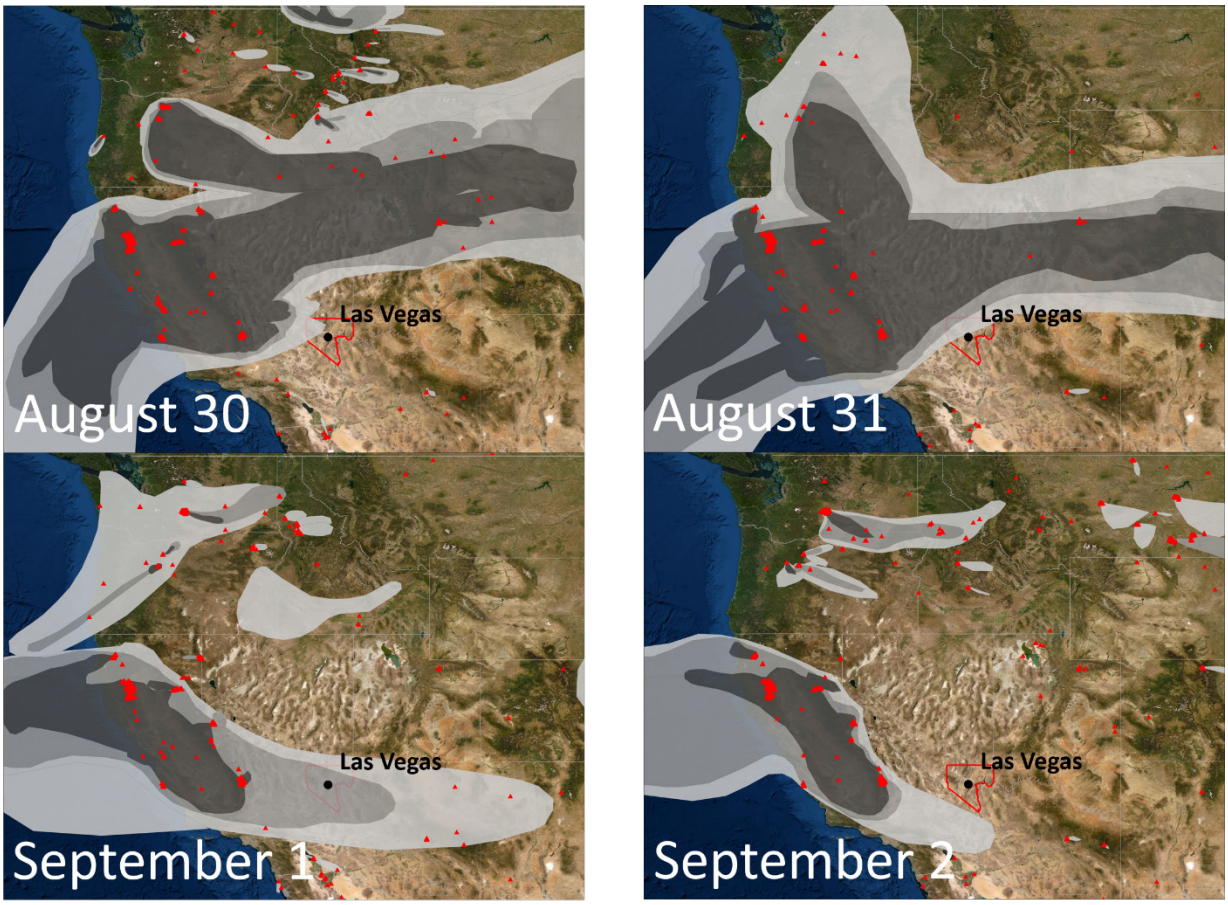

Figure 3-6. Daily HMS smoke and fire detections (red triangles) for the three days before the September 2 event and the day of the event.

3.1.2.3 Visible Satellite Imagery

Visible satellite imagery from the Moderate Resolution Imaging Spectroradiometer (MODIS) Aqua and Terra satellites show transport of smoke from the fires burning in central and southern California, and in the Pacific Northwest (including the White River Fire and the Lionshead Fire in Oregon) to Nevada between August 30 and September 2 (**Figures 3-7 through 3-10**). The visible satellite imagery mainly captures dense smoke plumes, but lack of a plume image does not rule out the presence of more diluted plumes. August 30 and 31 fires in Oregon show plumes traveling southeastward and California fires show smoke plumes traveling eastward toward Clark County. This is consistent with the locations of HMS smoke plumes transported from these fire locations. These characteristics correspond with the increase in high ozone and $PM_{2.5}$ concentrations in the Pacific Northwest, as shown in the AQI maps above. In addition, the transport of smoke southeastward from the Pacific Northwest is consistent with transport patterns observed in the HYSPLIT trajectory analysis presented in Section 3.1.3, as well as the satellite and ground-based measurements of smoke-associated species presented in Sections 3.2.3 and 3.2.4.

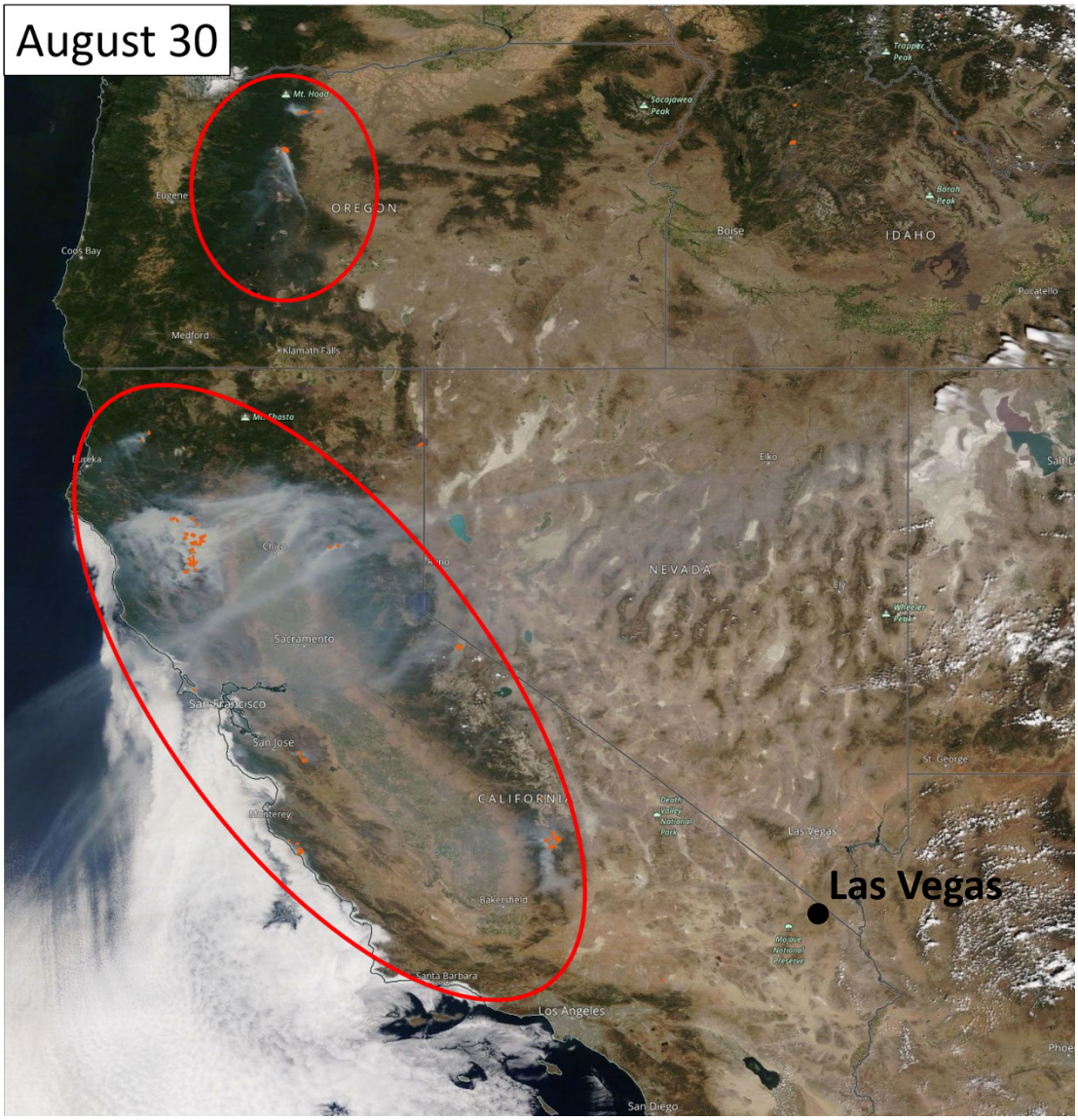

Figure 3-7. Visible satellite imagery from over western United States (including Oregon, California, and Nevada) on August 30, 2020. Source: NASA Worldview.

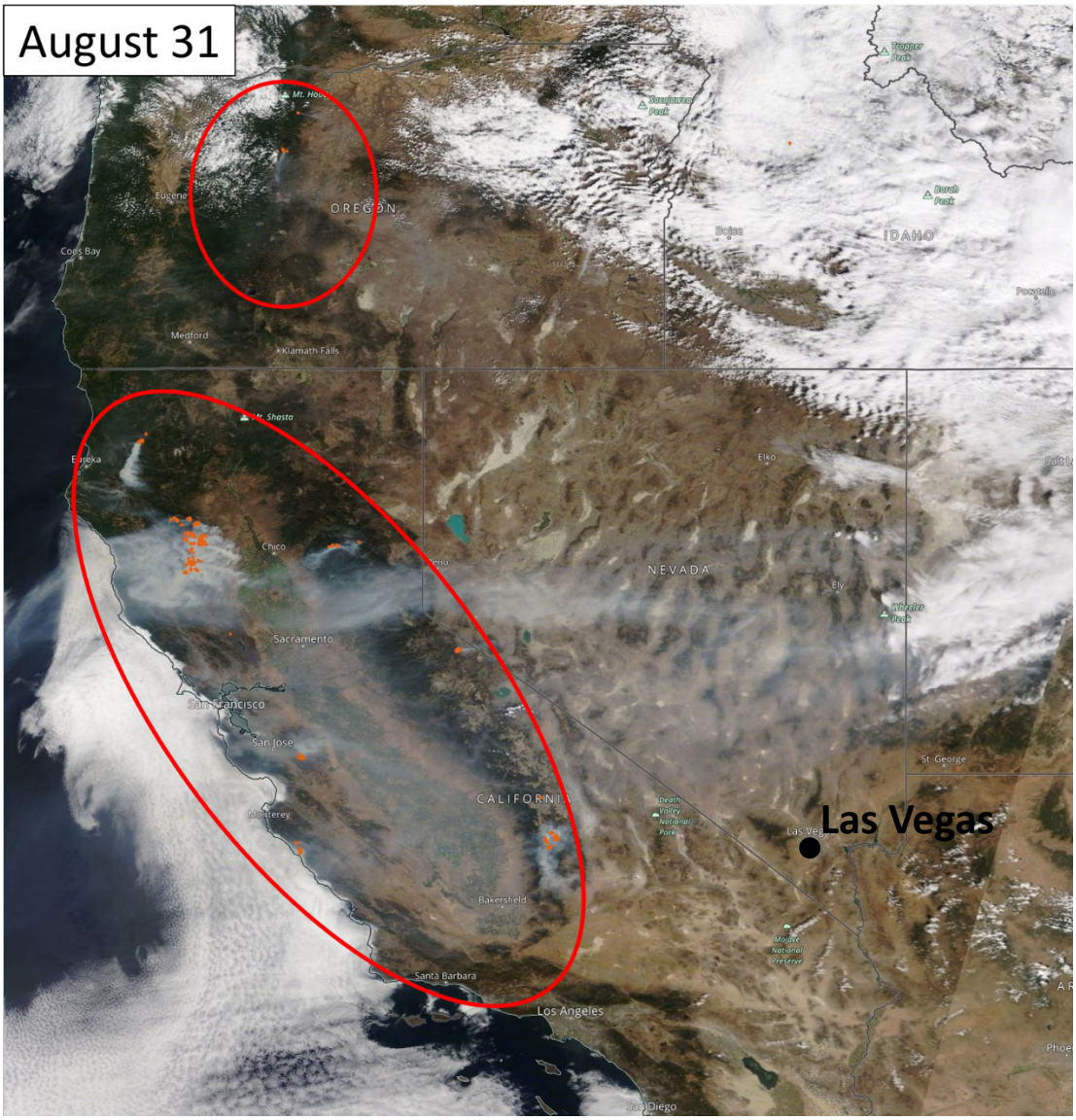

Figure 3-8. Visible satellite imagery from over western United States (including Oregon, California, and Nevada) on August 31, 2020. Source: NASA Worldview.

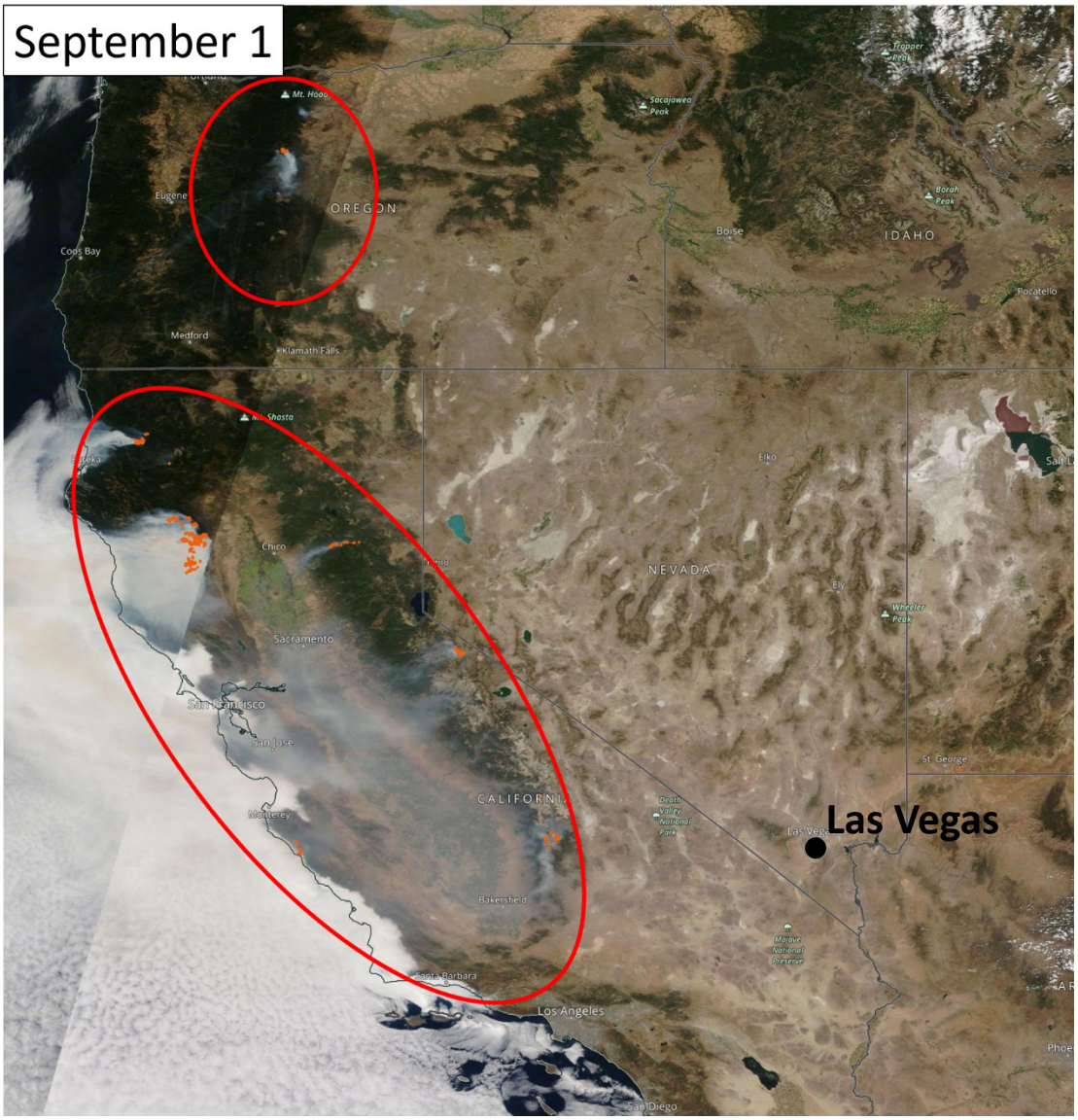

Figure 3-9. Visible satellite imagery from over western United States (including Oregon, California, and Nevada) on September 1, 2020. Source: NASA Worldview.

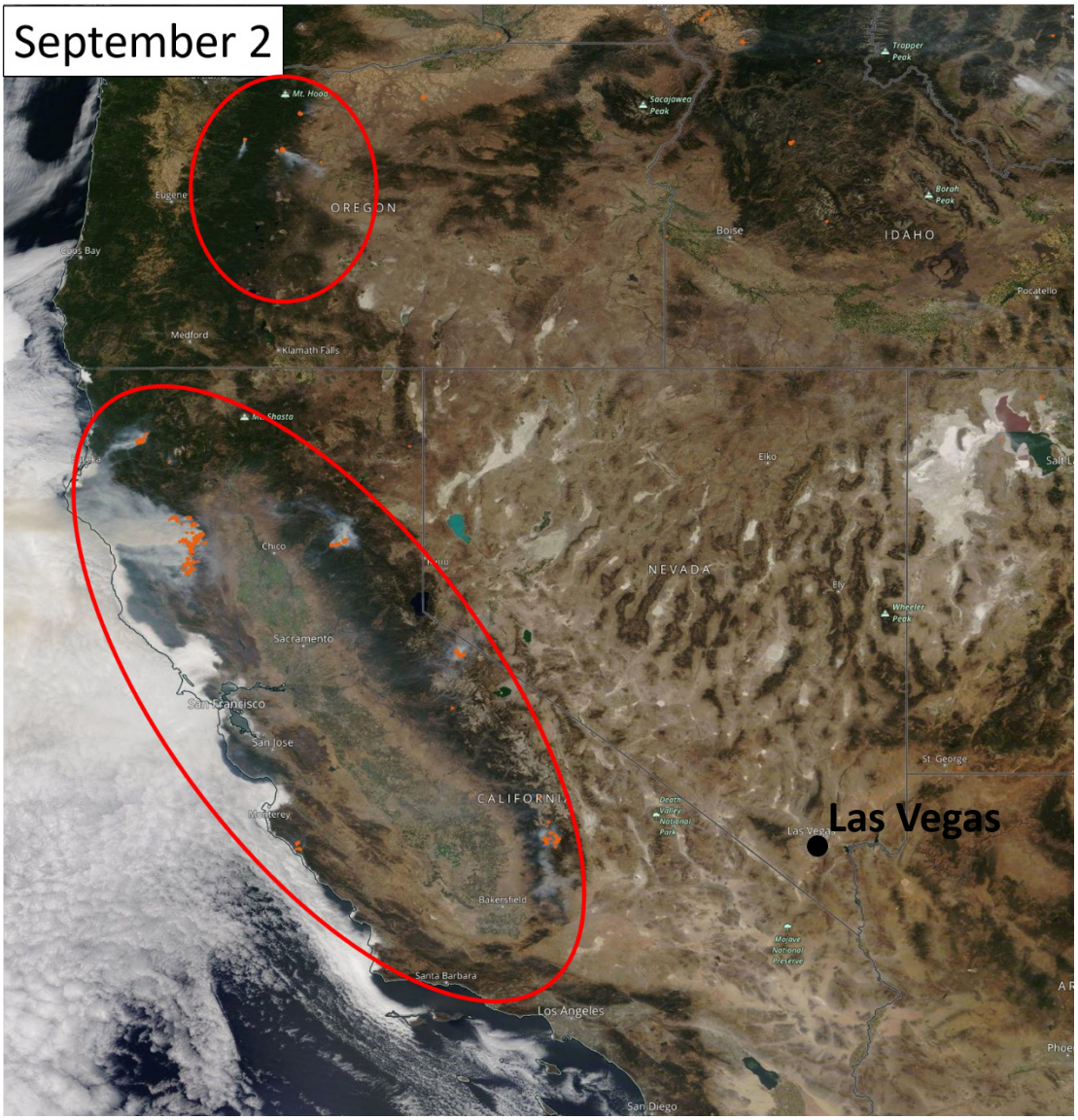

Figure 3-10. Visible satellite imagery from over western United States (including Oregon, California, and Nevada) on September 2, 2020. Source: NASA Worldview.

3.1.3 HYSPLIT Trajectories

HYSPLIT trajectories were run to demonstrate the transport of air parcels to Las Vegas from upwind areas and to show transport of smoke-containing air parcels from wildfires toward the affected monitors. These trajectories show that air was transported from fires in the Pacific Northwest (including the Evans Canyon Fire in Washington and the White River and Lionshead Fires in Oregon), and fires in California to the Clark County area in the days prior to the event and on September 2, 2020. Combined with satellite observations described in Sections 3.1.2 and 3.2.3, the trajectories

demonstrate that smoke was transported from the Pacific Northwest and California to Las Vegas, Nevada.

NOAA's online HYSPLIT model tool was used for the trajectory modeling (http://ready.arl.noaa.gov/HYSPLIT.php). HYSPLIT is a commonly used model that calculates the path of a single air parcel from a specific location and height above the ground over a period of time; this path is the modeled trajectory. HYSPLIT trajectories can be used as evidence that fire emissions were transported to an air quality monitor. This type of analysis is important for meeting Tier 1 requirements and is required under Tier 3.

Table 3-2 summarizes the model options used for this study. We used the meteorological data from the North American Mesoscale Forecast System (NAM, 12 km resolution) and High-Resolution Rapid Refresh (HRRR, 3 km resolution) model (ready.noaa.gov/archives.php). These data are high in spatial resolution, readily available for HYSPLIT modeling over the desired lengths of time, and expected to capture fine-scale meteorological variability. All backward trajectory start times were selected to be in the afternoon (22:00 UTC or 2:00 p.m. local standard time) to coincide with the maximum 1 hour ozone observed at the Walter Johnson monitoring site on September 2. As suggested in the EPA's EE guidance (U.S. Environmental Protection Agency, 2016), a backward trajectory length of 72 hours was selected to assess whether smoke from the current day or from the previous two days may have been transported over a long distance to the monitoring sites. Trajectories were initiated at 50 m, 500 m, and 1,000 m above ground level to capture transport throughout the mixed boundary layer, as ozone precursors may be transported aloft and influence concentrations at the surface through vertical mixing. Three backward trajectory approaches available in the HYSPLIT model were used in this analysis, including site-specific trajectories, trajectory matrix, and trajectory frequency. Site-specific back trajectories were run to show direct transport from the wildfire smoke to the affected site(s) – this analysis is useful in linking smoke impacts at a single location (i.e., an air quality monitor) to wildfire smoke. Matrix back trajectories were run to show the general air parcel transport patterns from the Las Vegas area to the wildfire smoke plumes. Similarly, matrix forward trajectories were run to show air parcel transport patterns from the fires to the Las Vegas area. Matrix trajectories are useful in analyzing air transport over areas larger than a single air quality site. Trajectory frequency analysis show the frequency with which multiple trajectories initiated over multiple hours pass over a grid cell on a map. Trajectory frequencies are useful in estimating the temporal and spatial patterns of air transport from a source region to a specific air quality monitor. Additionally, a forward trajectory matrix was run for locations of the White River and Lionshead Fires in Oregon, and the Slink Fire and SQF Lightning Complex in California to evaluate whether transport paths from these fires reached Clark County. Together, these trajectory analyses indicate the transport patterns into Clark County on September 2, 2020.

Table 3-2. HYSPLIT run configurations for each analysis type, including meteorology data set, time period of run, starting location(s), trajectory time length, starting height(s), starting time(s), vertical motion methodology, and top of model height.

HYSPLIT Parameter	Backward Trajectory Analysis – Site-Specific	Back Trajectory Analysis – Matrix	Backward Trajectory Analysis – Frequency	Forward Trajectory Analysis – Matrix	Backward Trajectory Analysis – High Resolution
Meteorology	12-km NAM	12-km NAM	12-km NAM	12-km NAM	3-km HRRR
Time Period	August 30 – September 2, 2020	September 2, 2020	August 30 – September 2, 2020	August 30 – September 2, 2020	September 1, 2020
Starting Location	36.1381 N, 115.2582 W	Evenly spaced grid covering Las Vegas, Nevada	36.1381 N, 115.2582 W	Evenly spaced grids covering Slink Fire, White River and Lionshead Fires (OR), and SQF Lightning Complex (CA)	36.1381 N, 115.2582 W
Trajectory Time Length	72 hours	72 hours	48 hours, 72 hours	48 hours, 72 hours	72 hours
Starting Heights (AGL)	50 m, 500 m, 1000 m	50 m	50 m, 1,000 m	500 m, 1,000 m, 2,250 m	50 m, 500 m, 1000 m
Starting Times	22:00 UTC	22:00 UTC	00:00 UTC, 02:00 UTC, 04:00 UTC, 06:00 UTC, 22:00 UTC	00:00 UTC, 02:00 UTC, 04:00 UTC, 06:00 UTC, 22:00 UTC	22:00 UTC
Vertical Motion Method	Model Vertical Velocity	Model Vertical Velocity	Model Vertical Velocity	Model Vertical Velocity	Model Vertical Velocity
Top of Model	10,000 m	10,000 m	10,000 m	10,000 m	10,000 m

Site-specific backward trajectories were calculated from the Las Vegas Valley (36.1489 N, 115.2019 W) on September 2, 2020. We modeled all trajectories for sites within the Las Vegas metropolitan area using the Las Vegas Valley location. The hour of 22:00 UTC (i.e., 14:00 PST) was chosen as the model starting time to align with the hour of maximum observed ozone at the Walter Johnson station. The backward trajectories from the Las Vegas Valley, together with measured ozone (8-hour begin time average), are shown in Figure 3-11. All three trajectories, each at a different height, follow a similar

backward path from the Las Vegas Valley, passing over northern Nevada, southern Idaho, and Washington state. Additionally, enhanced ozone concentrations were observed at the Las Vegas Valley.

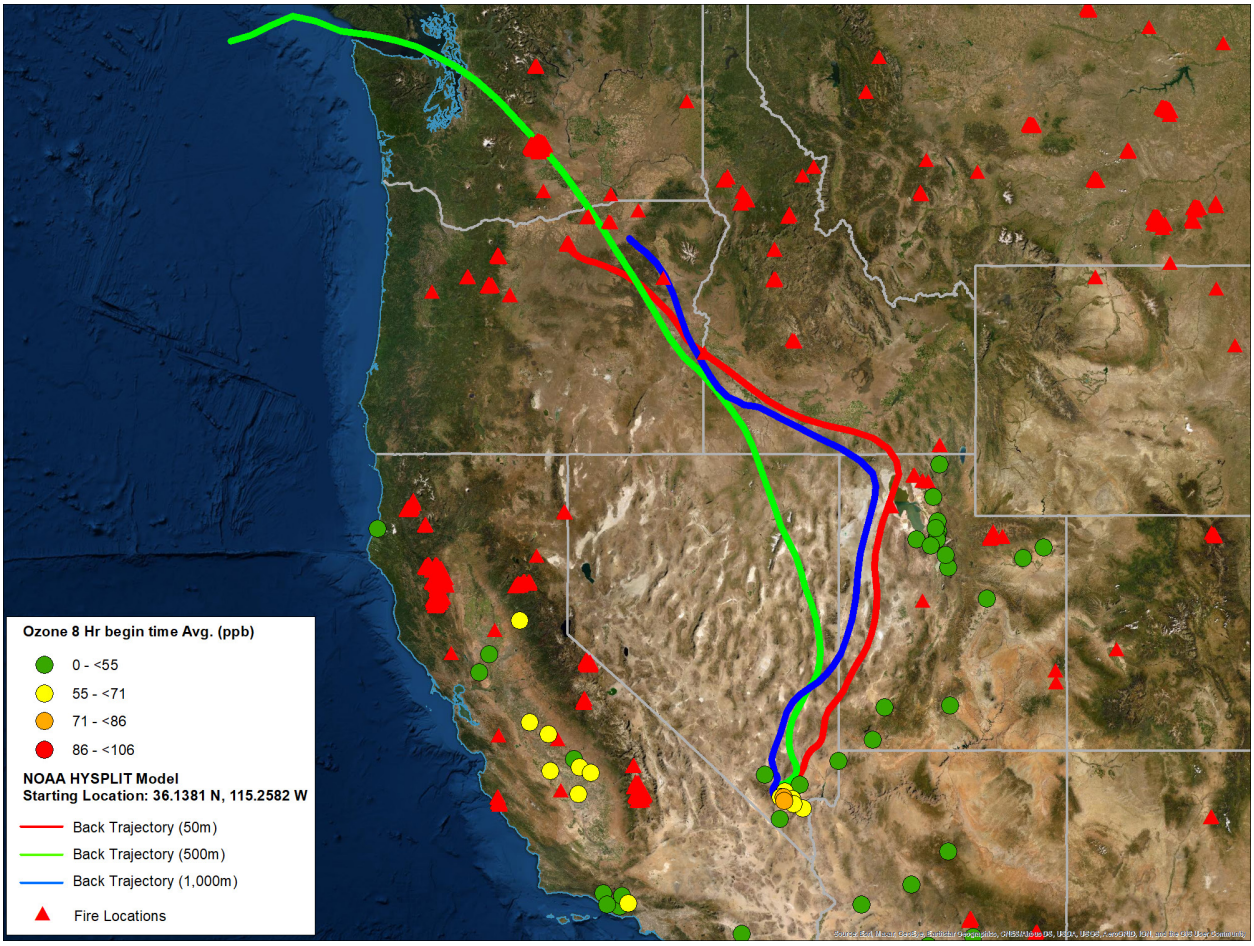

Figure 3-11. 72-hour HYSPLIT back trajectories from downtown Las Vegas, ending on September 2, 2020. NAM 12 km back trajectories are shown for 50 m (red), 500 m (green), and 1,000 m (blue) above ground level. Eight-hour ozone averages are shown as circles (green to red), and HMS fires are shown as red triangles.

To accurately trace the back trajectories from Las Vegas and see which smoke plumes they passed through in the days leading up to September 2, we combined HMS smoke data from August 30 and 31 with the same back trajectory from Figure 3-11 (with dates listed along the trajectory) and MDA8 ozone from September 2 in Figure 3-12. The Oregon fires were active on and before August 30, creating a dense smoke plume over the Pacific Northwest. Long-distance transport of wildfire smoke does have the potential to produce ozone enhancements downwind in >3-day aged plumes (Louisiana Department of Environmental Quality, 2018; Jaffe and Wigder, 2012). The backward trajectories from the Las Vegas Valley passed directly through that plume on August 30 and 31. On

September 1, transport patterns indicate that the smoke plume associated with the California fires was transported eastward and covered the Las Vegas region. Together, plumes from fires in California and in the Pacific Northwest (especially the White River and Lionshead Fires in Oregon) contributed smoke that was transported to Clark County on September 1, the day prior to the September 2 event. The smoke plume that covered much of the Pacific Northwest, northern and central California, and Nevada for the last two days of August came from both the California and the Oregon fires. The air parcels that reached the Las Vegas Valley on September 2 travelled through that plume during those two days. The air parcels then travelled southeastward over Nevada and Utah on September 1. By 2:00 p.m. PST on September 1, the air parcels carrying the plume reached southern Nevada and Clark County. Previous-day trajectory plots (**Figure 3-13**) show the formation of the smoke plume and its transport over the three days before the exceedance event. On August 30 and 31, a smoke plume covered much of northern and central California, Oregon, and Nevada was caused primarily by the large complex fires in California and the White River and Lionshead fires in Oregon. The back trajectories on these days missed this concentrated plume, which is likely why ozone concentrations were below the MDA8 standard in Las Vegas. By the afternoon of September 1, the plume from the California fires had transported further east, covering the Las Vegas region, but did not significantly elevate MDA8 ozone in Clark County on this day (possibly due to smoke reducing the photochemical potential for ozone production). **Figure 3-14** shows the high-resolution (3 km) backward trajectories from the Las Vegas Valley on September 1. The results are consistent in that all three trajectories pass through the Pacific Northwest.

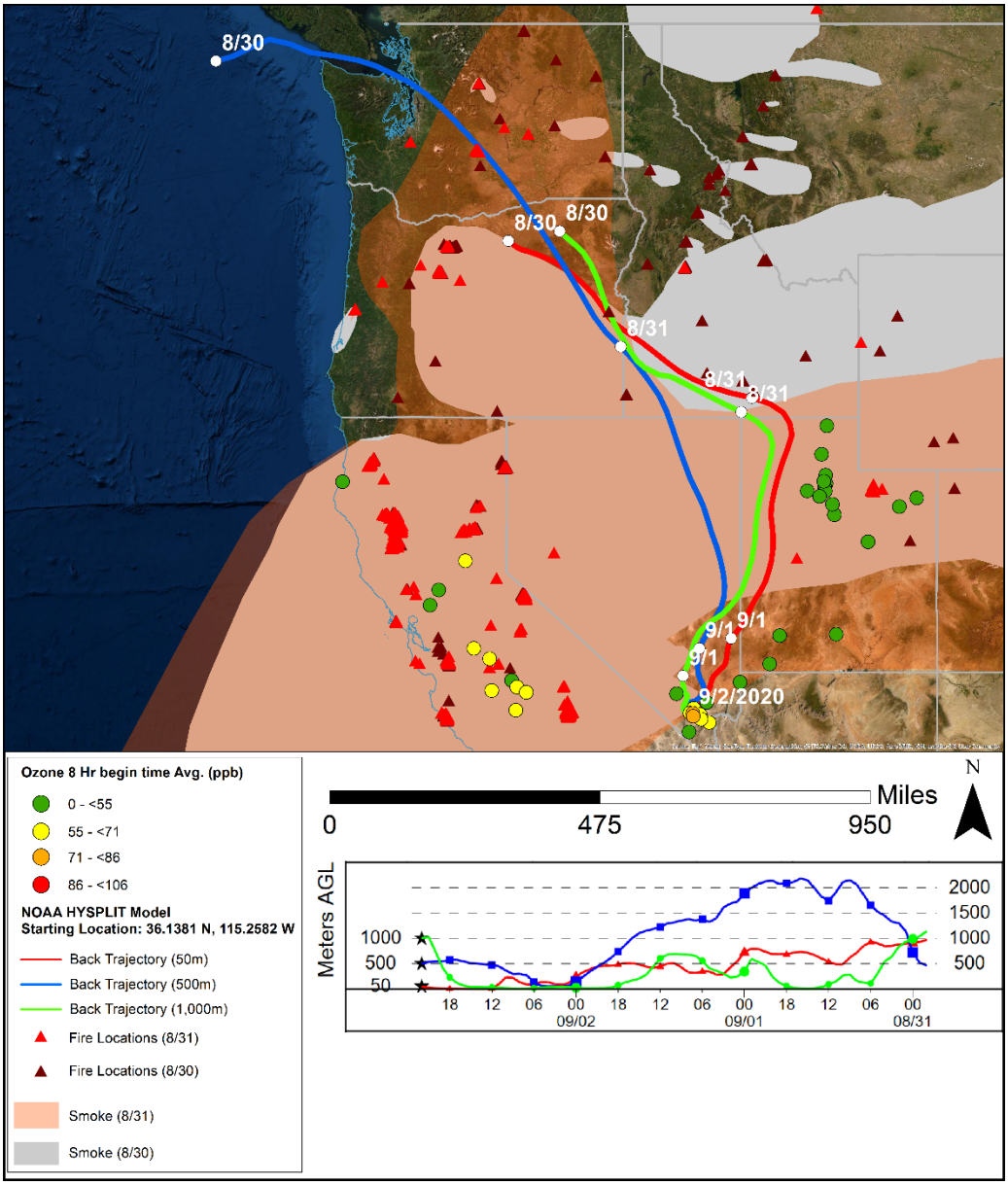

Figure 3-12. 72-hour HYSPLIT back trajectories with smoke from downtown Las Vegas, ending on September 2, 2020. NAM 12 km back trajectories are shown for 50 m (red), 500 m (green), and 1,000 m (blue) above ground level. The dots on each of the three trajectories mark the date (22:00 UTC) when that section of the trajectory ended. The HMS estimated smoke plume on August 30 is indicated by the red area while on August 31 it is indicated by the grey area.

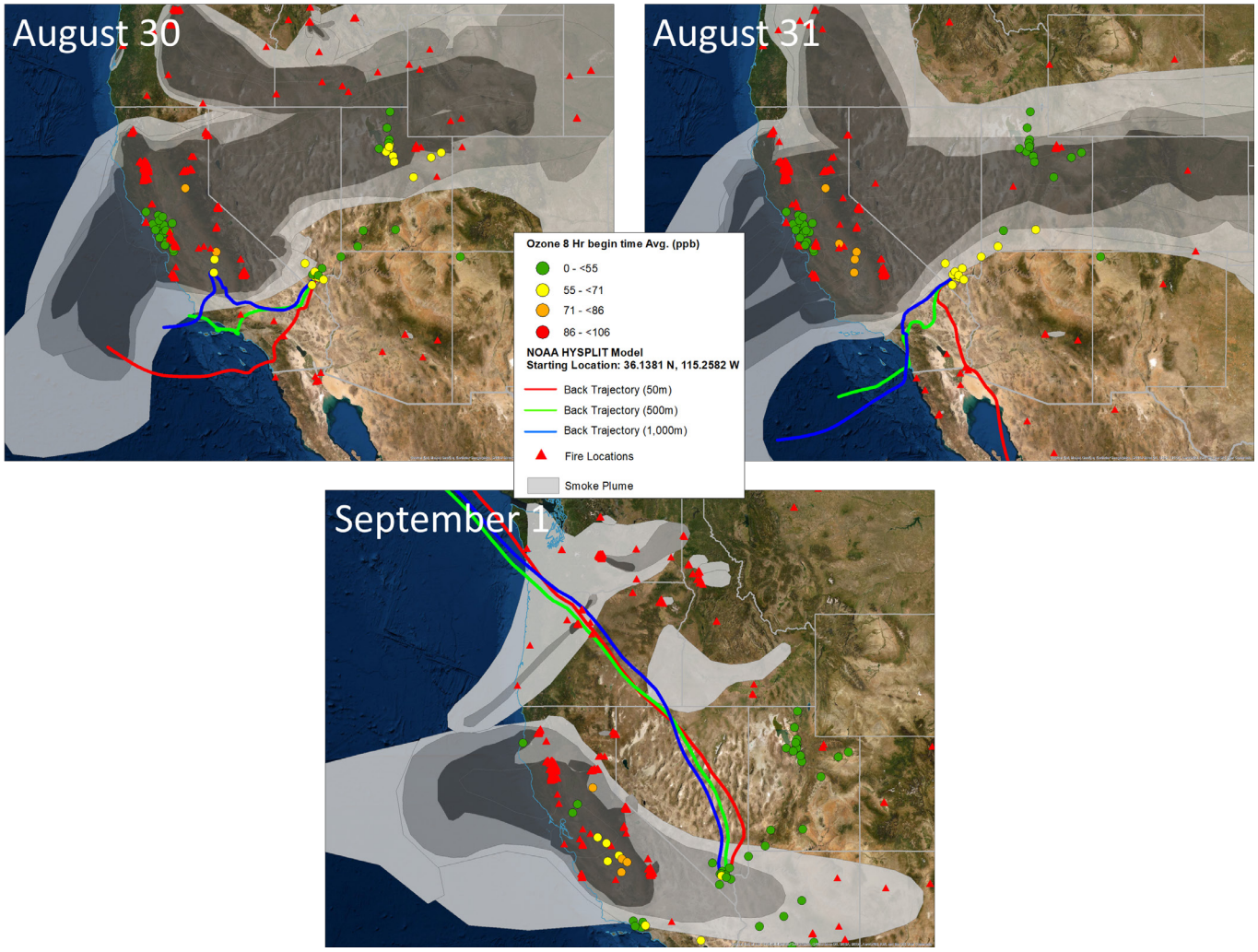

Figure 3-13. HYSPLIT back trajectories with smoke for August 30 to September 1, 2020. 72-hour, NAM 12 km back trajectories for the three days before the EE on September 2, initiated from downtown Las Vegas, are shown for 50 m (red), 500 m (green), and 1,000 m (blue) above ground level.

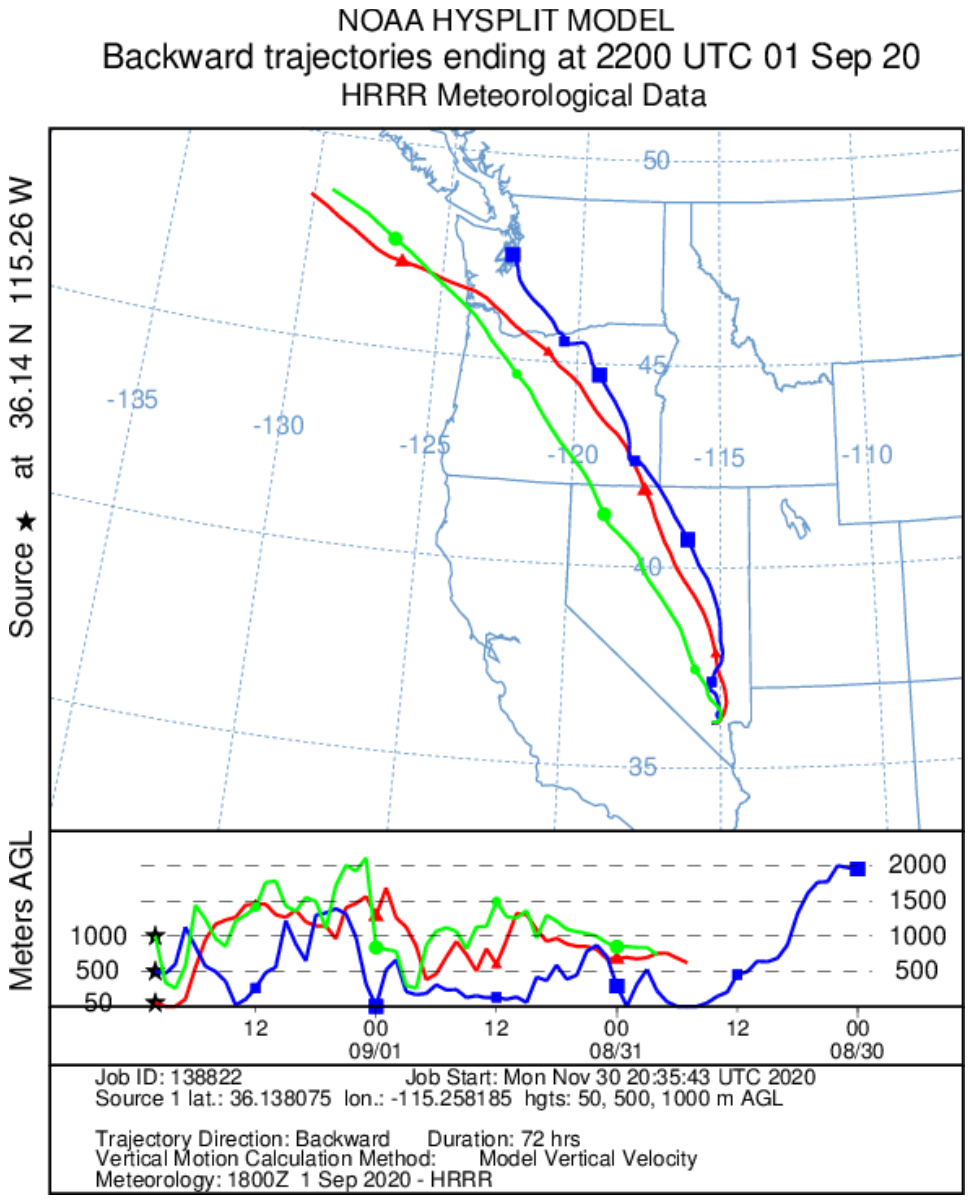

Figure 3-14. High-resolution HYSPLIT back trajectories. 72-hour, HRRR 3 km back trajectories initiated on September 2 from downtown Las Vegas are shown for 50 m (red), 500 m (blue), and 1,000 m (green) above ground level.

To identify variations in meteorological patterns of transported air to Las Vegas, we generated a HYSPLIT trajectory matrix. For this approach, trajectories are run in an evenly spaced grid of source locations. **Figures 3-15** shows 72-hour backward trajectory matrices with source locations encompassing Las Vegas. The backward trajectories were initiated from the afternoon (at 02:00 p.m. PST/10:00 p.m. UTC) of September 2, 2020, at a starting height of 50 m above ground level (AGL). As shown in the plot, the transported air intersecting Las Vegas on September 2, 2020, travelled through the Pacific Northwest. Consistent with the trajectories depicted in Figure 3-11, transported air from the Pacific Northwest traveled southeastward across Nevada and intersected Las Vegas at 50 m AGL,

which included emissions from the White River and Lionshead Fires in Oregon and fires throughout California on August 30 and 31.

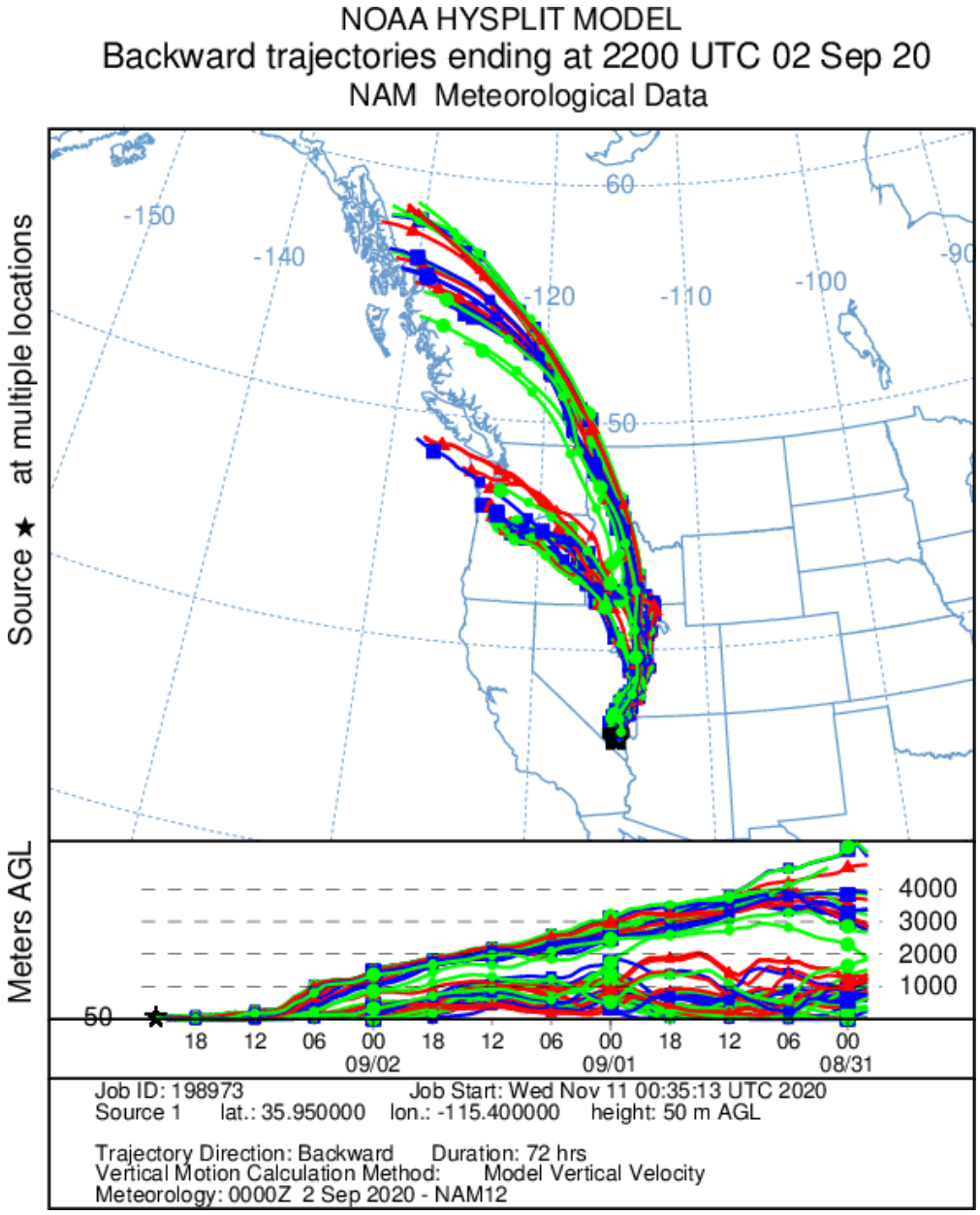

Figure 3-15. HYSPLIT back trajectory matrix. A 72-hour, NAM 12 km back trajectory matrix was initiated on September 2 at 22:00 UTC (2:00 p.m. Local Time) from downtown Las Vegas at 50 m above ground level.

A HYSPLIT frequency trajectory was the third trajectory approach used in this analysis. In this option, a trajectory from a single location and height starts every three hours. Using a continuous 0.25-degree grid, the frequency of trajectories passing through each grid cell is totaled and then normalized by the total number of trajectories. Figure 3-16 shows a 72-hour backward trajectory frequency plot starting from the Las Vegas Valley and 50 m AGL on September 2, 2020. The trajectory frequency plot yields similar results to those from the previous two approaches; transported air impacting the Las Vegas Valley on September 2, 2020, predominately came from the Pacific Northwest and also intersected the California fire plumes along the path. Figure 3-17 shows previous-day backward trajectory frequency plots at a starting height of 50 m AGL. Trajectories initiated on August 31 – September 1 show that air parcels originated from central and southern California and passed over large smoke plumes caused by fires throughout California. On the day before the event, air parcels from the smoke-inundated Pacific Northwest started to reach Las Vegas. Trajectory frequencies at 50 m AGL (Figure 3-18) and 1,000 m (Figure 3-19) initiated in the late afternoon through the evening of September 1 provide consistent evidence that in the hours leading up to the beginning of the exceptional event day, air came in part from central and southern California, where large fires produced extensive smoke plumes.

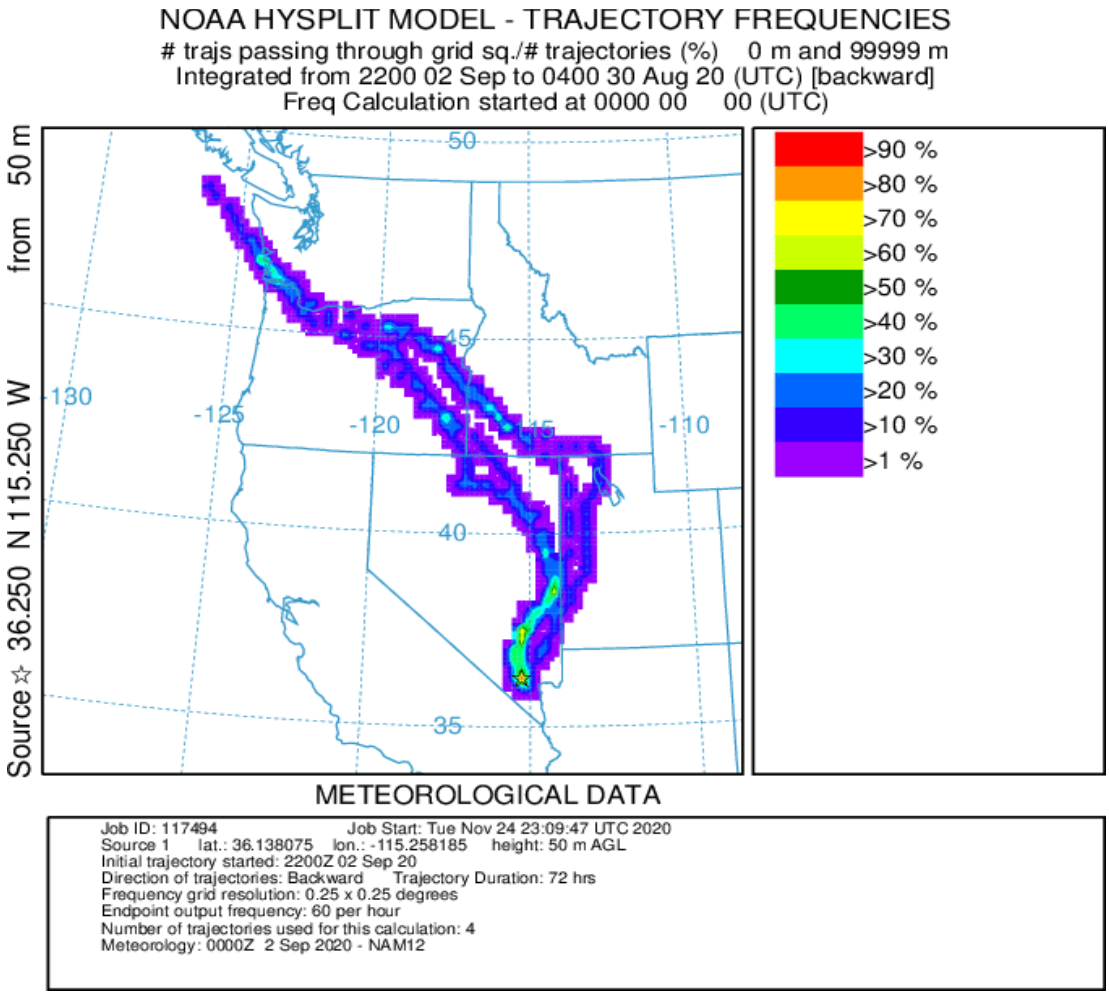

Figure 3-16. HYSPLIT back trajectory frequency. A 72-hour, NAM 12 km frequency of back trajectories was initiated on September 2 at 22:00 UTC (2:00 p.m. Local Time) from downtown Las Vegas at 50 m above ground level. The colors within the frequency plot indicate the percent of trajectories that pass through a grid square.

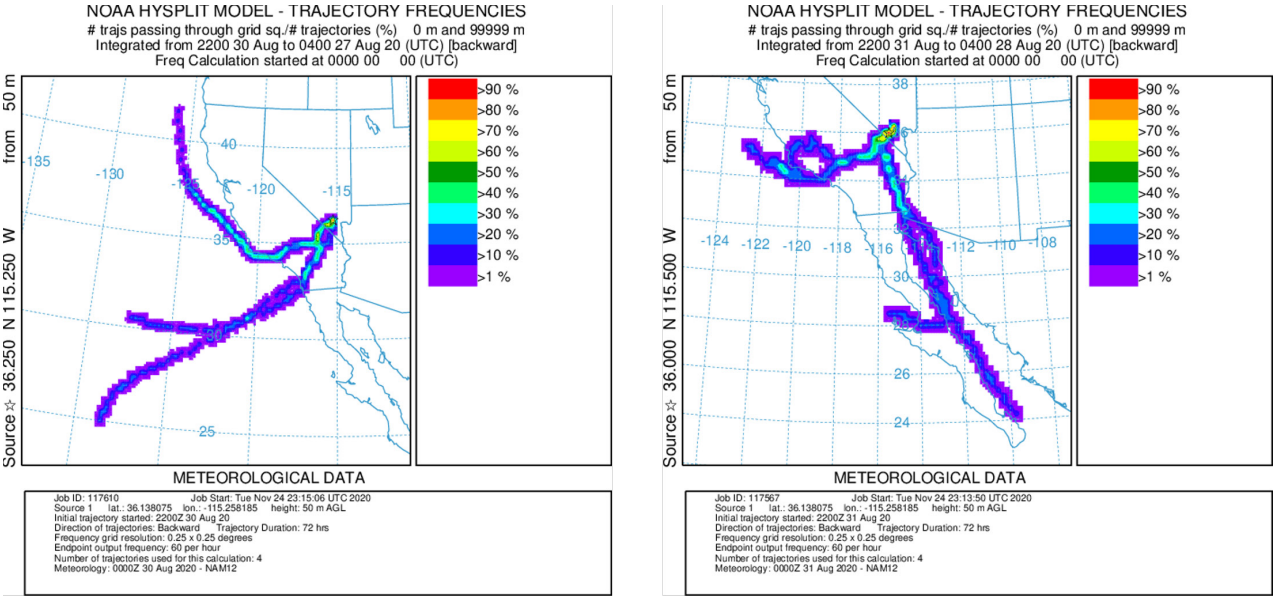

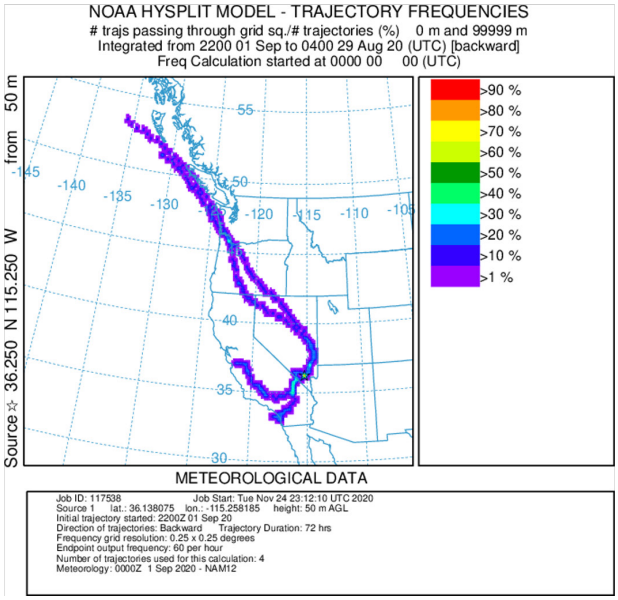

Figure 3-17. HYSPLIT back trajectory frequency – August 30 to September 1, 2020. A 72-hour, NAM 12 km frequency of back trajectories was initiated for the three days before the EE date from downtown Las Vegas at 50 m above ground level. The colors within the frequency plot indicate the percent of trajectories that pass through a grid square.

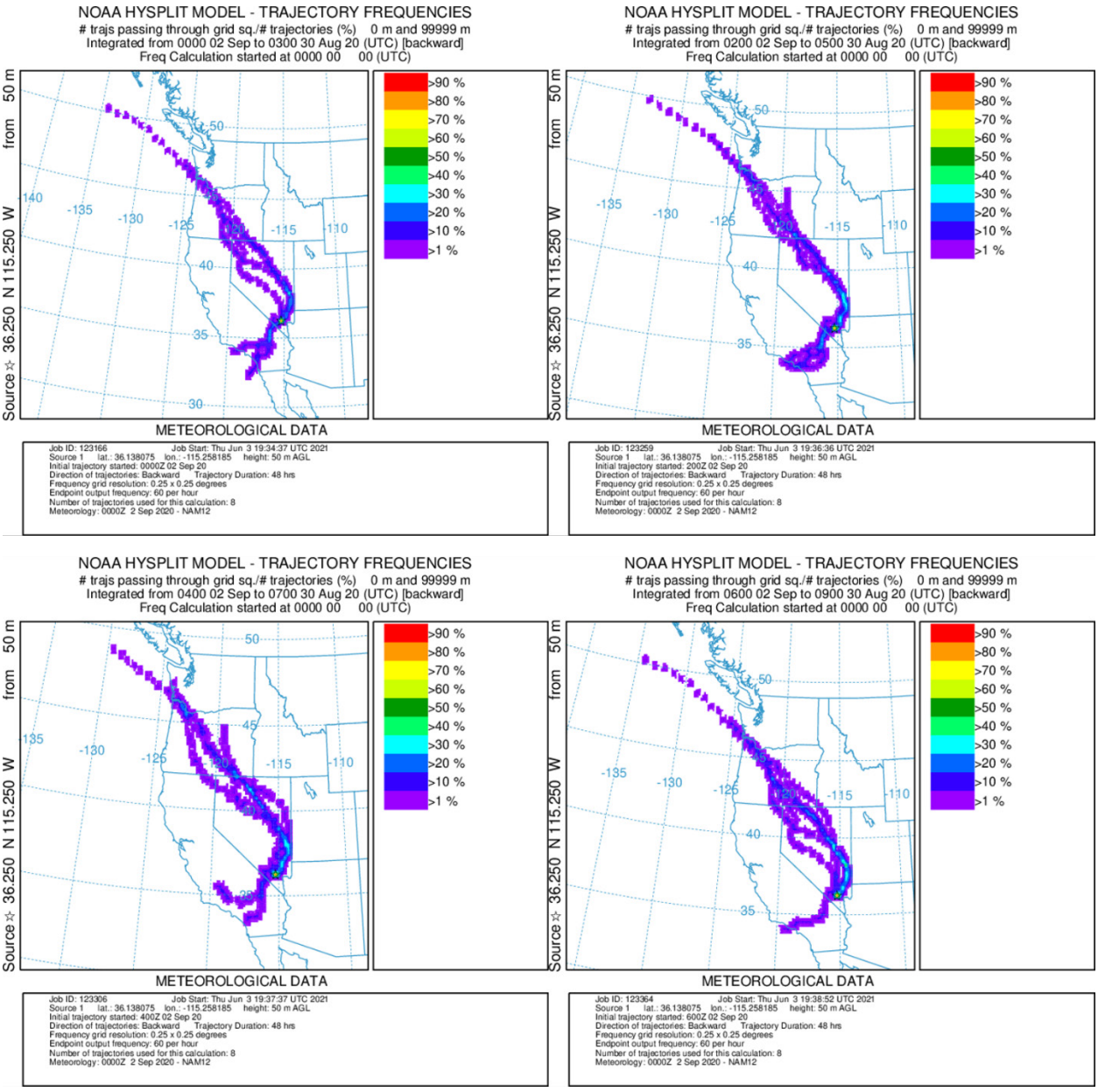

Figure 3-18. HYSPLIT back trajectory frequency initiated from 00:00 UTC to 06:00 UTC on September 2 (i.e., 6:00 p.m. on September 1 to 1:00 a.m. on September 2 PST). A 48-hour, NAM 12 km frequency of back trajectories was initiated for hours leading up to the EE date from downtown Las Vegas at 50 m above ground level. The colors within the frequency plot indicate the percent of trajectories that pass through a grid square.

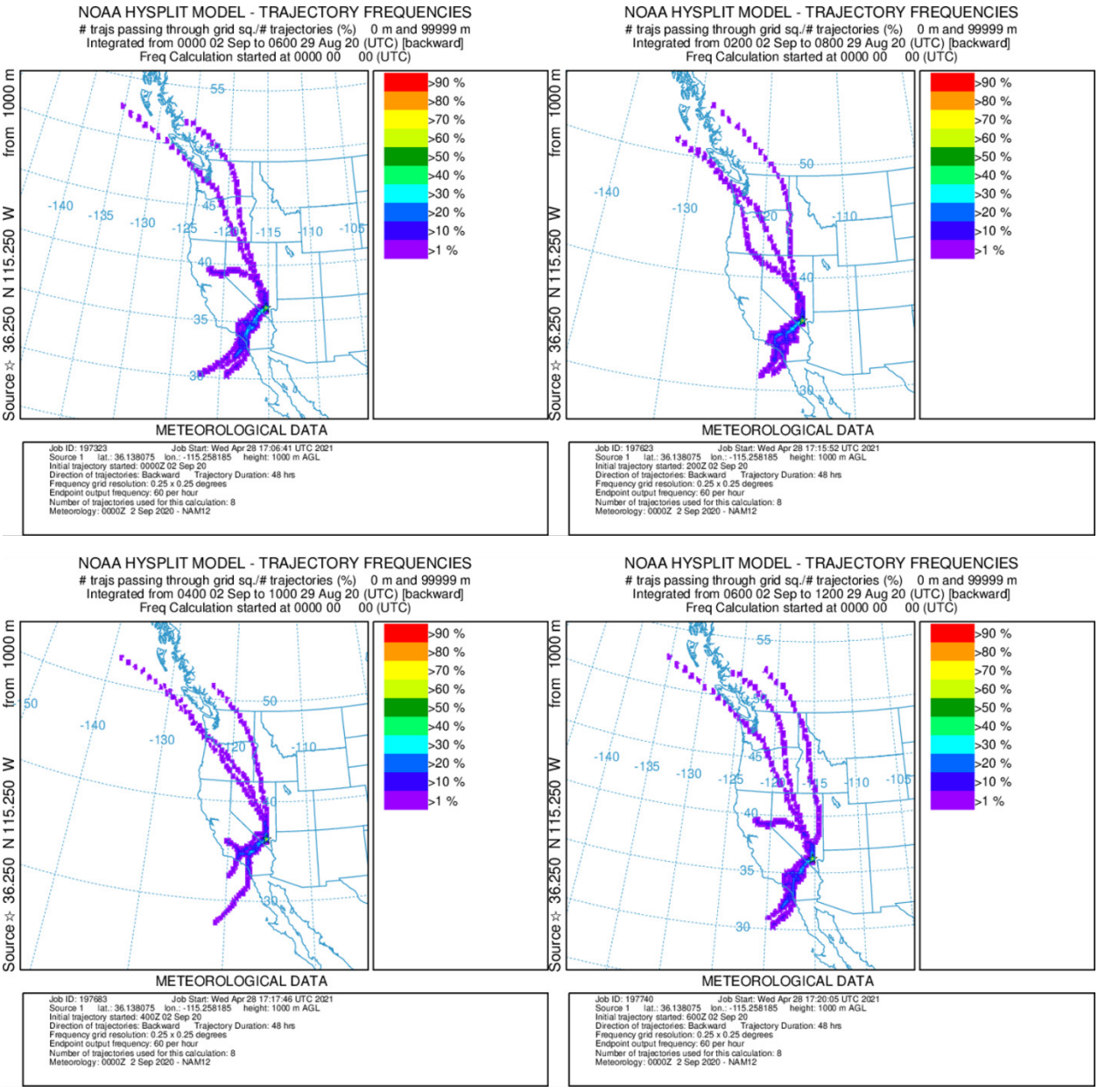

Figure 3-19. HYSPLIT back trajectory frequency initiated from 00:00 UTC to 06:00 UTC on September 2 (i.e., 6:00 p.m. on September 1 to 1:00 a.m. on September 2 PST). A 48-hour, NAM 12 km frequency of back trajectories was initiated for hours leading up to the EE date from downtown Las Vegas at 1000 m above ground level. The colors within the frequency plot indicate the percent of trajectories that pass through a grid square.

Forward trajectories were run from fire locations in Oregon (i.e., the White River and Lionshead Fires), and California (i.e., the Slink Fire), starting at 22:00 UTC on August 30 or 31 (Figure 3-20 through 3-21), which matches their corresponding ignition dates. These trajectories all show that smoke was transported from those fires in the Pacific Northwest and California to Clark County. Based on Figures 3-18 and 3-19, 48-hour forward trajectories were run from the SQF Lightning Complex at 500 m AGL

in the lower Sierra Nevada Mountain range every two hours starting at 00:00 UTC to 06:00 UTC on August 31 (i.e., 6:00 p.m. to 11:00 p.m. PST) (**Figure 3-22**). These trajectories show that some trajectories initiated over the SQF Lightning Complex travelled to Clark County by the hours leading up to the exceptional event day. These forward trajectories, combined with the back trajectories shown above, provide strong evidence for the transport of smoke from the Pacific Northwest and California fires to Clark County, Nevada.

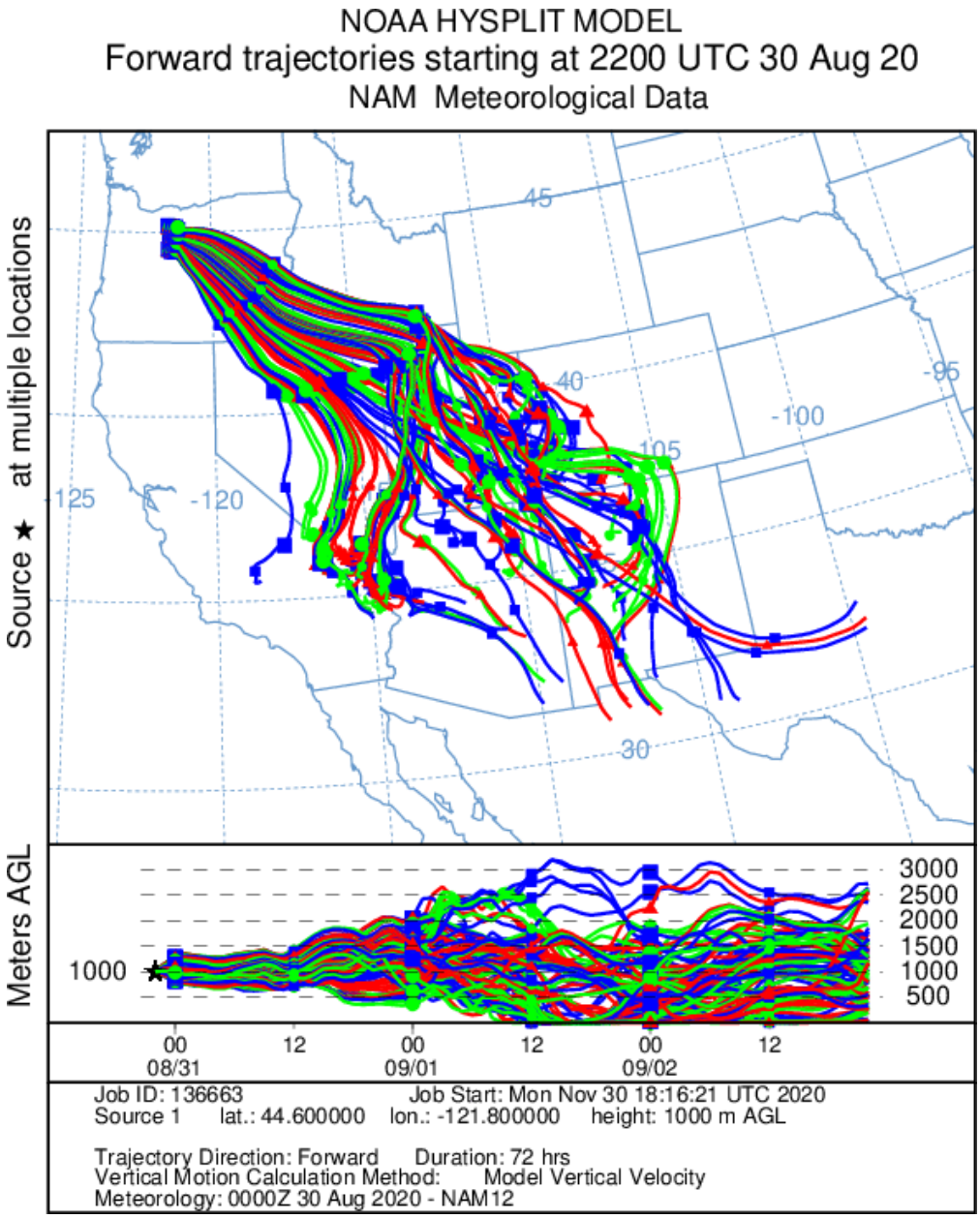

Figure 3-20. HYSPLIT forward trajectory matrix. A 72-hour, NAM 12 km forward trajectory matrix was initiated on August 30 at 22:00 UTC (2:00 p.m. Local Time) from the White River Fire and the Lionshead Fires (OR) at 1000 m above ground level.

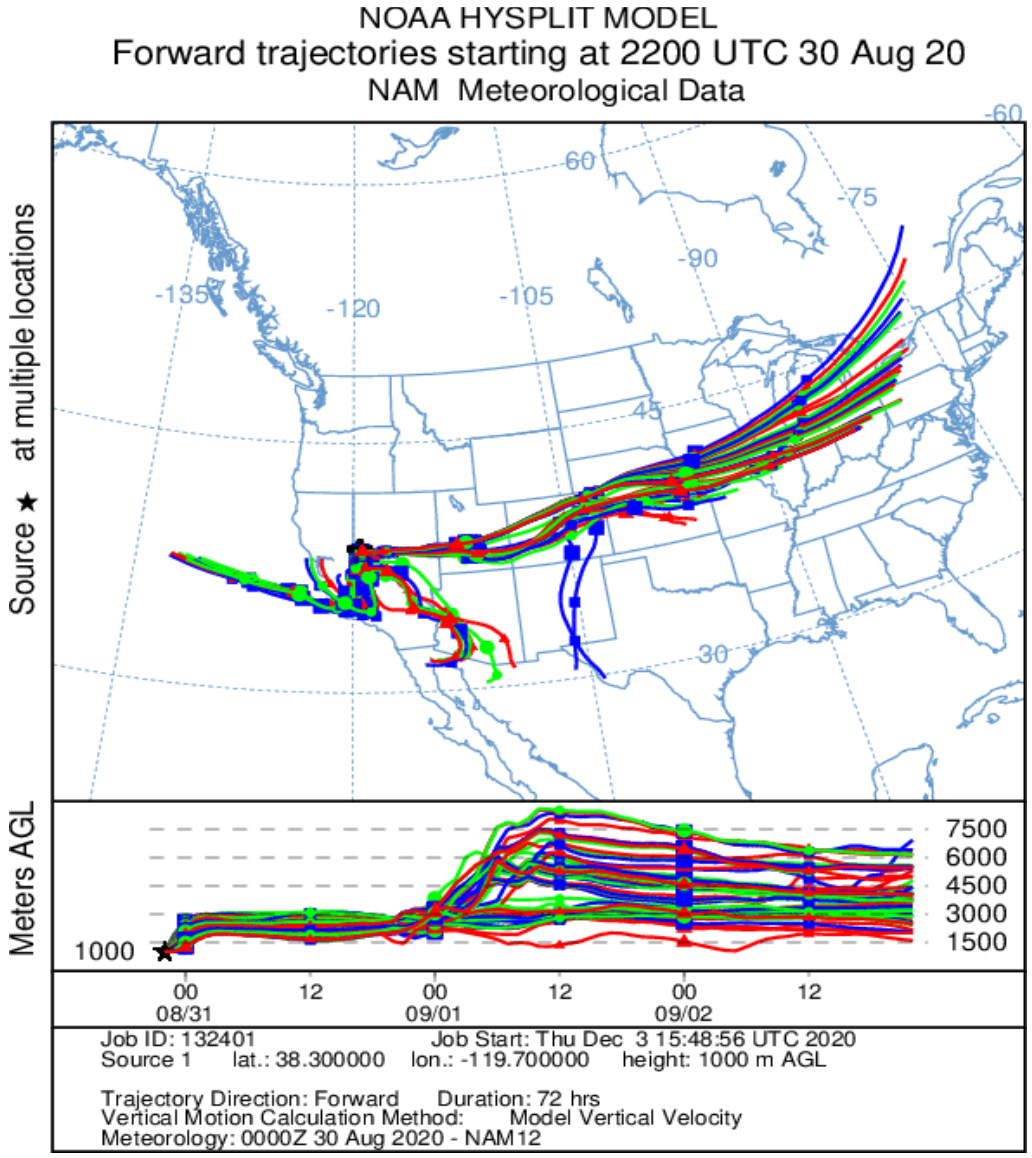

Figure 3-21. HYSPLIT forward trajectory matrix. A 72-hour, NAM 12 km forward trajectory matrix was initiated on August 30 at 22:00 UTC (2:00 p.m. Local Time) from the Slink Fire (CA) at 1000 m above ground level.

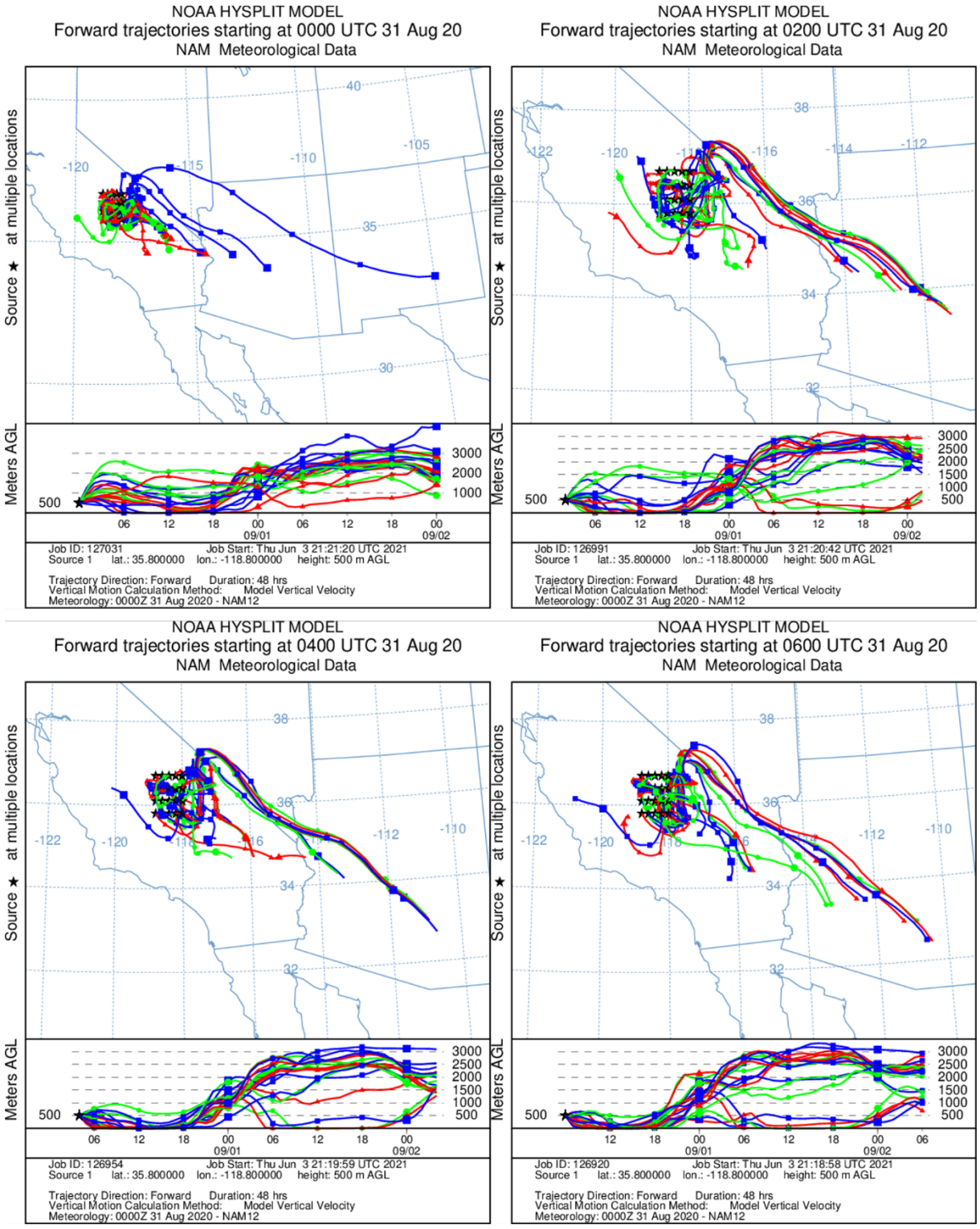

Figure 3-22. HYSPLIT forward trajectory matrix initiated from 00:00 UTC to 06:00 UTC on August 31 (i.e., 6:00 p.m. on August 30 to 1:00 a.m. on August 31 PST). A 48-hour, NAM 12 km from the SQF Lightning Complex (CA) at 500 m above ground level.

3.1.4 Media Coverage and Ground Images

News, weather, and environmental organizations provided widespread coverage of the effects of smoky conditions on air quality in Clark County. Media articles mentioned in this section are included in Appendix A. Regional fires in the southwest were cited as the source of the wildfire smoke. On September 2, the Clark County Department of Environment and Sustainability (DES) posted a warning on Facebook (Figure 3-23) for citizens to expect "continued smoke in the Vegas area as it gets trapped under high pressure buildings over the southwest U.S."[3]

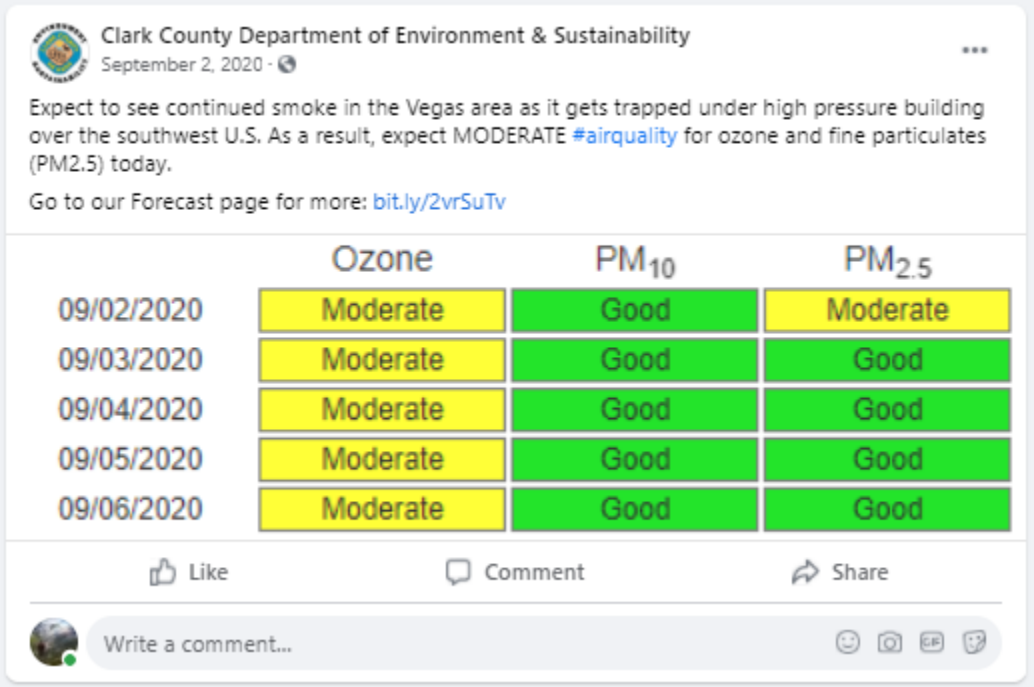

Figure 3-23 A Facebook post added by the Clark County Department of Environment and Sustainability on September 2, 2020, noting continued wildfire smoke impact on ozone levels in the Las Vegas area.

On September 2, Clark County DES released a formal smoke and ozone advisory as air quality continued to deteriorate. KLAS-TV in Las Vegas cited this advisory to further disseminate the information to Clark County residents (https://www.8newsnow.com/news/smoke-ozone-advisory-issued-for-thursday-and-friday-due-to-wildfires/).

The spread of wildfire smoke from California to surrounding states made headlines across the globe. The *Express*, a UK-based news organization, reported the headline "California fires: NASA Satellites reveal Poor Air Quality for Large Swathes of US" on September 2. The article describes the analysis of data from the Multi-angle Imaging SpectroRadiometer (MISR) onboard the Terra satellite and a

[3]https://www.facebook.com/SustainClarkCounty/posts/1973528412777370

subsequent warning from NASA to states surrounding California, including Nevada, to prepare for decreased air quality due to smoke particles transported from active fires in California. (https://www.express.co.uk/news/science/1330408/california-fires-map-nasa-satellite-images-wildfires-2020-space).

Ground images from the Clark County Department of Environment and Sustainability, Division of Air Quality's visibility cameras, located on the roof of the M Hotel in Las Vegas, show the smoky conditions that persisted on September 2 (Figure 3-24). When compared to images taken on a clear day (May 21, 2020) (Figure 3-25), the September 2 images show, particularly in the northwest direction, an opaque gray haze and slightly reduced visibility due to wildfire smoke.

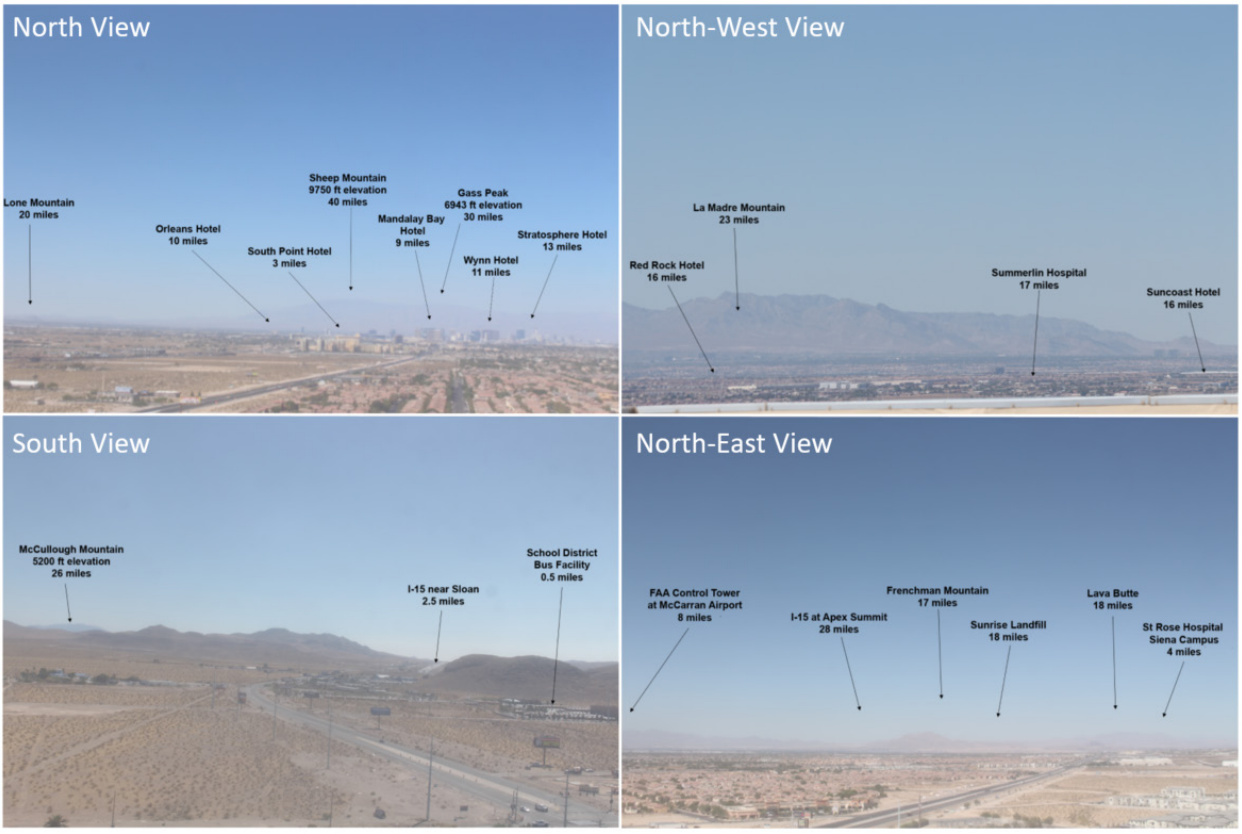

Figure 3-24. Clark County visibility images from September 2, 2020. Images taken from webcams set up in Clark County are shown for the EE on September 2. Each image is labeled with the viewing direction and landmarks.

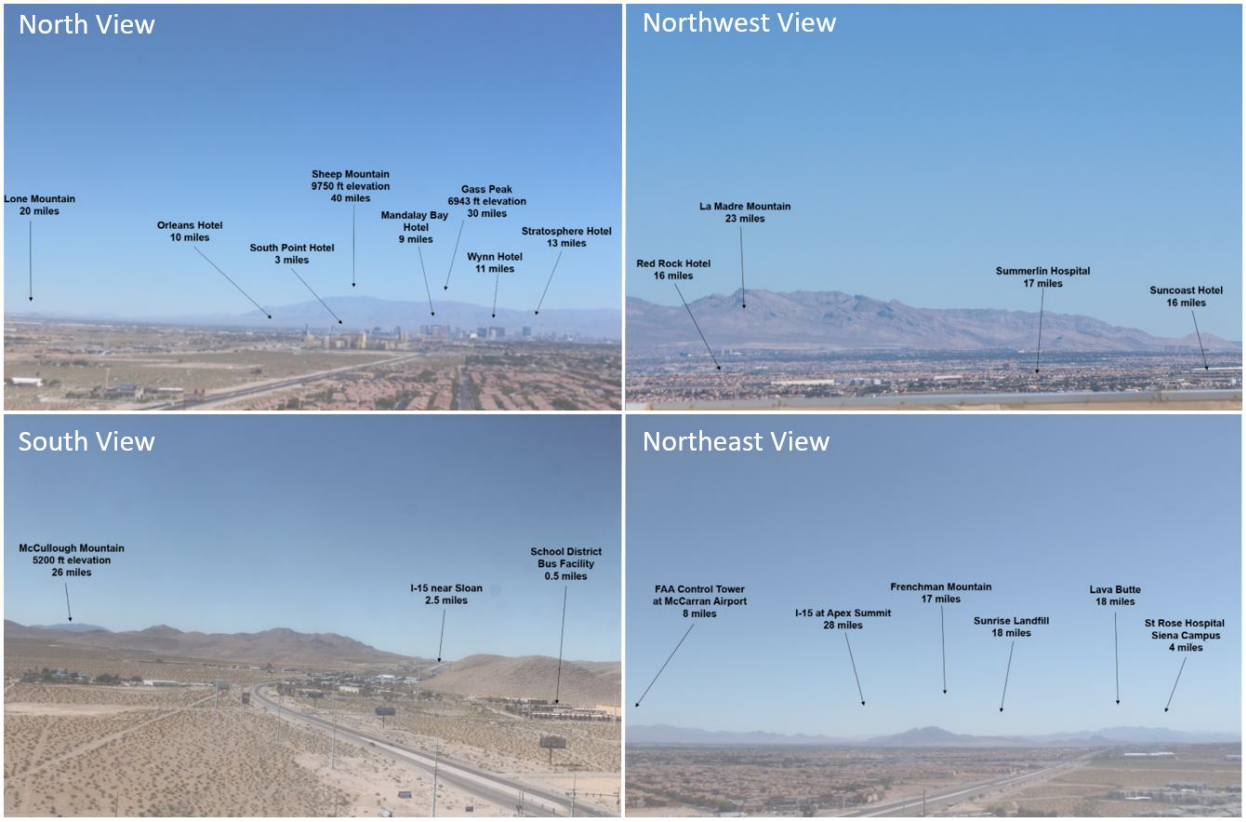

Figure 3-25. Visibility images taken from webcams set up in Clark County are shown for a clear day (May 21, 2020). Each image is labeled with the viewing direction and landmarks.

3.2 Tier 2 Analyses

This exceptional event demonstration meets the clear causal relationship criterion of the Exceptional Events Rule through a Tier 3 weight of evidence showing. EPA guidance says that "As part of the weight of evidence showing for the clear causal relationship rule element [for a tier 3 demonstration], air agencies should explain how the events, monitor and exceedance compare with the key factors outlined in Section 3.5.1 [Evidence that the Event, Monitor(s), and Exceedance Meet the Key Factors for Tier 2 Clear Causal Analyses]. The relationship of the event to the Tier 2 key factors may help inform the amount of additional information that will be needed to support Tier 3 analyses…") (U.S. Environmental Protection Agency, 2016). Tier 2 analyses include two key factors—Q/D analysis and comparison of event ozone concentrations with non-event concentrations—and select additional evidence to show that the fire emissions affected the monitor. This section of the demonstration presents the Tier 2 analysis results, which were used to guide the Tier 3 analyses. The Tier 2 results

are consistent with the Tier 3 analyses, and both sets of analyses contribute to the weight of evidence for the September 2 exceptional event.[4]

3.2.1 Key Factor #1: Q/d Analysis

The exceptional event guidance (U.S. Environmental Protection Agency, 2016) describes a method used to relate the quantity of smoke emissions and distance of the fire to an exceeding monitor. The resulting quantity, called Q/d, may be used to screen fires that meet a conservative threshold of air quality impacts.[5] This section provides the results of the Q/d analyses for fires that were likely to have contributed to the September 2 ozone event in Clark County.

Based on media coverage, transport analysis, and ground/satellite-based analyses in Section 3.1, the White River and Lionshead Fires in Oregon and multiple large complex fires in California likely contributed to smoky conditions and high ozone concentrations in Clark County. **Figure 3-26** shows large fires burning in California and Oregon on September 2, 2020. **Table 3-3** shows agency data available for each fire that could be linked through back trajectories with the September 2 EE event as of June 2021. Many of the fires (August Complex, SCU Lightning Complex, North Complex, SQF Lightning Complex, Lionshead, and White River) were started by lightning storms during dry conditions across the Pacific coast states. These fires grew very large very quickly due to lightning strikes in remote, forested areas that were inaccessible to most firefighting methods (**https://inciweb.nwcg.gov/incident/6983/**; **https://inciweb.nwcg.gov/incident/7056/**; **https://inciweb.nwcg.gov/incident/6997/**; **https://inciweb.nwcg.gov/incident/7048/**; **https://inciweb.nwcg.gov/incident/7049/**; **https://inciweb.nwcg.gov/incident/7013/**). Other major fires that may have contributed to smoke in Clark County on September 2 include the Red Salmon Complex (started on July 27, 2020; **https://inciweb.nwcg.gov/incident/6891/**), the Slink Fire (started on August 29, 2020; **https://inciweb.nwcg.gov/incident/7105/**), and the Dolan Fire (started on August 18, 2020; **https://inciweb.nwcg.gov/incident/7018/**). These fires were caused by lightning or are undetermined as of June 2021. All of the fires mentioned burned for a long period of time. Many have a final containment date in November 2020, while a few still do not have a containment date as of this report (June 2021). We provide the acreage burned as of September 2, 2020, in Table 3-3 based on agency information or fire pixel detections from MODIS if agency data is unavailable (these values are denoted with "*"). The total size of the fires burning on September 2 amounted to more than 800,000 acres.

---

[4] As noted in the ozone exceptional event guidance (U.S. Environmental Protection Agency, 2016), a Tier 3 demonstration must be presented when "the relationship between the wildfire-related emissions and the monitored exceedance or violation cannot clearly be shown using Tier 1 or Tier 2 analyses." Therefore, while the analyses presented in Section 3.2 provides evidence that is supportive of a clear causal relationship between the fires identified and the monitored exceedance, these analyses alone are not expected to be sufficient to demonstrate such a relationship in the absence of the Tier 3 analyses.

[5] Specifically, fires with a Q/d value meeting the 100 tons/km threshold may qualify for a tier 2 demonstration of a clear causal relationship. However, this threshold is insufficient to identify all cases where ozone impacts from smoke may have occurred. Pages 16-17 of the guidance state "To determine an appropriate and conservative value for the Q/D threshold (below which the EPA recommends Tier 3 analyses for the clear causal relationship), the EPA conducted a review… The reviews and analyses did not conclude that particular O_3 impacts will always occur above a particular value for Q/D. For this reason, a Q/D screening step alone is not sufficient to delineate conditions where sizable O_3 impacts are likely to occur." (U.S. Environmental Protection Agency, 2016).

Figure 3-26. Large fires burning on September 2, 2020, in the vicinity of Clark County are shown in red. The Clark County boundary is shown in black.

Table 3-3. Fire data for the California and Oregon fires associated with the September 2 EE. Information includes start/containment date, cause of the fire, the agency estimates of the area burned by the EE date (September 2, 2020), and the total reported acres burned. NA means a date has not officially been determined, while '*' means agency data was unavailable; in these instances, MODIS fire hotspot estimates were used to calculate the burned area. The SCU Lightning Complex and Dolan Fire do not fall within one of the back-trajectory buffers and are not candidates for Q/d calculation. However, long range transport was likely to bring smoke from these fires to Clark County over times scales greater than 24-hours, potentially impacting air quality.

Fire Name	Start Date	Contained Date	Cause	Area Burned by EE Date (acres)	Total Area Burned (acres)
Red Salmon Complex	7/27/2020	11/17/2020	Lightning	29,675	144,474
August Complex	8/17/2020	11/15/2020	Lightning	287,106	1,032,648
SCU Lightning Complex	8/16/2020	10/1/2020	Lightning	327,280*	396,624
North Complex	8/17/2020	11/30/2020	Lightning	65,919	318,935
Dolan Fire	8/18/2020	12/31/2020	Unknown	31,409	124,924
SQF Lightning Complex	8/19/2020	1/6/2021	Lightning	46,328	174,178
Slink Fire	8/29/2020	NA	Lightning	14,200	26,759
Lionshead Fire	8/16/2020	10/30/2020	Lightning	13,389	204,469
White River	8/17/2020	9/28/2020	Lightning	16,952	17,442

Key factor #1 for a Tier 2 demonstration requires an analysis of wildfire smoke emissions from a qualifying fire and the distance of the fire to the affected monitor or monitors. To identify qualifying fires, the guidance "recommends generating 24-hour back trajectories from the affected O_3 monitoring site(s) beginning at each hour of these two or three dates" (U.S. Environmental Protection Agency, 2016). Three dates would be used only if the 8-hour averaging period for the daily maximum 8-hour ozone data include hours falling on two dates (i.e., the 8-hour average includes at least 11 p.m. and midnight on two distinct calendar days). For this demonstration, 24-hour HYSPLIT back trajectories were generated from the monitor location starting on each hour of the day of the exceedance, as well as the day prior to the exceedance (September 1 and 2). The guidance states that "…fires that are close to any of these back trajectories" may be used to calculate Q/d (U.S. Environmental Protection Agency, 2016). To identify fires that fall near the HYSPLIT trajectories, trajectories were buffered by a distance of 25% of the distance traveled by the trajectory, which is consistent with uncertainty reported for HYSPLIT trajectory modeling (Draxler, 1991). **Figure 3-27** shows the back trajectories and buffer of uncertainty from Clark County, Nevada. All fires falling within the uncertainty buffer of one or more trajectories were considered candidates for calculating Q/d. Candidate fires included the August Complex, Lionshead Fire, North Complex, Red Salmon Complex, Slink Fire, SQF Complex, and White River Fire.

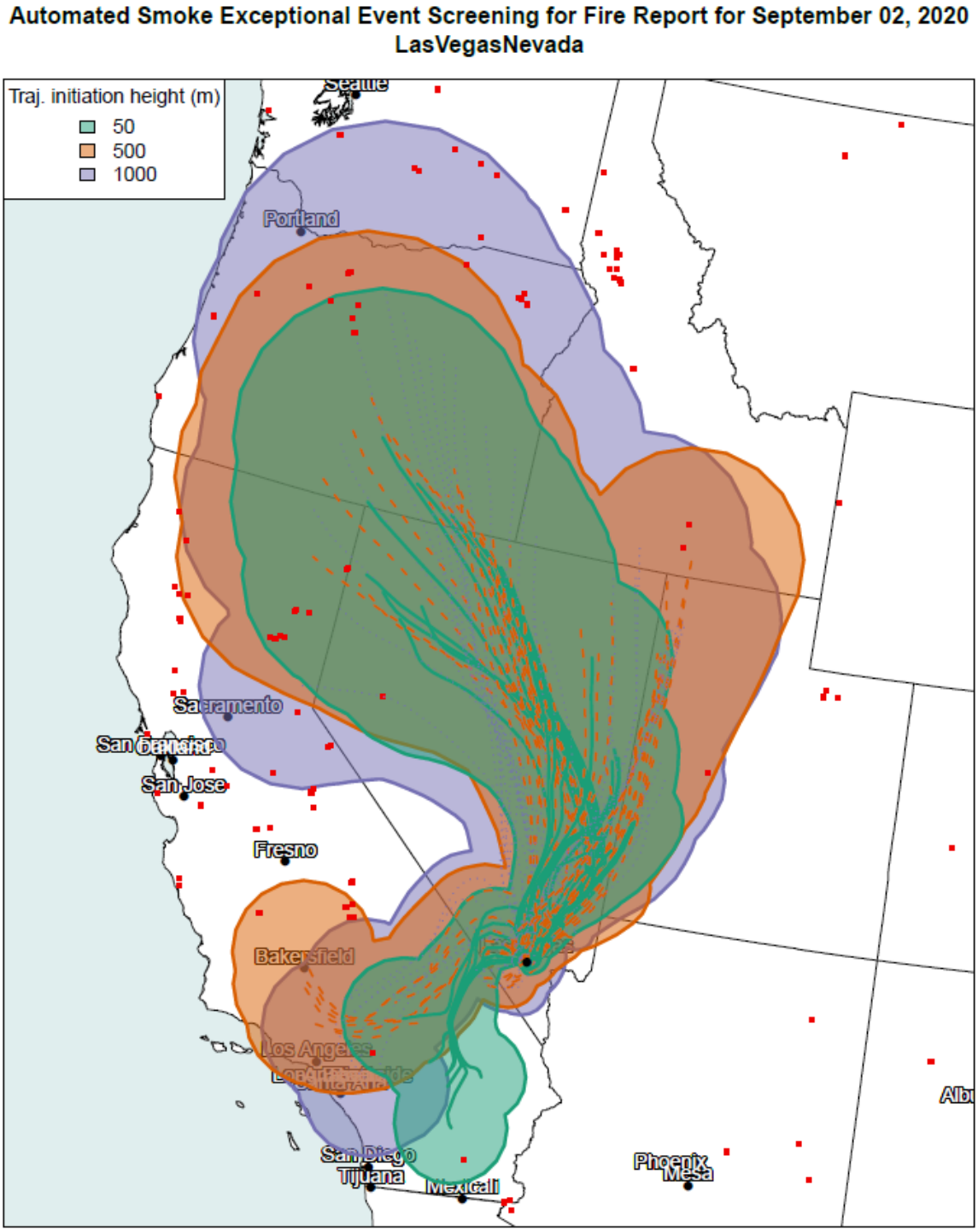

Figure 3-27. Q/d analysis. 24-hour back trajectories are shown as solid or dotted lines. The starting height of the back trajectory is indicated by the color. Uncertainty buffers, calculated as 25% of the distance traveled by the trajectory, are shown in colored polygons. Active fires on September 2 are shown as red squares. Fires falling within one or more uncertainty buffer(s) were used to calculate individual and aggregate Q/d values.

To calculate Q/d for qualifying fires, the total daily emissions of NO_x and reactive VOCs (rVOCs) in tons is divided by the distance from the fire to impacted monitors. BlueSky Playground Version 3.0.1 (https://tools.airfire.org/playground/v3/) was used to estimate emissions of NO_x and VOCs for each fire on a daily basis for September 1 and 2. Daily fire growth was identified using agency reports directly or news reports citing official sources. Each fire's location—as reported in InciWeb or by CAL FIRE—was used to identify the distance to the impacted monitors and fuelbed type. Emissions calculations were based on very dry conditions.

EPA guidance recommends that an event may qualify for a Tier 2 demonstration if the Q/d value for a fire, or the aggregate Q/d across multiple fires, exceeds a conservative value of 100 tons/km. Daily Q/d results indicate that significant emissions of NO_x and rVOCs occurred from the candidate fires during the day of the exceedance (Table 3-4) and the day prior (Table 3-5). However, due to the significant distance between the fire and the monitor location, the emissions were not large enough to reach the Q/d threshold of 100 tons/km for a Tier 2 demonstration, and it was determined that Tier 3 analyses were needed to demonstrate a clear causal relationship.

The Q/d analysis, as described in the ozone exceptional event guidance (U.S. Environmental Protection Agency, 2016) and presented here, would not reflect the impact of transport occurring over more than 24 hours. The trajectories and uncertainty buffers in Section 3.1.3 and Figure 3-26 show that transport from the Dolan Fire and SCU Lightning Complex occurred over more than 24 hours. In addition, trajectory uncertainty shown in Figure 3-26 suggests that transport from fires in Oregon (White River and Lionshead Fires) may have occurred within a 24-hour time frame, but Section 3.1.3 trajectories suggest that transport was most likely to have occurred over longer time frames. Because this demonstration includes wildfire smoke that was transported over longer time frames, we conducted an extended analysis to investigate emissions and transport of smoke from fires over more than 24 hours. The results are presented in Appendix B. These analyses provide evidence that the identified fires emitted ozone precursors in the days leading up to the September 2 wildfire smoke event, including August 30 and 31. Further, the trajectories provided here and in Section 3.1.3 show that these precursor emissions were likely to be transported to Clark County on the day of the ozone exceedance.

The results of the Q/d analysis presented in this section, as well as the extended emissions transport assessment included in Appendix B, agree with and further strengthen the conceptual model and Tier 3 weight of evidence of a clear causal relationship between the identified wildfires smoke emissions and the monitored ozone exceedance identified in this demonstration.

Table 3-4. Daily growth, emissions, and Q/d for the fires with potential smoke contribution on September 2, 2020. Growth for all dates were obtained from agency estimates available from the Incident Information System (InciWeb). Aggregate Q/d calculated for all fires shown is 26.7. Column "E (Tons)" represents the sum of NO_x and Reactive VOC emissions.

Fire Name	Area (Acres)	Daily Growth (Acres)	NO_x (Tons)	VOCs (Tons)	Reactive VOCs (Tons)	E (Tons)	Distance (Km)	Q/d (Tons/km)	Fuel Loading	Fire Size Data Source
White River Fire	16,952	596	29.28	1206.5	724	753	1,138	0.7	Grand fir-Douglas fir forest	https://inciweb.nwcg.gov/incident/7013/
Lionshead Fire	8,785	267	10.31	432.69	260	270	1,098	0.2	Douglas-fir-western hemlock-western redcedar/vine maple forest	https://inciweb.nwcg.gov/incident/7050/
Red Salmon Complex	29,675	3,070	99.12	2874.73	1,724.838	1,824	907	2.0	Douglas-fir-madrone-tanoak forest	https://inciweb.nwcg.gov/incident/6891/
August Complex	287,106	25,902	531.13	17046.55	10,227.93	10,759	772	13.9	Jeffrey pine-ponderosa pine-Douglas-fir-California black oak forest	https://inciweb.nwcg.gov/incident/6983/
North Complex	65,919	1,446	52.35	1966.16	1,179.696	1,232	665	1.9	Douglas-fir-madrone-tanoak forest	https://inciweb.nwcg.gov/incident/6997/
Slink Fire	14,200	0	0	0	0	0	470	0	Ponderosa pine-Jeffrey pine forest	https://inciweb.nwcg.gov/incident/7105/
SQF Complex	46,328	3,754	167.3	6111.4	3,666.8	3834.2	296	13.0	Red fir forest	https://inciweb.nwcg.gov/incident/7048/

Table 3-5. Daily growth, emissions, and Q/d for the fires with potential smoke contribution on September 1, 2020. Growth for all dates shown were obtained from agency estimates available from the Incident Information System (InciWeb). Aggregate Q/d calculated for all fires shown is 31.4. Column "E (Tons)" represents the sum of NO_x and Reactive VOC emissions.

Fire Name	Area (Acres)	Daily Growth (Acres)	NOx (Tons)	VOCs (Tons)	Reactive VOCs (Tons)	E (Tons)	Distance (Km)	Q/d (Tons/km)	Fuel Loading	Fire Size Data Source
White River Fire	16,356	945	46.42	1912.98	1,148	1,194	1,138	1.0	Grand fir-Douglas fir forest	https://inciweb.nwcg.gov/incident/7013/
Lionshead Fire	8,518	553	21.36	896.17	538	559	1,098	0.5	Douglas-fir-western hemlock-western redcedar/vine maple forest	https://inciweb.nwcg.gov/incident/7050/
Red Salmon Complex	26605	727	23.47	680.76	408.456	432	907	0.5	Douglas-fir-madrone-tanoak forest	https://inciweb.nwcg.gov/incident/6891/
August Complex	261204	18263	374.49	12019.19	7211.514	7,586	772	9.8	Jeffrey pine-ponderosa pine-Douglas-fir-California black oak forest	https://inciweb.nwcg.gov/incident/6983/
North Complex	64473	2198	79.58	2988.68	1793.208	1,873	665	2.8	Douglas-fir-madrone-tanoak forest	https://inciweb.nwcg.gov/incident/6997/
Slink Fire	14200	5900	139.65	5044.38	3026.628	3,166	470	6.7	Ponderosa pine-Jeffrey pine forest	https://inciweb.nwcg.gov/incident/7105/
SQF Complex	42,574	4,846	215.99	7,889.15	4,733.49	4,949	296	16.7	Red fir forest	https://www.kerntoday.com/september-1st-update-sqf-complex-at-37728-acres/

3.2.2 Key Factor #2: Comparison of Event Concentrations with Non-Event Concentrations

Another key factor in determining whether the September 2, 2020, exceedance event is exceptional is to compare event ozone concentrations with non-event concentrations via percentile and rank-order analysis. Table 3-6 shows September 2, 2020, concentrations as a percentile in comparison with the last six years of data (with and without the other proposed 2018 and 2020 EE days included) at each site in Clark County. For the two monitoring sites (i.e., Paul Meyer and Walter Johnson) that show a NAAQS standard exceedance on September 2, all of the exceedances are greater than or equal to the 99th percentile when compared to the last six years of data, even with all other proposed 2018 and 2020 EE days included. Without the other EE days included, the percentiles are slightly higher (also >99th percentile). To confirm that the calculated percentiles are not biased by non-ozone season data, Table 3-7 shows the September 2 percentile ranks for all monitoring sites around Clark County in comparison with the last six years of ozone season (May to September) data. The Walter Johnson and Paul Meyer monitoring sites show six-year ozone season percentile ranks above the 98th percentile (with all proposed 2018 and 2020 EE days included) for September 2. When the other possible EE days are excluded, the percentile rank for September 2 increases to >99th percentile for both sites. Although the sites do not show a >99th percentile rank for September 2 compared with the last six ozone seasons, this analysis confirms that the September 2 EE included unusually high concentrations of ozone when compared with the last six years of data and the last six ozone seasons.

Table 3-6. Six-year percentile ozone. The September 2 EE ozone concentration at each site is calculated as a percentile of the last six years with and without other 2018 and 2020 EEs included in the historical record.

AQS Site Code	Site Name	6-Year Percentile	6-Year Percentile w/o EE Dates
320030071	Walter Johnson	99.3	*99.7*
320030043	Paul Meyer	99.1	*99.6*

Table 3-7. Six-year, ozone-season percentile ozone. The September 2 EE ozone concentration at each site is calculated as a percentile of the last six years' ozone season (May-September) with and without other 2018 and 2020 EEs included in the historical record.

AQS Site Code	Site Name	6-Year Percentile	6-Year Percentile w/o EE Dates
320030071	Walter Johnson	98.4	*99.2*
320030043	Paul Meyer	97.9	*99.1*

We also compared the rank-ordered concentrations at each site for 2020. As shown in Figures 2-3 and 2-4, 2020 ozone concentrations were not atypically low, which might bias our rank-ordered analysis for September 2, 2020. Tables 3-8 and 3-9 show the rank-ordered ozone concentrations for 2018 through 2020 and the design values for 2020 and include the proposed 2018 and 2020 EEs. For the Walter Johnson monitoring site, September 2 was the fifth highest ozone concentration of 2020, while the ozone concentration at Paul Meyer was not in the top five. However, without including the other proposed EE event in 2020, all affected sites show September 2 ranked as the second highest ozone event in 2020.

Table 3-8. Site-specific ozone design values for the Paul Meyer monitoring site. The top five highest ozone concentrations for 2018-2020 at Paul Meyer are shown and proposed EE days in 2018 and 2020 are included.

Paul Meyer Rank	2018	2019	2020
Highest	79	74	79
Second Highest	76	72	78
Third Highest	75	70	77
Fourth Highest	75	69	77
Fifth Highest	74	69	76
Design Value		73	

Table 3-9. Site-specific ozone design values for the Walter Johnson monitoring site. The top five highest ozone concentrations for 2018-2020 at Walter Johnson are shown and proposed EE days in 2018 and 2020 are included.

Walter Johnson Rank	2018	2019	2020
Highest	79	77	82
Second Highest	77	69	82
Third Highest	77	69	78
Fourth Highest	76	68	77
Fifth Highest	76	68	75
Design Value		73	

For further comparison with non-event ozone concentrations, Table 3-10 shows five-year (2015-2019) MDA8 ozone statistics for the week before and after September 2. In this two-week window

analysis, each affected monitoring site shows MDA8 ozone concentrations on September 2, 2020, to be well above the average and 95th percentile of the last five years of data.

Table 3-10. Two-week non-event comparison. September 2, 2020, MDA8 ozone concentrations for each affected site are shown in the top row. Five-year (2015-2019) average MDA8 ozone statistics for August 26 through September 10 are shown for each affected site around Clark County to compare with the event ozone concentrations.

	Paul Meyer 320030043	Walter Johnson 320030071
Sep. 2	73	75
Mean	56	55
Median	57	56
Mode	58	53
St. Dev	8	9
Minimum	35	34
95 %ile	66	66
99 %ile	74	75
Maximum	76	77
Range	41	43
Count	96	96

The percentile, rank-ordered analyses, and the two-week window analysis, indicate that all affected monitoring sites on September 2, 2020, showed unusually high ozone concentrations compared with non-event concentrations. This conclusion supports a key factor, suggesting that September 2 was an EE in Clark County, Nevada.

3.2.3 Satellite Retrievals of Pollutant Concentrations

Satellite retrievals of pollutants associated with wildfire smoke, such as AOD, CO, and NO_x, provide evidence of total column wildfire emission and associated smoke plumes. We examined maps of Multi-Angle Implementation of Atmospheric Correction (MAIAC) AOD from the Moderate Resolution Imaging Spectroradiometer (MODIS) instrument onboard the Aqua and Terra satellites, CO retrievals from the Atmospheric Infrared Sounder (AIRS) instrument onboard the Aqua satellite, and NO_2 retrievals from the Ozone Monitoring Instrument (OMI). These maps provide source region and smoke transport information for the fires in the Pacific Northwest, including the White River and Lionshead Fires in Oregon and the fires in California. MODIS AOD measurements indicate the

concentration of light-absorbing aerosols, including those emitted by wildfires, in the total atmospheric column. Between August 30 and September 2, AOD measurements show areas of widespread enhanced aerosols over the US states of California and Oregon, including over the White River and Lionshead Fires in Oregon (Figure 3-28). This widespread plume persists over California and spreads into central Nevada in the days preceding September 2. As mentioned in Section 3.1.3, frequency back trajectories and forward matrix trajectories from fire locations show that air from southern and central California, where large fires created widespread smoke and enhanced AOD measurements, was transported to the Las Vegas Valley by late September 1. Trajectories in Section 3.1.3 show that these plumes were upwind of the Las Vegas Valley in the days and hours leading up to the exceptional event day. However, MODIS AOD retrievals do not indicate increased aerosols in the Clark County area on September 2 based on total column measurements (Figure 3-29).

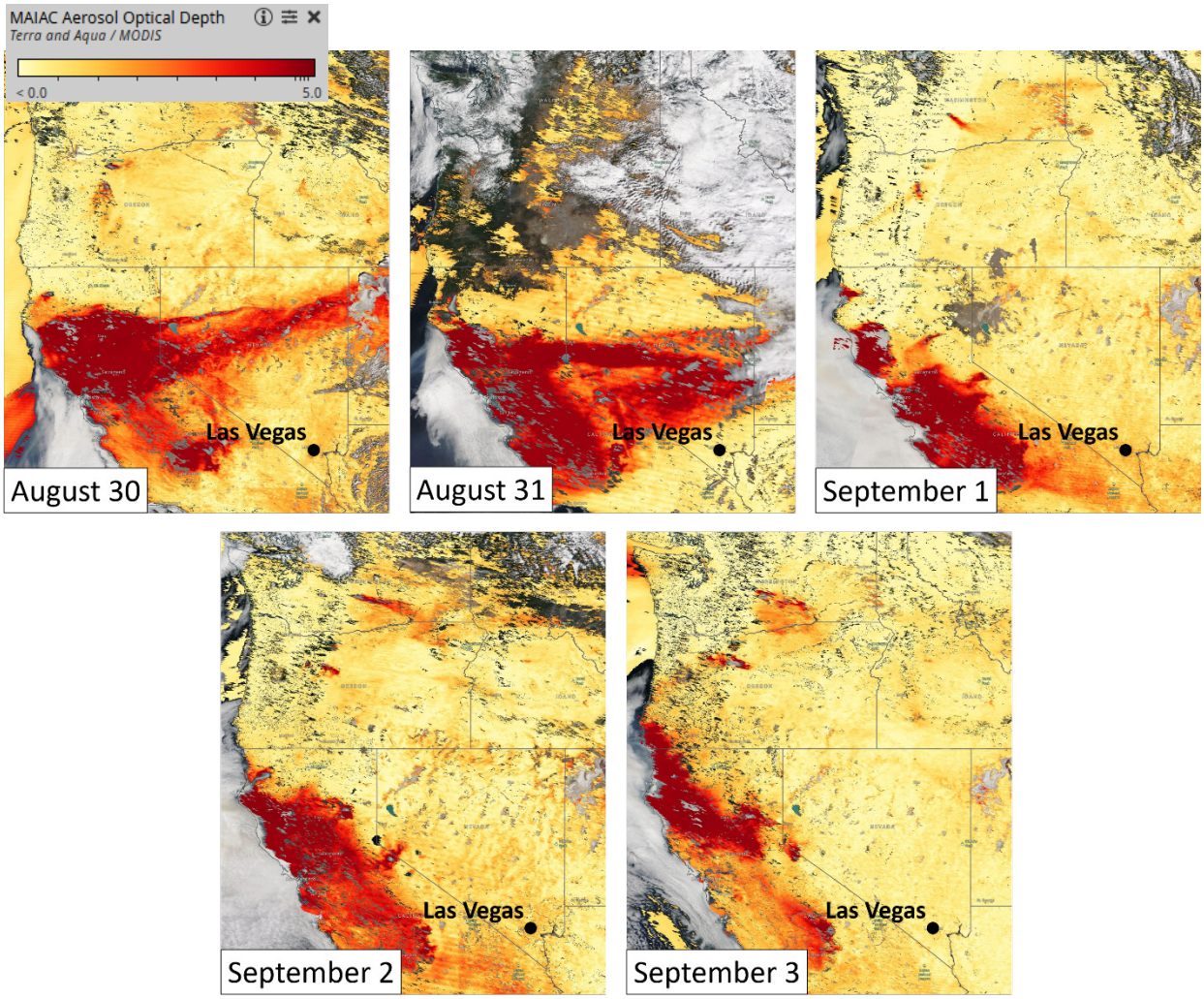

Figure 3-28. MAIAC MODIS Aqua/Terra combined AOD retrievals for the three days before, during the EE on September 2, and the day after the EE are shown.

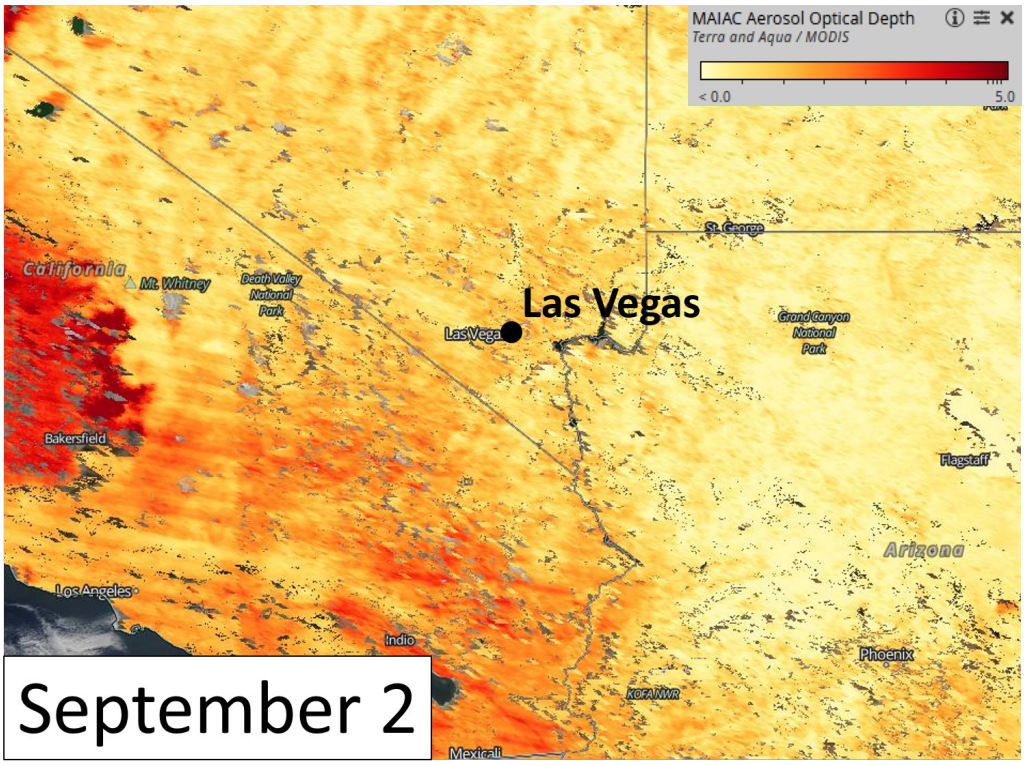

Figure 3-29. A zoomed-in view (over Clark County) of the MAIAC MODIS Aqua/Terra combined AOD retrieval during the EE on September 2, 2020.

CO measurements at 500 hPa from AIRS show a similar pattern of smoke plume seen in the MODIS AOD data noted above. Unfortunately, CO measurements from AIRS were unavailable in the days leading up to September 2. The map of CO concentrations on September 2 shows widespread enhanced CO at 500 hPa throughout California, western Nevada, and over the fires in the Pacific Northwest (Figure 3-30). On September 2, CO concentrations in areas around Clark County were not as enhanced as CO concentrations directly over the fires throughout the western United States, and were only up to approximately 100 ppbv at 500 hPa.

We additionally examined OMI retrievals of tropospheric NO_2 (Figure 3-31). Over areas of dense, visible smoke and near actively burning fires where significant smoke is present in the troposphere, OMI retrievals show an increase in measured NO_2. Elevated levels of NO_2 are especially pronounced over the North Complex and SQF Lightning Complex in California. NO_2 concentrations were not elevated over Clark County. These images show enhanced AOD, CO, and NO_2 concentrations in the wildfire smoke source regions identified through trajectory analysis, but do not show total-column enhanced concentrations in Clark County on the EE date. Therefore, this evidence is inconclusive, specifically in Clark County, but confirms enhanced concentrations in the source regions shown to impact Clark County on September 2.

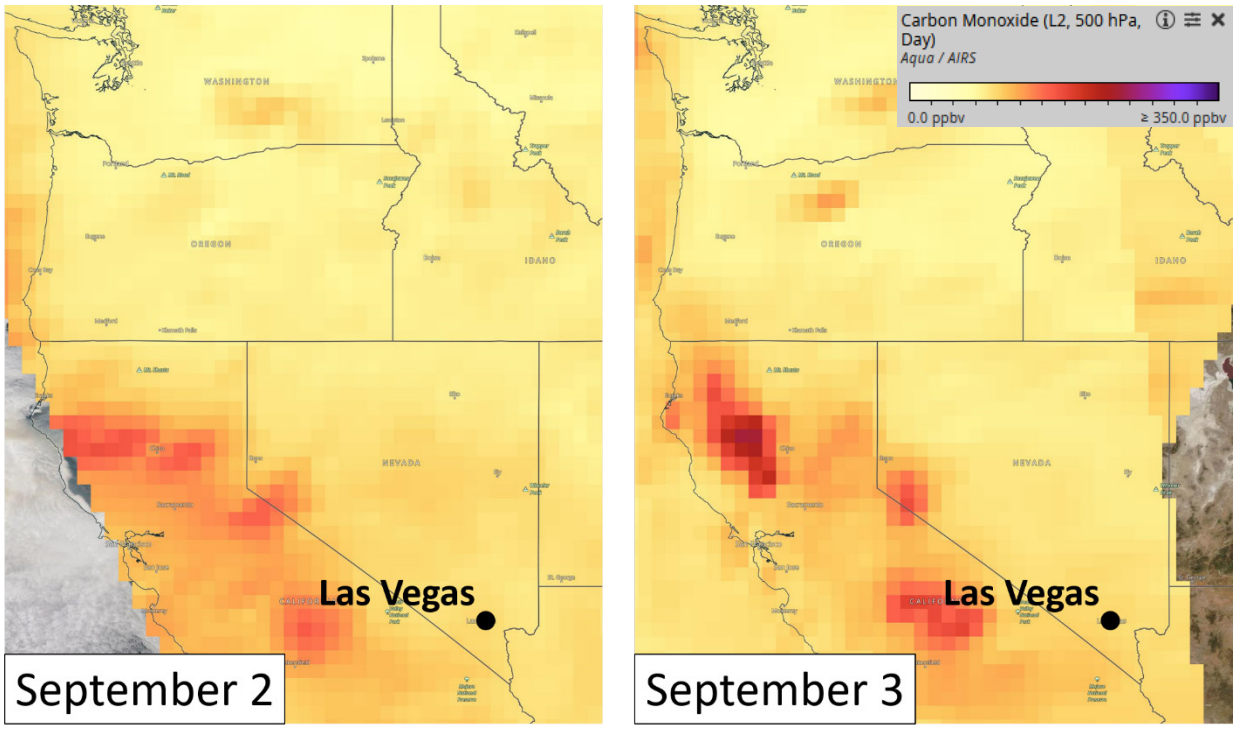

Figure 3-30. A zoomed-in view (over Clark County and the fires in California and Oregon) of the Aqua AIRS CO retrieval during the EE on September 2, 2020.

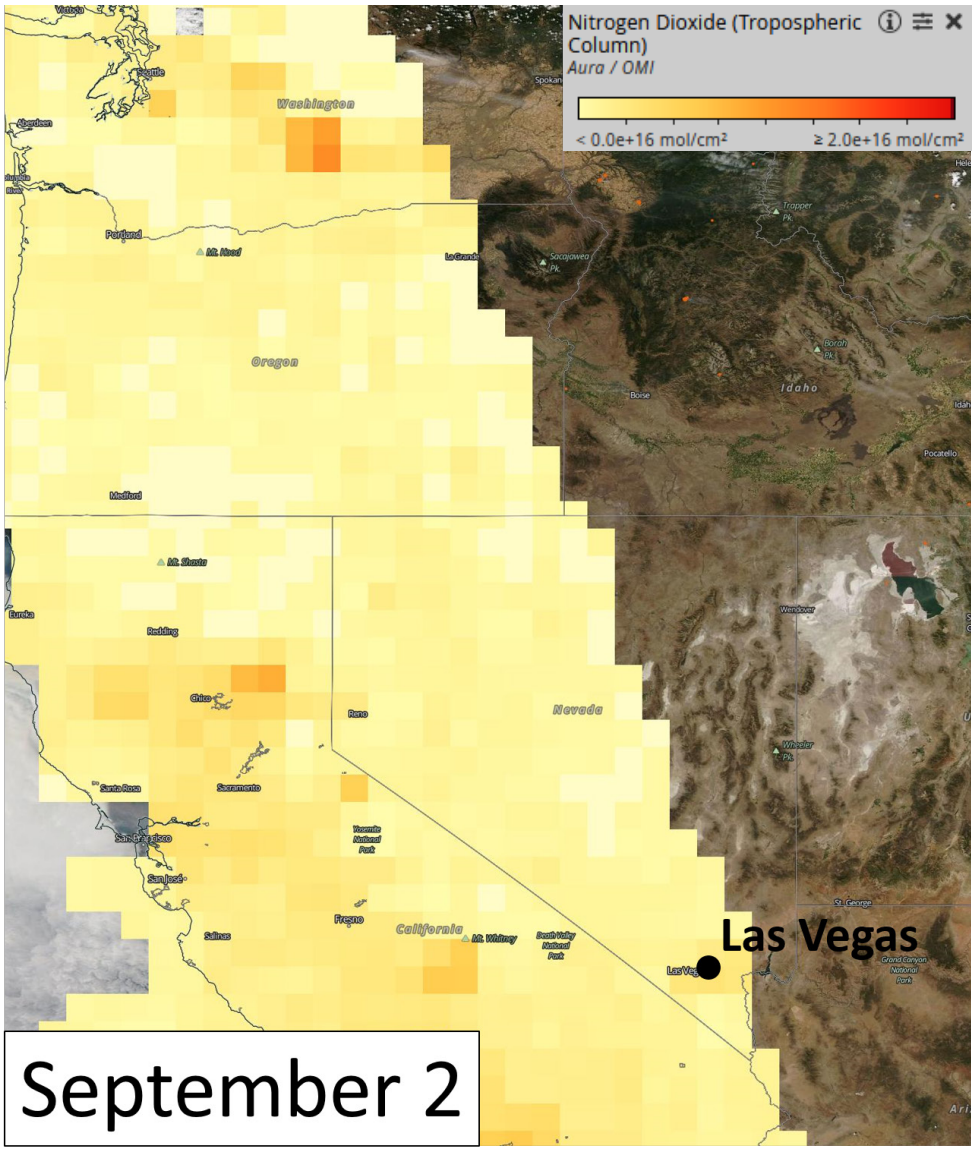

Figure 3-31. OMI Aura NO_2 retrieval for the EE on September 2, 2020.

3.2.4 Supporting Pollutant Trends and Diurnal Patterns

Ground measurements of wildfire plume components (e.g., $PM_{2.5}$, CO, NO_x, and VOCs) further demonstrate that smoke impacted ground-level air quality if enhanced concentrations or unusual diurnal patterns were observed. We examined concentrations of $PM_{2.5}$, CO, NO, NO_2, and TNMOC measured at all exceedance sites as well as other nearby sites in Clark County. If $PM_{2.5}$, CO, NO_x, and VOCs were enhanced at the time the smoke plume arrived in Clark County, these measurements would provide additional supporting evidence of smoke and/or wildfire emissions impacts in Clark County.

Figure 3-32 shows an overall view of pollutants measured around Clark County in the week before and after the September 2 event. The peak daily concentration of $PM_{2.5}$ at exceedance-affected monitoring sites shows an increase the day before the event, suggesting the influence of an additional source of $PM_{2.5}$ right before the EE event. Increases in NO, NO_2, and TNMOC concentrations compared to the week previous begin on September 2, and all these pollutants remain elevated for several days afterwards. The increased concentrations of NO, NO_2, and TNMOC provide support for the presence of smoke at the surface. The rest of this sections examines supporting pollutants on a site-by-site basis to identify deviations from expected diurnal patterns in concentrations that indicate the presence of wildfire smoke in Clark County on September 2. Less than one year of TNMOC data is available at any Clark County monitoring site, so this pollutant is excluded from the site-specific examinations shown below.

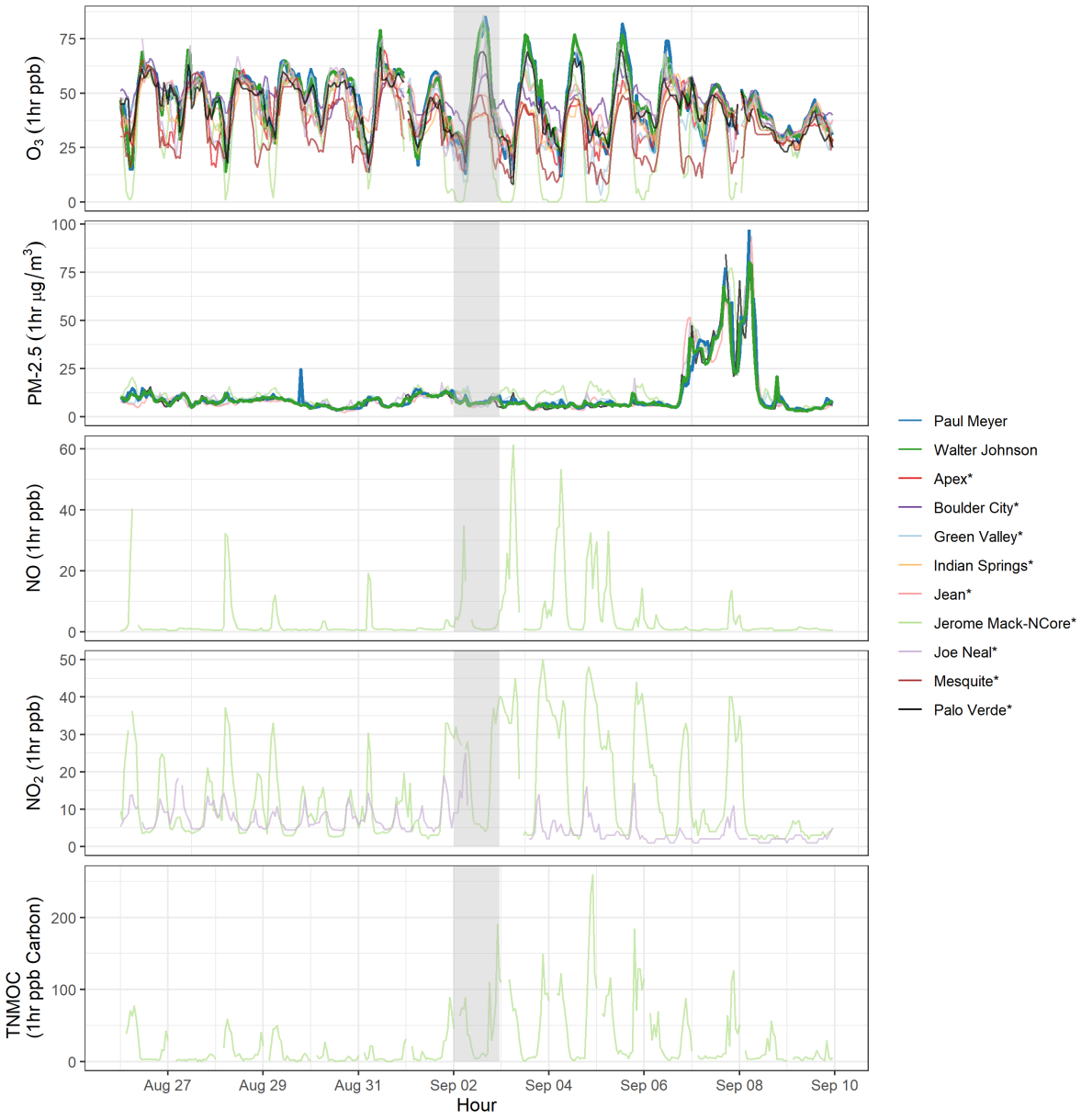

Figure 3-32. Hourly concentrations of ozone, $PM_{2.5}$, NO_x, and total non-methane organic compound (TNMOC). Colored lines represent sites in exceedance on September 2. Gray lines represent supporting sites in Clark County. The gray bar represents September 2.

Unusual diurnal patterns of supporting measurements during the period surrounding the event date can provide evidence that smoke impacted Clark County air quality. Figure 3-33 shows the diurnal profile for ozone and $PM_{2.5}$ at each site that experienced an ozone exceedance on September 2 alongside the seasonal (May to September) average concentrations. Five years of ozone data is available from each site. Four years of $PM_{2.5}$ data is available from Paul Meyer, and one year is available from Walter Johnson. On a typical day, the diurnal profile of ozone shows a peak around midday and an overnight trough. At both sites, the peak ozone concentration on September 2 is well

above average. The diurnal profile of $PM_{2.5}$ exhibits maximum levels overnight and a trough in the afternoon. On September 1, the day before the exceedance event, $PM_{2.5}$ concentrations were persistently well above average throughout the day before dropping to normal levels shortly after midnight. On September 2, a spike in $PM_{2.5}$ around 6:00 a.m. aligned with the initial daily rise in ozone levels. After this morning peak, $PM_{2.5}$ levels showed a constant rise throughout the day, and did not drop to a typical afternoon trough. $PM_{2.5}$ concentrations were above average for the majority of the day, indicating smoke (or other unusual $PM_{2.5}$ concentration events) in the region.

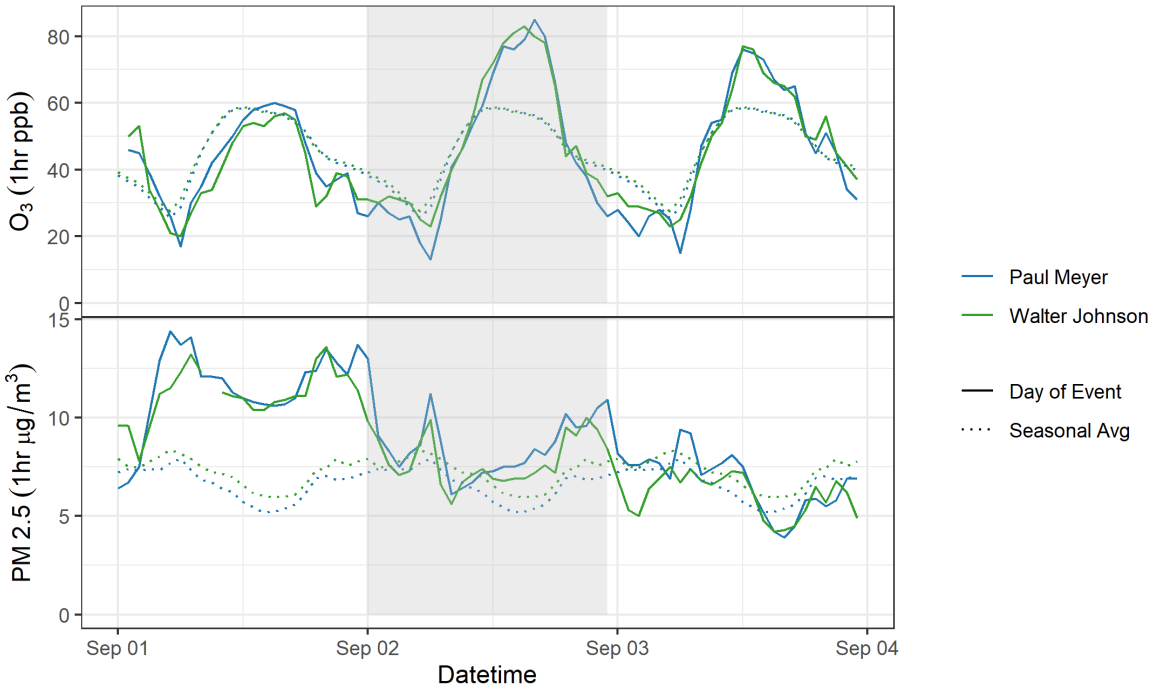

Figure 3-33. September 2 diurnal profile of ozone and $PM_{2.5}$ (solid line), and the seasonal (May-Sept) average (dotted line) at sites in exceedance on September 2, 2020. The event date, September 2, is shaded in gray. Five years of ozone data is available at each site. Four years and one year of $PM_{2.5}$ data is available from Paul Meyer and Walter Johnson, respectively.

Figures 3-34 and 3-35 further display the diurnal profile and average seasonal diurnal profile of ozone and $PM_{2.5}$ separated by event-affected monitoring site, along with the five-year 5^{th} to 95^{th} percentile range. On September 2, concentrations of ozone at every site rose above the five-year 95^{th} percentile at the peak value for the day. September 1 $PM_{2.5}$ concentrations are abnormally high at both exceedance sites. At Paul Meyer, concentrations skirt the 95^{th} percentile throughout the day and exceed the 95^{th} percentile in the early evening. On the event date, September 2, unusual 6 a.m. spike is visible at both exceedance-affected sites. Though the magnitude is not extremely high compared to expected concentrations, an early morning spike deviates from the typical diurnal trend. Observed $PM_{2.5}$ concentrations continue to deviate from the expected trend throughout the day. At Paul Meyer, $PM_{2.5}$ concentrations rise steadily from daybreak to 11 p.m. local time,

throughout the time period when a trough is expected in the afternoon. The deviation is less apparent at Walter Johnson, though $PM_{2.5}$ concentrations remain at a constant, above-average magnitude throughout the afternoon and increase sharply in the evening. These abnormal magnitudes and trends in $PM_{2.5}$ concentrations on September 1 and 2 at each exceedance affected provide evidence of an unusual $PM_{2.5}$ source impacting Clark County during the event period.

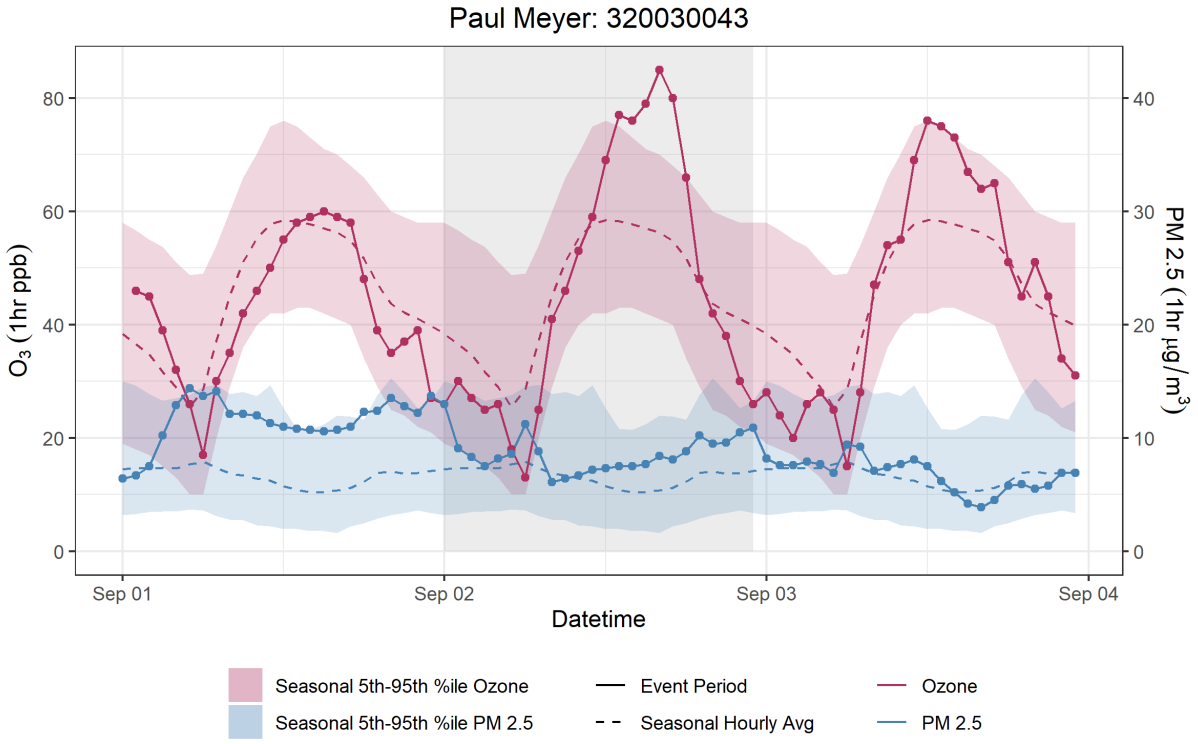

Figure 3-34. Diurnal profile of ozone (red) and $PM_{2.5}$ (blue) concentrations at Paul Meyer, including concentrations on September 2 (solid line) and the seasonal (May-Sept) average (dotted line). Five years of ozone data and four years of $PM_{2.5}$ data is available from Paul Meyer. Shaded ribbons represent the five-year 5^{th}-95^{th} percentile range.

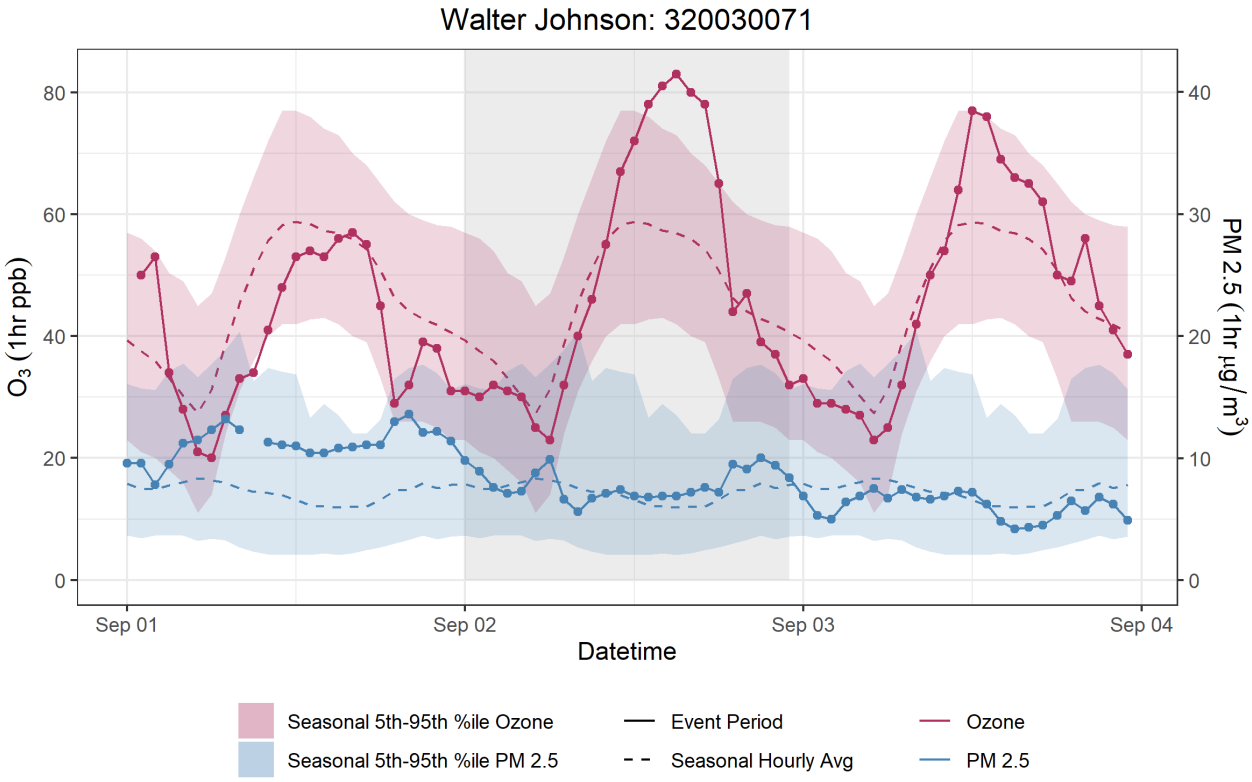

Figure 3-35. Diurnal profile of ozone (red) and $PM_{2.5}$ (blue) concentrations at Walter Johnson, including concentrations on September 2 (solid line) and the seasonal (May-Sept) average (dotted line). Five years of ozone data and one year of $PM_{2.5}$ data is available from Walter Johnson. Shaded ribbons represent the five-year 5^{th}-95^{th} percentile range.

The ratio of PM_{10} to $PM_{2.5}$ concentrations was examined to determine if a dust event—rather than a smoke event—resulted in increased $PM_{2.5}$ concentrations during the event period. If PM_{10} increased more quickly than $PM_{2.5}$, an event might be attributed to dust. Figures 3-36 and 3-37 show a time series of the $PM_{10}/PM_{2.5}$ ratio from September 1 through September 4, with the five-year diurnal average profile and the 5^{th} to 95^{th} percentile range also shown. The notable enhancement in $PM_{2.5}$ concentrations throughout September 1 at each exceedance-affected site is not accompanied by an increase in the ratio of $PM_{10}/PM_{2.5}$. At both the Paul Meyer and Walter Johnson stations, the $PM_{10}/PM_{2.5}$ ratio is below average on September 1, which indicates that the increase in $PM_{2.5}$ at each site during the event period was not unusually influenced by dust. This confirms the assertion that smoke influenced pollutant concentrations on September 2 in Clark County. Though there was significant increase in the $PM_{10}/PM_{2.5}$ ratio above the expected profile on the morning of September 2 at the Paul Meyer station, this seems to be a locally isolated occurrence at Paul Meyer because the Walter Johnson station does not show any similar observation, and the ratio dropped back to an average level soon after.

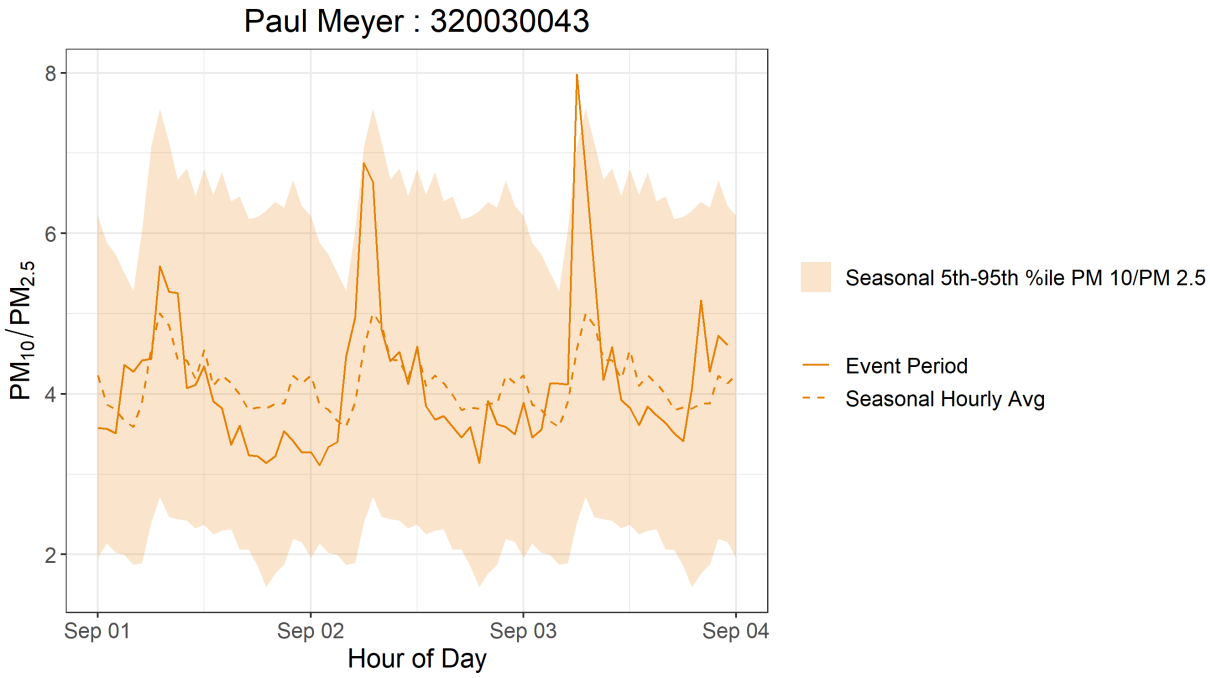

Figure 3-36. $PM_{10}/PM_{2.5}$ ratio at the Paul Meyer exceedance site during the September 2 event period. The five-year average $PM_{10}/PM_{2.5}$ ratio is displayed as a dotted line, and the 5th to 95th percentile range is shown as a shaded ribbon.

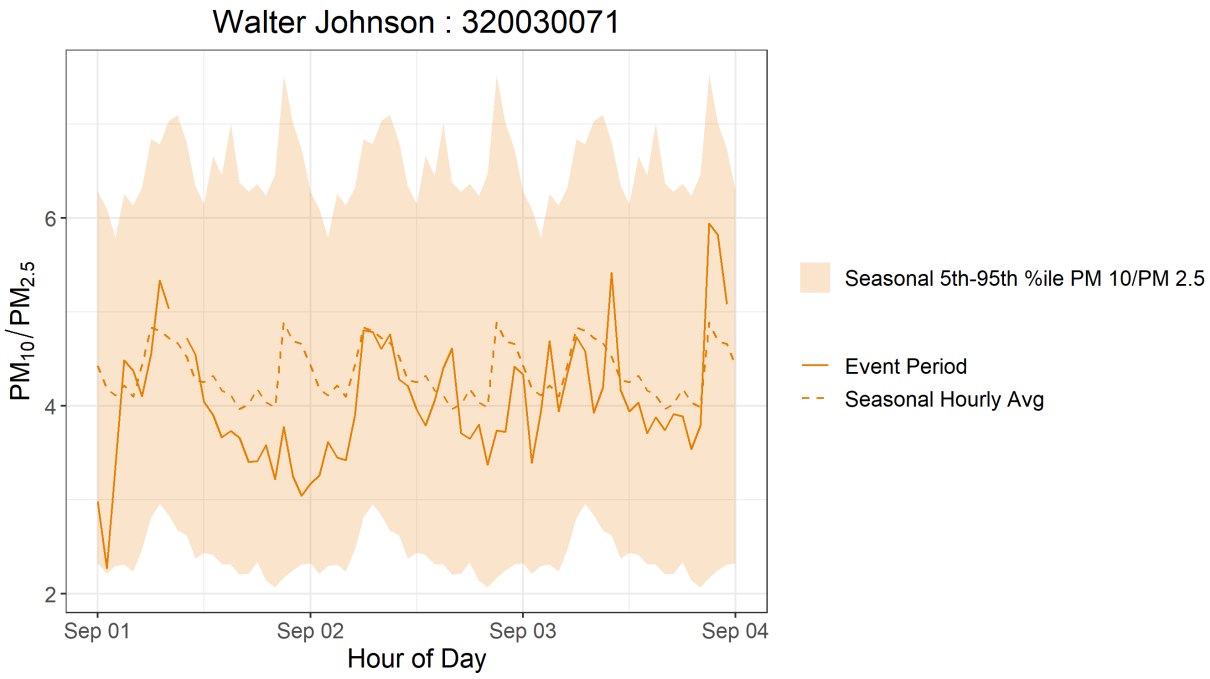

Figure 3-37. $PM_{10}/PM_{2.5}$ ratio at the Walter Johnson exceedance site during the September 2 event period. The five-year average $PM_{10}/PM_{2.5}$ ratio is displayed as a dotted line, and the 5th to 95th percentile range is shown as a shaded ribbon.

Diurnal profiles of ozone and CO in Clark County on September 2 are displayed in **Figures 3-38 and 3-39.** CO data is available from two non-exceedance-affected sites in Clark County, Green Valley and Joe Neal. Observations from these sites are included to provide a reference for regional CO concentrations in Clark County, but should not be used as a direct proxy for concentrations at either event site due to local variation. Five years of ozone data is available from each site. Two years and one year of CO data is available from Joe Neal and Green Valley, respectively. The average and 5^{th}-95^{th} percentile range of seasonal CO concentrations are included on each plot. The diurnal profile of CO at both sites shows two peaks, during the morning and evening, with troughs near midday and after midnight. CO concentrations at both reference sites are elevated above average on September 1 and 2, rising above the 95^{th} percentile concentration more than once at each site across these two days. At Joe Neal, the magnitude of both the morning and evening peak on September first is well above average, and CO remains elevated during the typical trough in the first few hours of September 2. Though data on September 2 is incomplete, the evening peak again reaches a magnitude above the 95^{th} percentile concentration. Similar deviations from the diurnal profile occur at Green Valley. The evening peak CO concentration on September 1 is above average, and CO remains elevated close to the 95^{th} percentile concentration through the night. The morning peak CO concentration rises well above the 95^{th} percentile on the event date, September 2, and the magnitude of peak evening CO concentrations is also quite high compared to the expected diurnal profile. The most pronounced abnormality at Green Valley is a midday peak in CO concentrations. During hours when a trough in CO typically occurs, CO rises well above the 95^{th} percentile. Though CO data is not available from exceedance-affected sites Paul Meyer and Walter Johnson, examination of CO at other sites in Clark County shows significant deviations from the typical diurnal profile of CO. The abnormally high magnitudes and unusually timed peaks in CO concentrations on September 1 and 2 lend evidence to the presence of wildfire emissions in Clark County prior to and during the ozone exceedance on September 2.

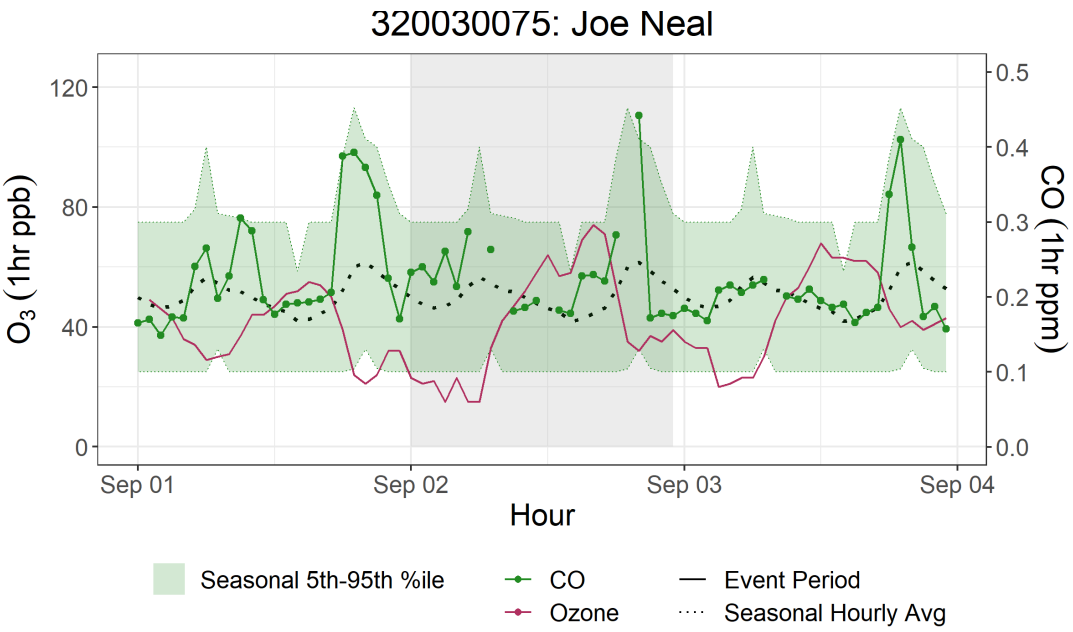

Figure 3-38. Ozone (red) and CO (green) concentrations for Joe Neal on September 1 through 3. The dashed and dotted lines show the seasonal (May to Sept) average. The green ribbon area indicates the seasonal 5th to 95th percentile values for statistical reference. The gray area represents the event date, September 2. Five years of ozone data and two years of CO data is available from Joe Neal.

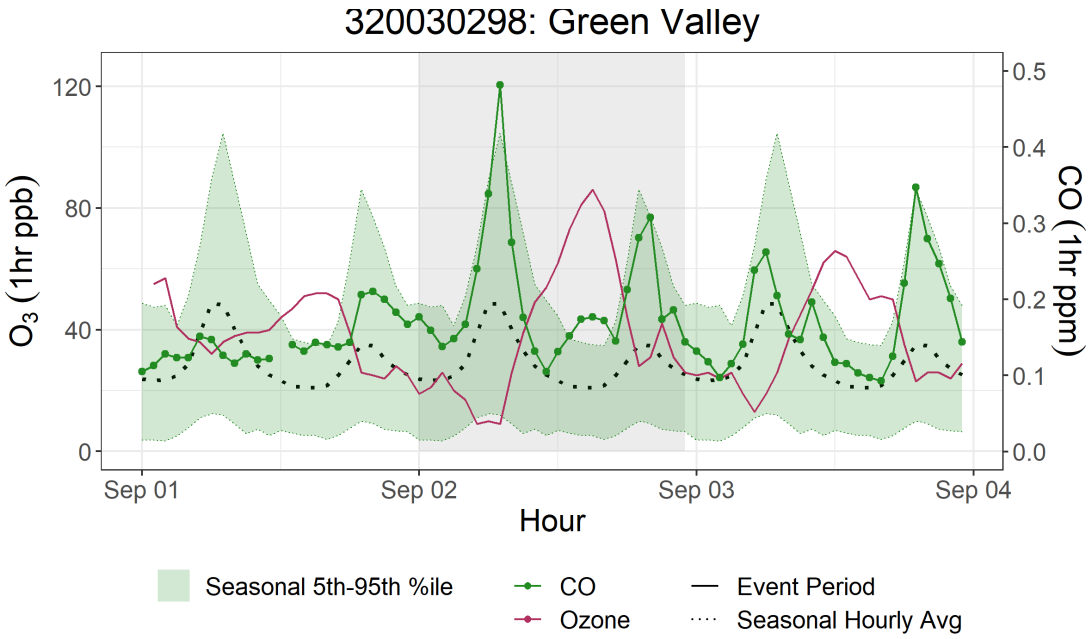

Figure 3-39. Ozone (red) and CO (green) concentrations for Green Valley on September 1 through 3. The dashed and dotted lines show the seasonal (May to Sept) average. The green ribbon area indicates the seasonal 5th to 95th percentile values for statistical reference. The gray area represents the event date, September 2. Five years of ozone data and one year of CO data is available from Green Valley.

Lastly, concentrations of NO_x (NO and NO_2) were examined for the September 2 event in Clark County. In Clark County, neither NO nor NO_2 data is available from either exceedance-affected site, though observations at other sites in Clark County provide a reference for regional deviations of NO_x from the typical diurnal profile. As shown in in the middle panel of **Figure 3-40**, NO data is available only at the NCore reference site, Jerome Mack. The five-year diurnal NO trend shows a peak in the morning that quickly drops to near-zero values before 12:00 p.m.

The bottom panel of Figure 3-40 shows the diurnal average of NO_2 at supporting sites Jerome Mack and Joe Neal. Four and five years of NO_2 data are available from Jerome Mack and Joe Neal, respectively. In comparison to average, NO_2 observations at Jerome Mack were enhanced above average on September 2. Though data on September 2 is not available from Joe Neal after 7 a.m., NO_2 concentrations exceeded the 95th percentile concentration on the night of September 1, the day before the exceedance event. The elevated NO and NO_2 above typical concentrations on September 1 and 2 at supporting monitoring sites provide evidence of wildfire emissions at the surface in Clark County during the event period.

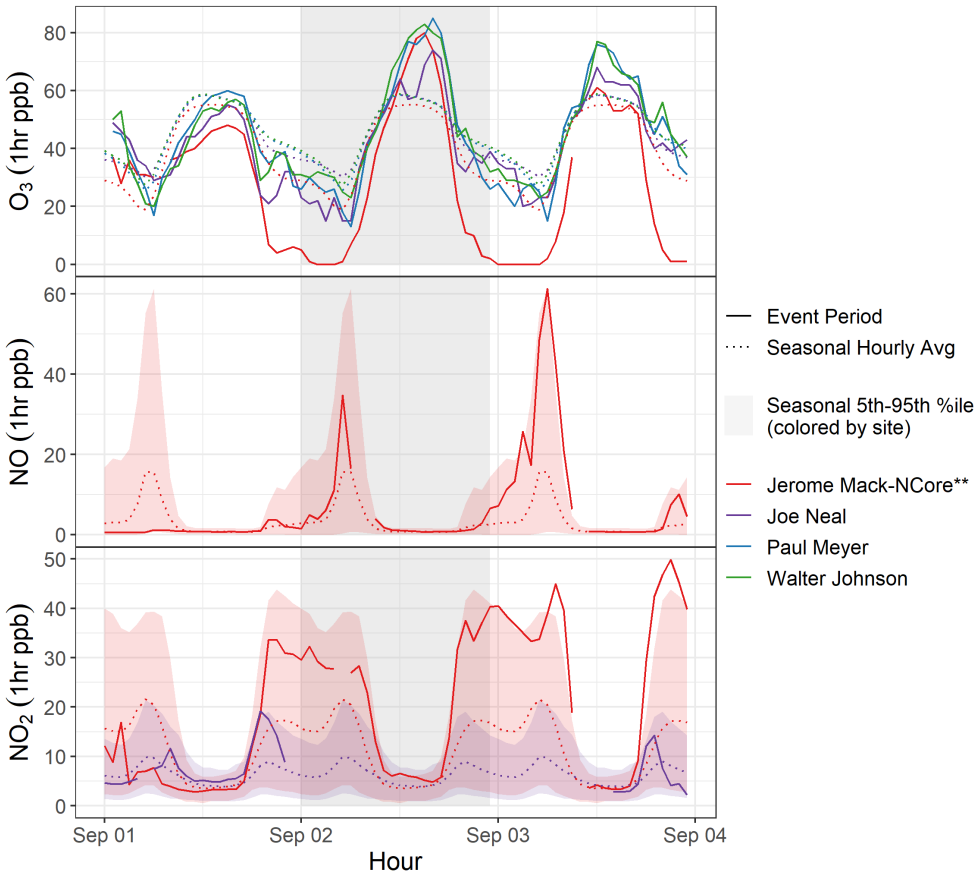

Figure 3-40. Ozone and NO_x concentrations during the September 2 EE. The top figure shows ozone concentrations from all sites on September 2 (solid lines) and five-year seasonal averages (May - Sept) for each site (dotted lines). The middle plot shows NO concentrations on September 2 (solid line), the seasonal average (dotted line), and the seasonal 5th to 95th percentile (shaded area) for select sites with NO measurements. The bottom plot shows the same information as the middle plot, but for NO_2. 5 years of NO data is available from Jerome Mack, and 4 and 5 years of NO_2 data is available from Jerome Mack and Joe Neal, respectively.

The supporting pollutant trends and diurnal patterns, showing $PM_{2.5}$, CO, NO_x, and ozone concentrations outside of their normal seasonal and yearly historical averages provide additional proof of smoke impacts on the Clark County area during September 2, 2020. Wildfires can generate the precursors needed to create ozone, NO_x, and VOCs. While ozone concentrations can be suppressed very near a fire due to NO_x titration, downwind areas are likely to see an increase in ozone concentrations due to the presence of both precursor gases and sufficient UV radiation (i.e., when an air mass leaves an area of very thick smoke that inhibited solar radiation) (Finlayson-Pitts and Pitts Jr, 1997; Jaffe et al., 2008; Bytnerowicz et al., 2010). Ozone precursors from wildfire smoke can also be transported a significant distance downwind, and if these compounds are mixed into an urban area (such as Las Vegas), the ozone concentrations produced can be significantly higher than

they would be from either the smoke plume or the urban area alone (Jaffe et al., 2013; Wigder et al., 2013; Lu et al., 2016; Brey and Fischer, 2016). Since we find evidence of smoke impacts on September 2 in Clark County via supporting pollutant measurements and other analyses in Sections 3.1 and 3.2, we suggest that both the direct transport of ozone and the transport of ozone precursor gases likely caused the ozone exceedance.

Filter samples were also taken at the Jerome Mack (including a collocated sample) in Clark County every three days during 2020. From these filter samples, concentrations of levoglucosan, a wildfire smoke tracer, were analyzed by the Desert Research Institute (DRI) via gas chromatography-mass spectroscopy (GC-MS). Levoglucosan is produced by the combustion of cellulose and is emitted during wildfire events that can be transported downwind (Simoneit et al., 1999; Simoneit, 2002; Bhattarai et al., 2019). Levoglucosan has an atmospheric lifetime of one to four days before it is lost due to atmospheric oxidation and can therefore be used as a tracer of biomass burning (wildfires) far downwind from its source (Hoffmann et al., 2009; Hennigan et al., 2010; Bhattarai et al., 2019; Lai et al., 2014). In the Las Vegas region, residential wood combustion has historically not been a significant contributor to levoglucosan concentrations during the late summer time frame (Kimbrough et al., 2016). Table 3-11 shows levoglucosan concentration, uncertainty, and positive/negative detection certainty during the September 2 EE event. Table 3-11 also shows the average levoglucosan concentration from nineteen 2018-2019 background days together with its standard deviation, and propagated uncertainty at the Jerome Mack site for comparison. On these background days, no ozone exceedance was observed, and fire/smoke influence was minimal according to HMS. During the September 2 EE event, non-zero levoglucosan concentrations and positive detections are seen after smoke is transported to Clark County from the California and Oregon fires. The detected 16 ng/m^3 of levoglucosan in Clark County at the Jerome Mack monitoring site is significantly higher than the background average of 2±3 ng/m^3, providing certain evidence that wildfire smoke affected the area during the September 2 ozone exceedance.

Table 3-11. Levoglucosan concentrations at monitoring sites around Clark County, Nevada, during September 2 ozone event. The average levoglucosan concentration together with its standard deviation, and propagated uncertainty from background days in 2018 and 2019 for the Jerome Mack site are also provided for comparison. Positive or negative detection is also shown.

Sample Date	Sampling Site	Levoglucosan (ng/m^3)	Levoglucosan Uncertainty (ng/m^3)	Levoglucosan Detected?
Background days (2018-2019)	Jerome Mack	2±3	1	N/A
9/2/2020	Jerome Mack	16	1	Positive

3.3 Tier 3 Analyses

3.3.1 Total Column & Meteorological Conditions

Satellite analyses and HYSPLIT trajectories shown in Section 3.1 provide strong evidence that smoke was present over Clark County at the time of the EE on September 2, 2020. However, the visible true color, AOD, and CO satellite data do not provide information about the vertical distribution of visible or measured smoke components. We examined satellite-retrieved aerosol vertical profiles and ceilometer mixing height measurements to determine whether the smoke plume was present at or near the surface on September 2.

The Cloud-Aerosol Light Detection and Ranging (LIDAR) and Infrared Pathfinder Satellite Observation (CALIPSO) system is a remote sensing instrument mounted on the CloudSat satellite that provides vertical profile measurements of atmospheric aerosols and clouds. Detected aerosols are classified into marine, marine mixture, dust, dust mixture, clean/background, polluted continental, smoke, and volcanic aerosol types.

The best CALIPSO aerosol retrieval over Clark County for the September 2 ozone event is available at approximately 3:20 a.m. local time on August 30 and 2:40 p.m. local time on September 2 (**Figures 3-41 through 3-44**). Unfortunately, the CALIPSO vertical profile does not capture information directly over Clark County during the event; it does, however, provide information about the column above areas to the north of Clark County in central and northern Nevada, and to the west of Clark County in western Nevada and southern California. Increased backscatter between the altitudes of approximately 1,000 to 5,000 m on August 30, and between 1,000 to 3,000 m on September 2, provides evidence of increased aerosols at low levels in the vertical columns that could be transported to Clark County and mixed down to the surface (**Figures 3-45 through 3-48**). CALIPSO figures on both August 30 and September 2 provide evidence that significant amounts of smoke were upwind of the Las Vegas area in the days leading up to the ozone exceedance. The HYSPLIT trajectories shown in Section 3.1.3 provide evidence of smoke transport from the California and Oregon fires to Clark County but do not provide information about the characteristics of aerosols in the vertical profile of the atmosphere near these fires. The CALIPSO aerosol retrieval, however, provides evidence that enhanced aerosol concentrations were present in the vertical atmospheric column near Clark County on the morning of August 30 and on the afternoon of September 2, while the HYSPLIT trajectories provide evidence of transport from the California and Oregon fires to Clark County. This evidence suggests that the smoke plumes from these fires reached Clark County and likely affected air quality by September 2, 2020.

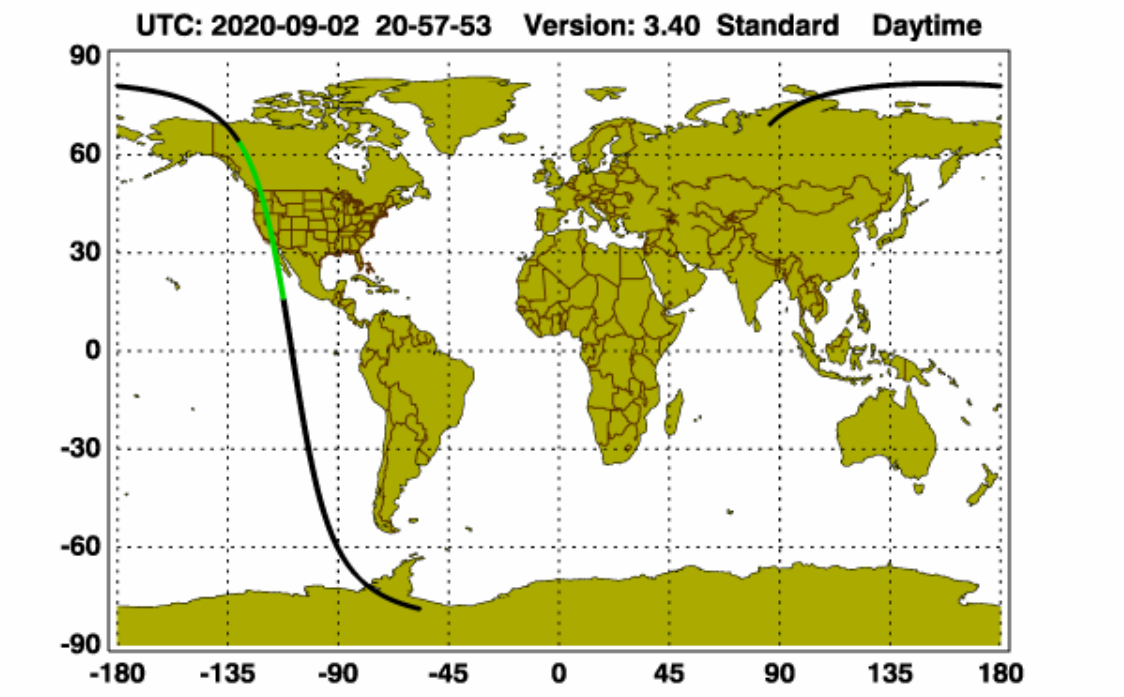

Figure 3-41. The CALIPSO retrieval path for September 2, 2020. This overpass was the closest to Clark County and the nearest in time.

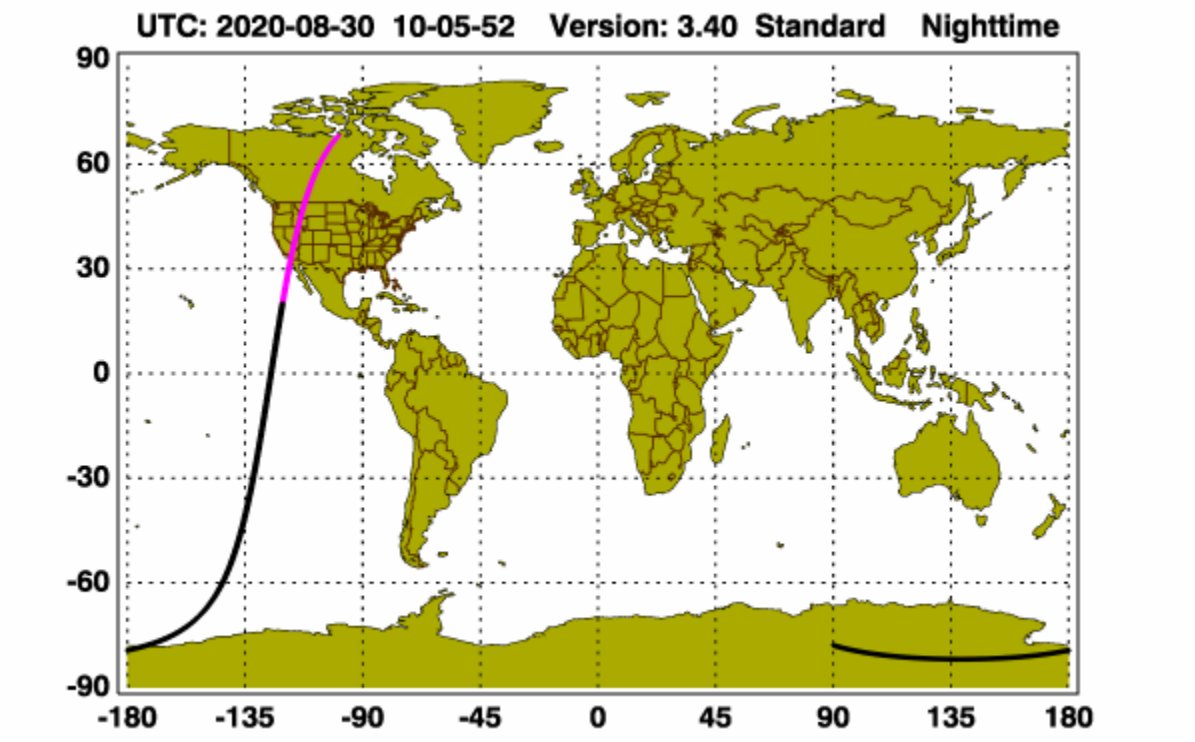

Figure 3-42. The CALIPSO retrieval path for August 30, 2020.

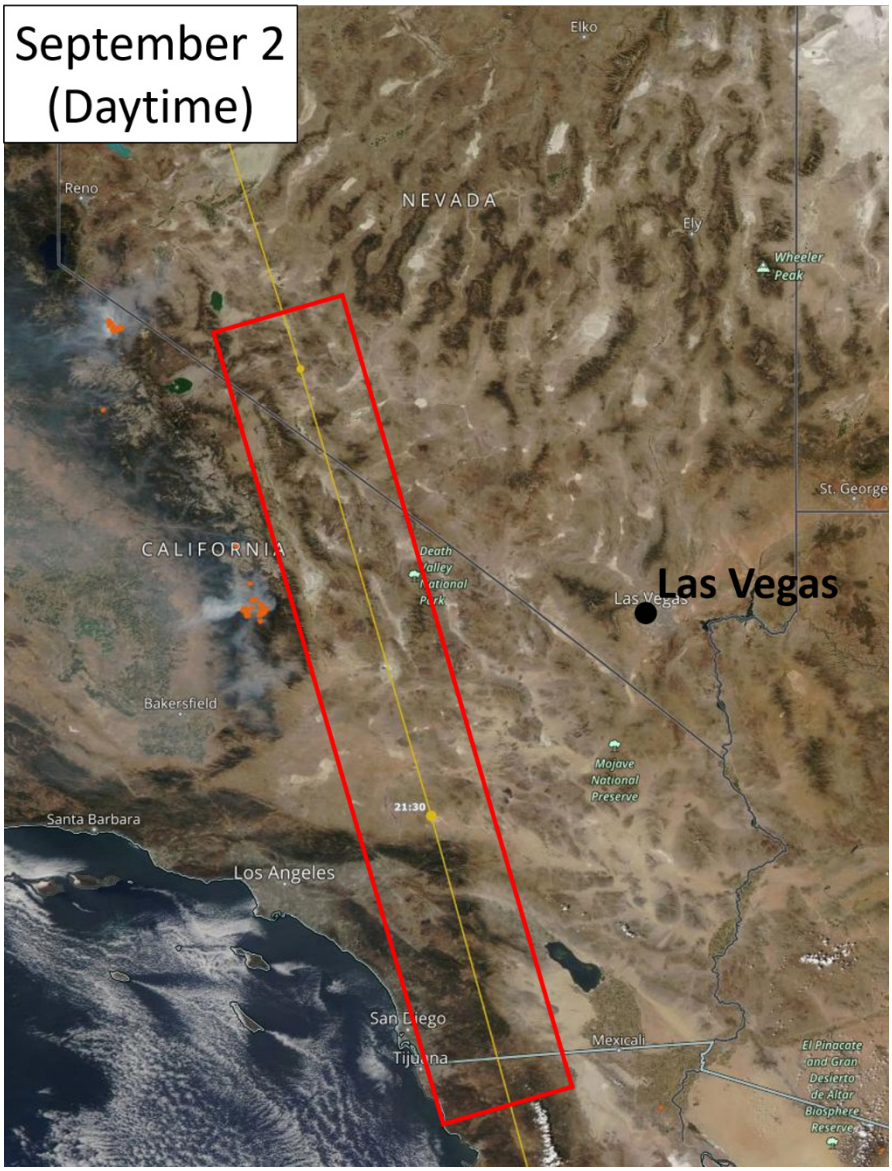

Figure 3-43. The CALIPSO retrieval path for September 2, 2020. This overpass was the closest to Clark County and the nearest in time. Approximate areas indicated by the red box.

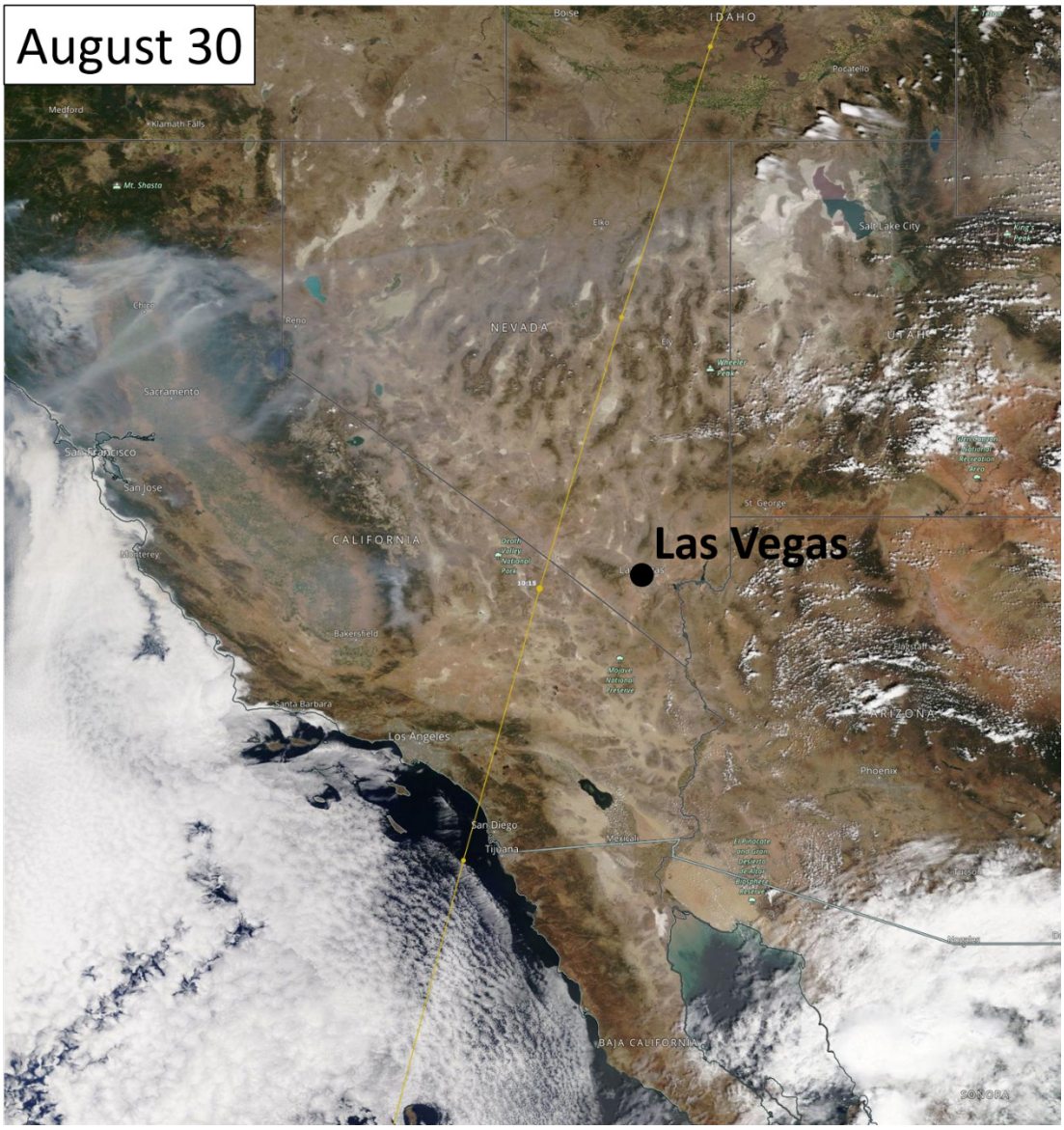

Figure 3-44. The CALIPSO retrieval path for August 30, 2020.

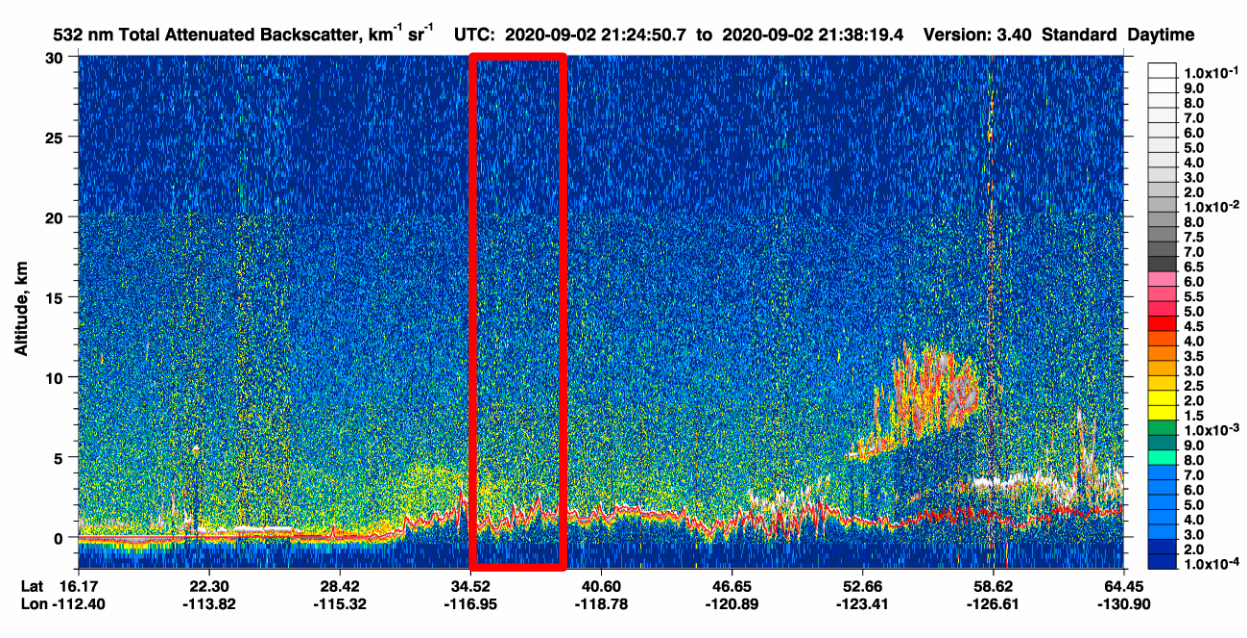

Figure 3-45. CALIPSO total column profile backscatter information for the September 2 overpass near Clark County, Nevada (approximate areas indicated by a red box).

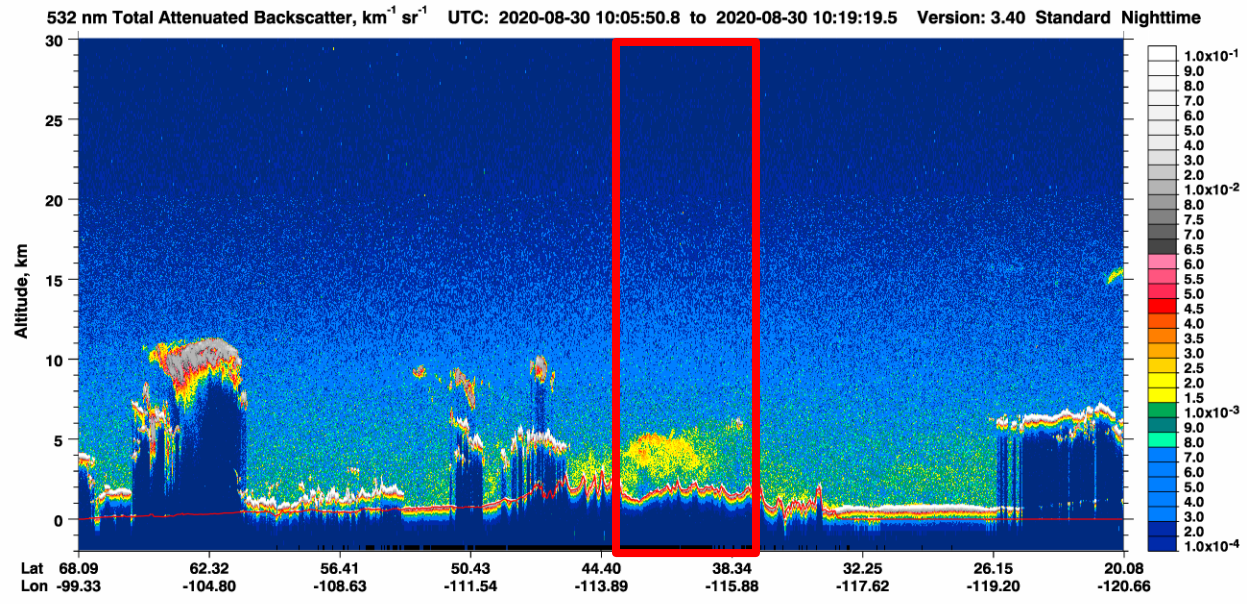

Figure 3-46. CALIPSO total column profile backscatter information for the August 30 overpass near Clark County, Nevada (approximate areas indicated by a red box).

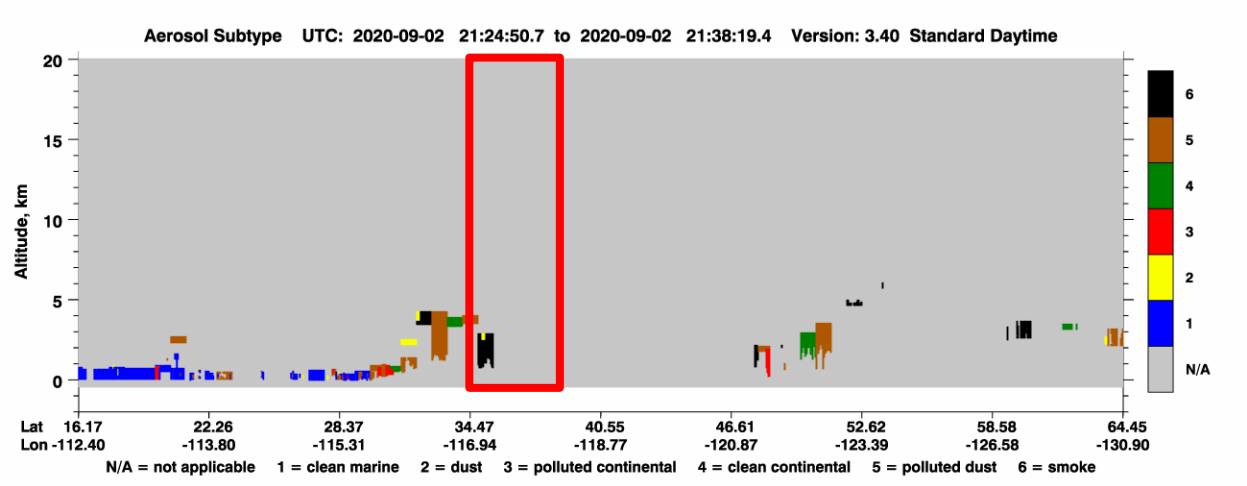

Figure 3-47. CALIPSO total column profile aerosol subtype information for the September 2 overpass near Clark County, Nevada (approximate areas indicated by a red box).

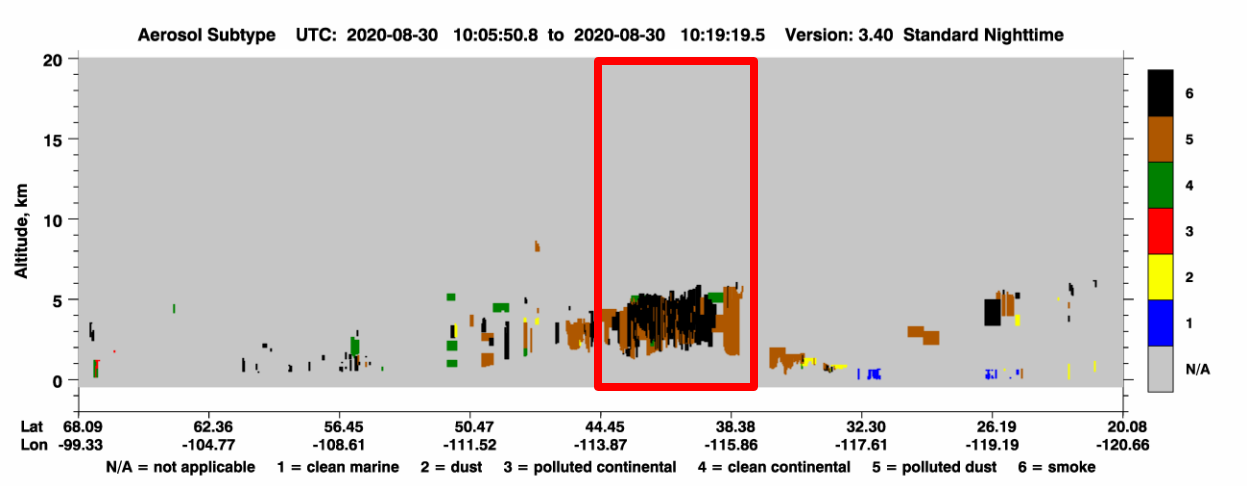

Figure 3-48. CALIPSO total column profile aerosol subtype information for the August 30 overpass near Clark County, Nevada (approximate areas indicated by a red box).

The mesoscale and local meteorological conditions from August 30 to September 2 provide evidence for transport of smoke from the fires in California and the Pacific Northwest to Clark County, Nevada, and subsequent vertical mixing of smoke from aloft to the surface. Upper-level wind barbs at 500 hPa from Oregon to Nevada from August 30 and August 31 to September 1 indicate a strong shift from a primarily westerly direction to a northerly direction causing smoke from the fire in California and the Pacific Northwest to move into the Clark County area (Figure 3-49).

Local observations of mixing heights in the Las Vegas area on September 1 and September 2 suggest that smoke likely mixed into the lower levels of the atmosphere. Ceilometer data from the Jerome Mack site indicate mixing heights on September 1 and September 2 between approximately 1,500 m

and 2,250 m for several hours during each day (Figure 3-50). Furthermore, a surface low-pressure system was centered over the border of Nevada and California between August 30 and September 2. Low pressure at the surface is often associated with enhanced vertical mixing in the lower troposphere (Figure 3-51). Mixing height data from the ceilometer and the surface weather maps provide evidence of enhanced vertical mixing in the lower troposphere when smoke was present over Clark County.

In addition to the ceilometer-based measurements of mixing heights, vertical temperature profiles (Skew-T diagrams) can be used to estimate mixing heights. The vertical temperature profile at Las Vegas from August 30 to September 2 shows the vertical atmospheric profile becoming drier in the lower troposphere—as shown by the widening between the temperature profile and the dewpoint profile—with wind directions consistently from the north, northwest, and northeast (Figures 3-52 and 3-53), indicating smoke transport in the lower levels of the atmosphere from the fires in California and the Pacific Northwest into Clark County. Enhanced vertical mixing from August 30 to September 2 can be seen from a pronounced, sizeable mixed layer—as indicated by temperatures decreasing with height approximately along the dry adiabat up to at least 600 hPa—with associated warm temperatures and very dry air.

To summarize:

- The CALIPSO vertical profile of aerosols over Clark County on the morning of August 30 and in the afternoon of September 2 clearly show smoke upwind and to the west of Clark County (Figures 3-47 and 3-48)
- The upper-level and surface weather maps show conditions consistent with transporting smoke from the Pacific Northwest and California into Clark County
- The ceilometer data, the surface weather map, and the vertical temperature and wind profiles (skew-T diagrams) suggest the existence of smoke within the mixed layer, the transport of smoke from the fires in California and the Pacific Northwest to Clark County, and subsequent mixing in the lower troposphere.

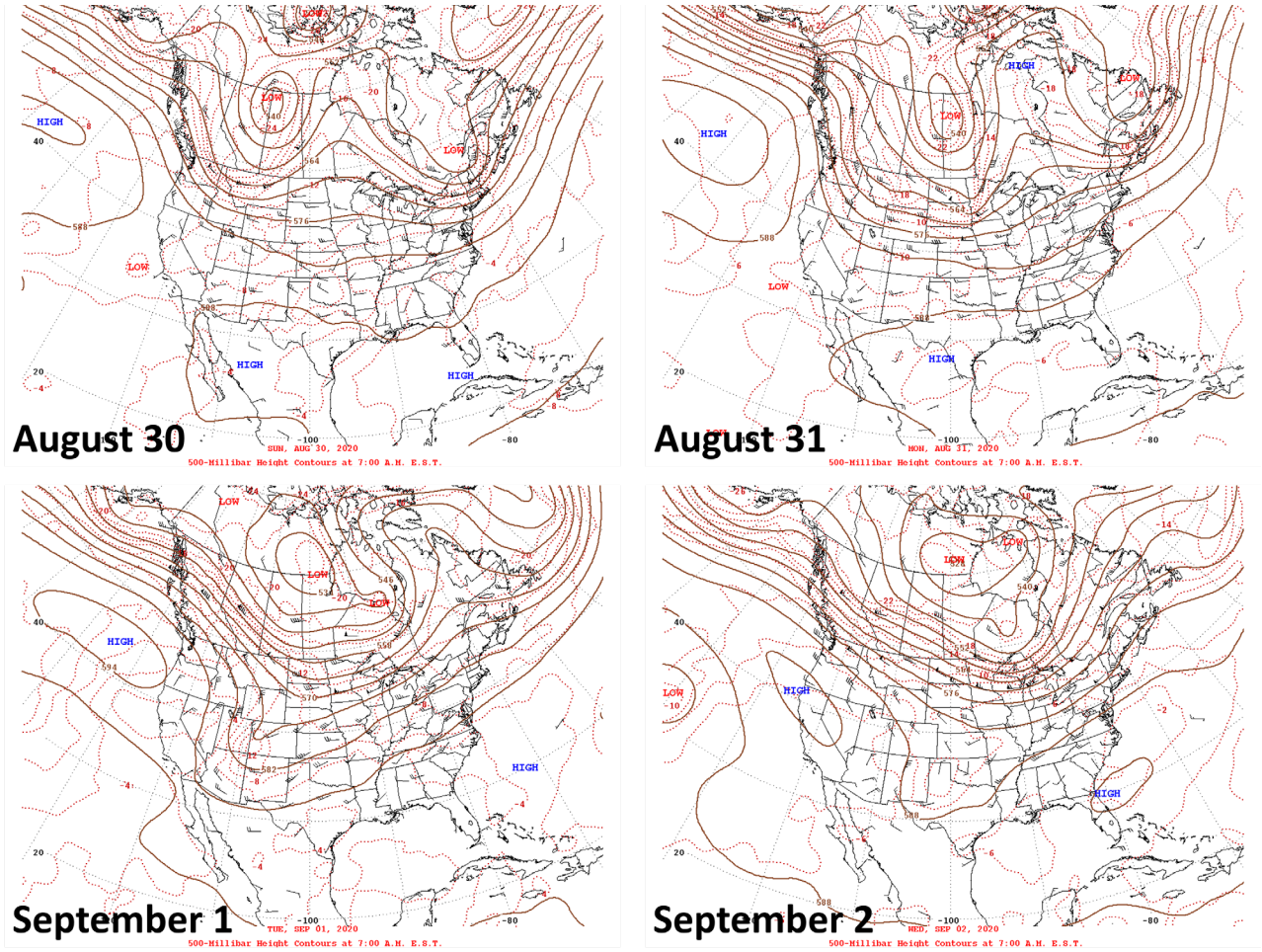

Figure 3-49. Daily upper-level meteorological maps for the three days leading up to the EE and during the September 2 EE.

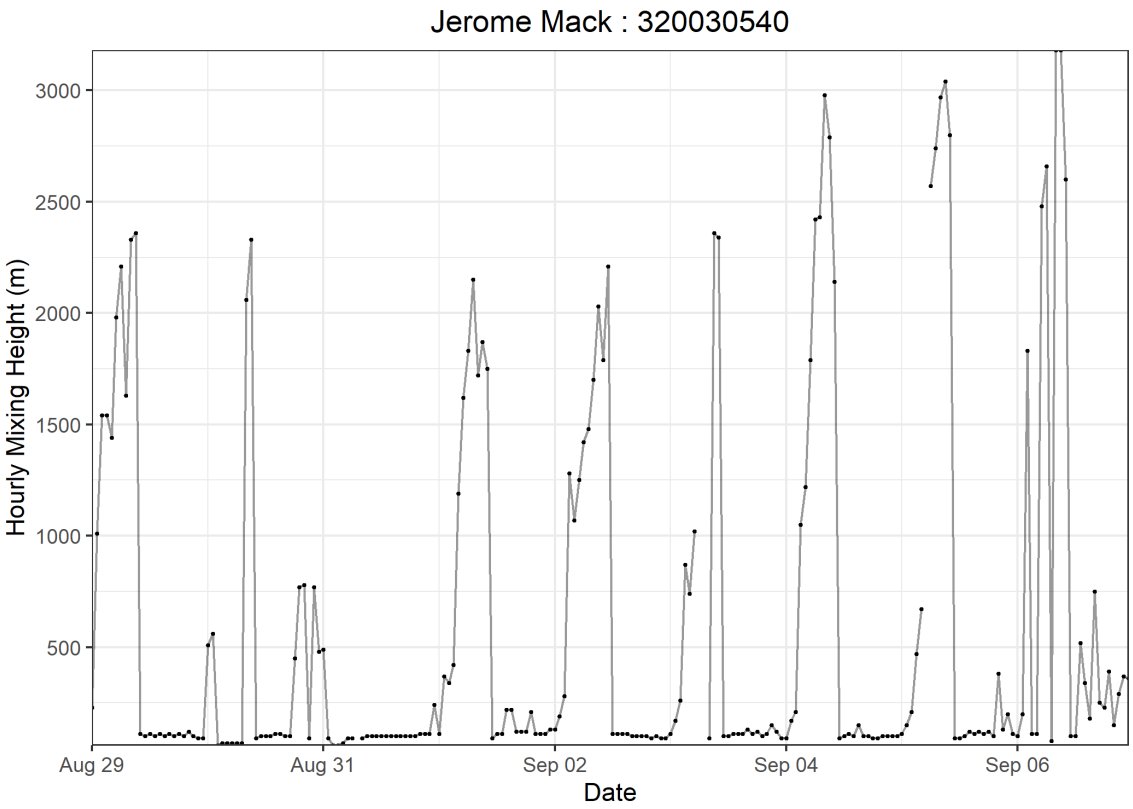

Figure 3-50. Time series of mixing heights taken from Jerome Mack (NCore Site) for two weeks before and after the September 2 EE.

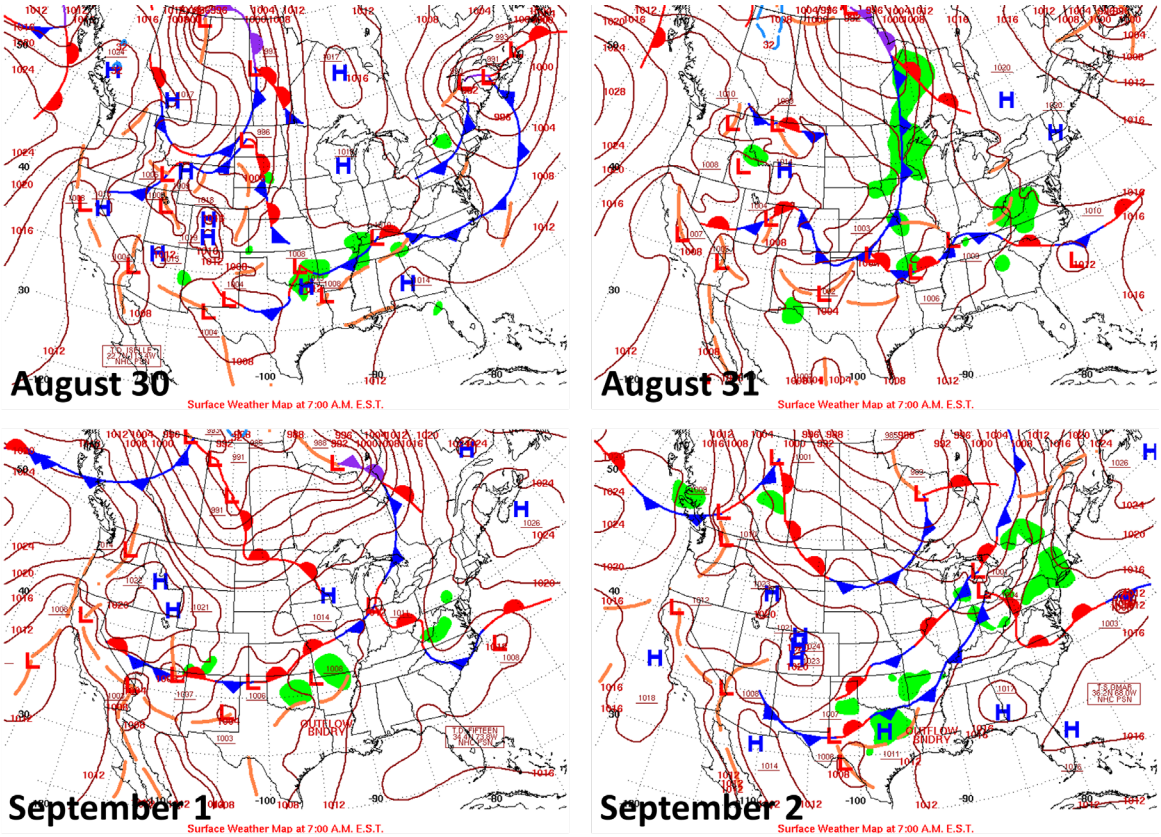

Figure 3-51. Daily surface meteorological maps for the three days leading up to the EE and during the September 2 EE.

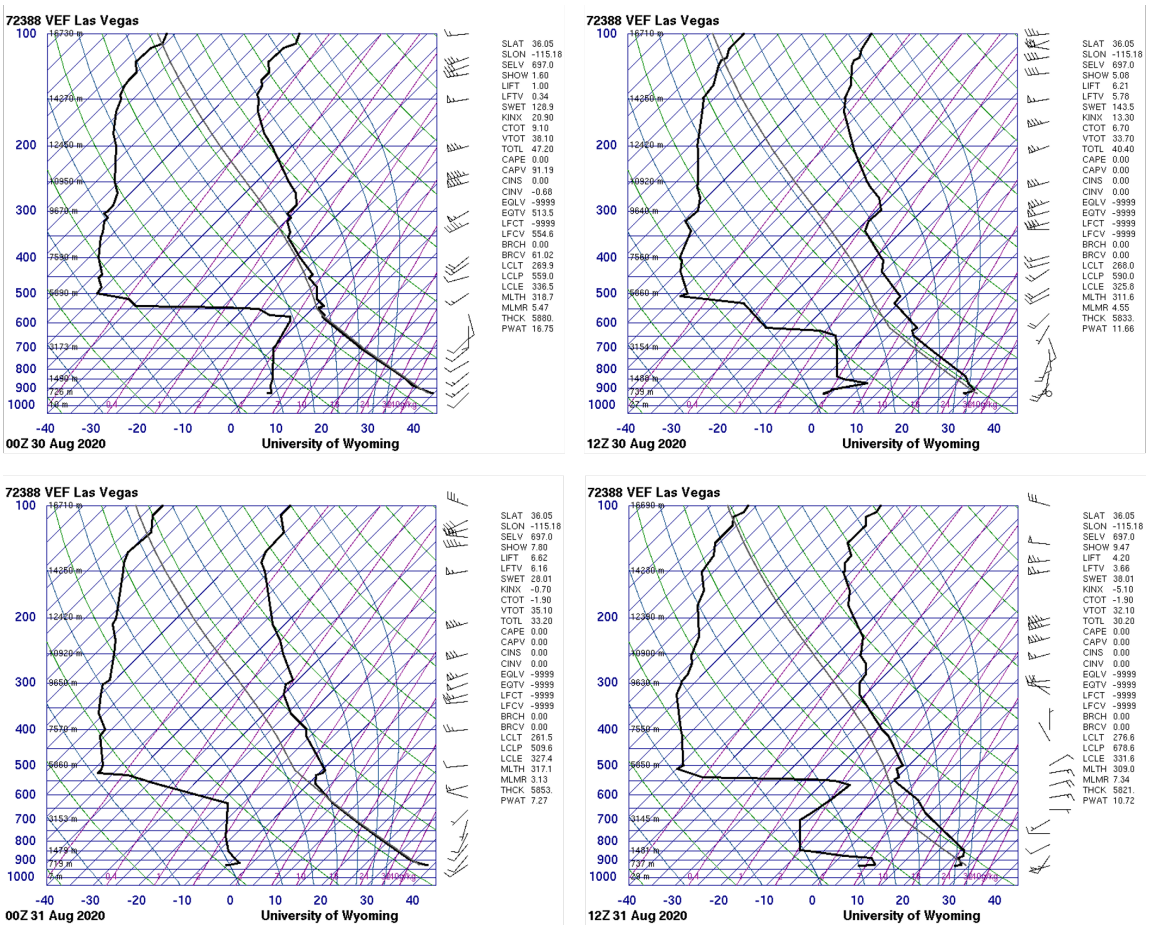

Figure 3-52. Skew-T diagrams from August 30 and 31, 2020, in Las Vegas, Nevada.

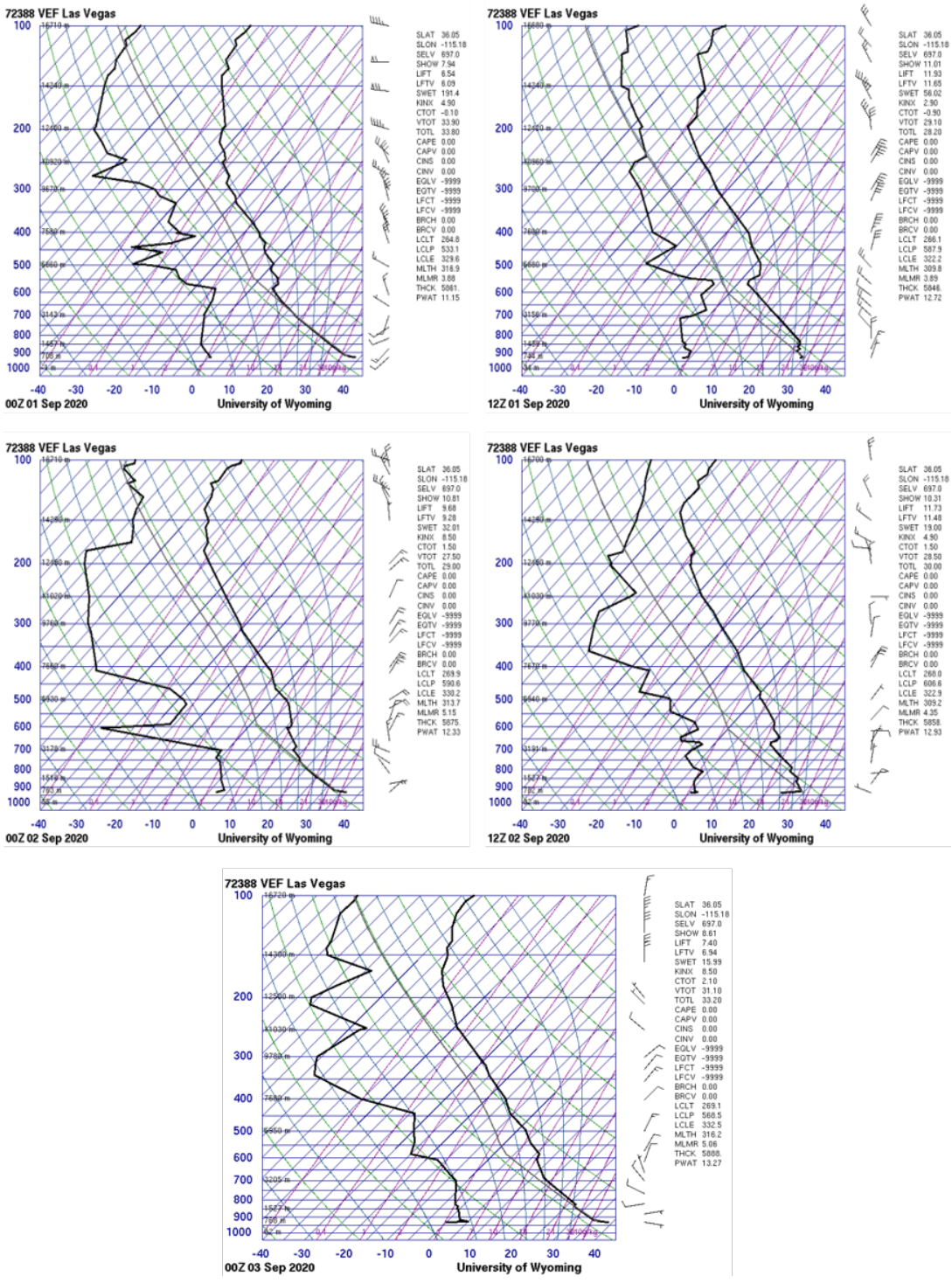

Figure 3-53. Skew-T diagrams from September 1 to 3, 2020, in Las Vegas, Nevada.

3.3.2 Matching Day Analysis

Ozone production and transport strongly depend on regional and local meteorological conditions. A comparison of ozone concentrations on suspected exceptional event days with non-event days that share similar meteorology can help demonstrate that ozone production was affected by an atypical source. Given that similar meteorological days are likely to have similar ozone concentrations, noticeable differences in ozone concentrations between the event date and meteorologically similar days provide a clear causal relationship between wildfire smoke and elevated ozone concentrations.

Identify Meteorologically Similar Days

In order to identify the best matching meteorological days, both synoptic and local conditions were examined from days in the ozone season (April 1 through September 30) between 2014 and 2020. This data set excludes days with suspected exceptional events in the 2018 and 2020 seasons, and all dates within 5 days of the EE event date (September 2) to ensure that lingering effects of smoke transport or stratospheric intrusion did not appear in the data.

To best represent similar air transport patterns, twice-daily HYSPLIT trajectories (initiated at 18:00 and 22:00 UTC) from Clark County for 2014-2020 were clustered by total spatial variance. The calculation, based on the difference between each point along a trajectory, provides seven distinct pathways of airflow into Clark County. The cluster that best represents the trajectory on the exceptional event day was chosen, and ozone-season days within the cluster were then subset for regional meteorological comparison to the exceptional event day.

For the meteorological comparison, a correlation score was assigned to each day from the cluster subset. The National Centers for Environmental Prediction's (NCEP) reanalysis data was compiled for the ozone seasons in 2014-2020. Daily average wind speed, geopotential height, relative humidity, and temperature were considered at 1,000 mb and 500 mb. At the surface, daily average atmospheric pressure, maximum temperature, and minimum temperature were utilized. Pearson product-moment coefficient of linear correlation (pattern correlation) was calculated between the exceptional event date and each cluster-subset ozone-season day in 2014-2020 for each parameter. The pattern correlation calculates the similarity between two mapped variables at corresponding grid locations within the domain. The statistic was calculated using a regional domain of 30°N – 45°N latitude and 125°W - 105°W longitude. The correlation score for each day was defined as the average pattern correlation of all parameters at each height level. The correlations scores were then ranked by the highest correlation for 1,000 mb, the surface, and finally 500 mb. Dates within 5 days of the current exceptional event were removed from the similar day analysis to ensure the data are mutually exclusive. 50 dates with the highest rank correlation scores were then chosen as candidate matching days for further analysis.

Local meteorological conditions for the subset of candidate matching days were then compared to conditions on September 2, and filtered to identify five or more days that best matched the event date. Meteorological maps at the surface and 500 mb, as well as local meteorological data describing temperature, wind, moisture, instability, mixing layer height, and cloud cover, were examined. The data source for each parameter is summarized in Table 3-12.

Table 3-12. Local meteorological parameters and their data sources.

Meteorological Parameter	Data Source
Maximum daily temperature	Jerome Mack - NCore Monitoring Site
Average daily temperature	Jerome Mack - NCore Monitoring Site
Resultant daily wind direction	Jerome Mack - NCore Monitoring Site (calculated vector average)
Resultant daily wind speed	Jerome Mack - NCore Monitoring Site (calculated vector average)
Average daily wind speed	Jerome Mack - NCore Monitoring Site
Average daily relative humidity (RH)	Jerome Mack - NCore Monitoring Site
Precipitation	Jerome Mack - NCore Monitoring Site
Total daily global horizontal irradiance (GHI)	UNLV Measurement and Instrumentation Data Center (MIDC) in partnership with NREL (https://midcdmz.nrel.gov/apps/daily.pl?site=UNLV&start=20060318&yr=2021&mo=4&dy=29)
4:00 p.m. local standard time (LST) mixing layer mixing ratio	Upper air soundings from KVEF (http://weather.uwyo.edu/upperair/sounding.html)
4:00 p.m. LST lifted condensation level (LCL)	Upper air soundings from KVEF (http://weather.uwyo.edu/upperair/sounding.html)
4:00 p.m. LST convective available potential energy (CAPE)	Upper air soundings from KVEF (http://weather.uwyo.edu/upperair/sounding.html)
4:00 p.m. LST 1,000-500 mb thickness	Upper air soundings from KVEF (http://weather.uwyo.edu/upperair/sounding.html)
Daily surface meteorological map	NOAA's Weather Prediction Center Daily Weather Maps (https://www.wpc.ncep.noaa.gov/dailywxmap/index.html)
Daily 500 mb meteorological map	NOAA's Weather Prediction Center Daily Weather Maps (https://www.wpc.ncep.noaa.gov/dailywxmap/index.html)

Matching Day Analysis

Table 3-13 displays the percentile ranking of each examined meteorological parameter at the Jerome Mack NCore site in the 30-day period surrounding September 2 (August 18 through September 17) across the years 2014 through 2020. Wind speeds were abnormally low on September 2. Both the resultant average speed and the mean scalar speed are the minimum measurement across the seven years of data for this time period. Total GHI was also quite low, at the 6th percentile. As is typical in Clark County, there was no precipitation on September 2.

Table 3-13. Percentile rank of meteorological parameters on September 2, 2020, compared to the 30-day period surrounding September 2 over seven years (August 18 through September 17, 2014-2020).

Date	Max Temp (°F)	Avg Temp (°F)	Resultant Wind Direction (°)	Resultant Wind Speed (mph)	Avg Wind Speed (mph)	Avg RH (%)	Precip (in)	Total GHI (kWh/m^2)	Mixing Layer Mixing Ratio (g/kg)	LCL (mb)	CAPE (J/kg)	500-1000 mb Thickness (m)
2020-09-02	59	33	NA	0	0	61	NA	6	59	63	62	64

From the subset of synoptically similar days filtered according to the methodology described above, dates were further filtered according to parameters listed in Table 3-12 to match local meteorological conditions. A priority was placed on matching wind speeds rather than direction since the average scalar wind speed was just above 1 knot, the National Weather Service's definition of "calm". This indicates that wind direction was likely variable and therefore did not have a strong influence on ozone concentration. Table 3-14 shows the six days that best match the meteorological conditions that existed on September 2, 2020; it also shows the MDA8 concentration on each of these dates at each site that experienced an exceedance on September 2. Surface and upper-level maps for September 2 and each date listed in Table 3-14 show highly consistent conditions. All dates show a surface low pressure system and an upper-level region of high pressure over Clark County, with a very low gradient of height contours at 500 mb. Surface and upper-level maps are included in **Appendix C.**

Table 3-14 shows the average MDA8 ozone concentration across these six days with an expected range defined by one standard deviation, a conservative estimate given the small sample size. The expected MDA8 ozone concentration is well below the 70-ppb standard, ranging from 58 to 59 ppb. Further, the upper end of the provided range at each site also falls below the ozone standard. Neither of the sites that had an ozone exceedance on September 2 exceeded the 70-ppb ozone standard on any of these meteorologically similar days. If meteorology were the sole cause of the ozone exceedance on September 2, we would expect to see similarly high ozone levels on each of the similar days listed in Tables 3-14, especially those with even warmer temperatures than experienced on September 2. These findings further demonstrate that an unusual source of ozone beyond typical photochemistry contributed to the ozone exceedance on September 2, 2020.

Table 3-14. The top six matching meteorological days to September 2, 2020. Concentrations recorded at the Paul Meyer (PM) and Walter Johnson (WJ) monitoring sites are shown for each of these days. Average MDA8 ozone concentrations of the meteorologically similar days are shown plus-or-minus one standard deviation, rounded to the nearest ppb.

Date	Max Temp (°F)	Avg Temp (°F)	Resultant Wind Direction (°)	Resultant Wind Speed (mph)	Avg Wind Speed (mph)	Avg RH (%)	Precip (in)	Total GHI (kWh/m^2)	Mixing Layer Mixing Ratio (g/kg)	LCL (mb)	CAPE (J/kg)	500-1000 mb Thickness (m)	MDA8 Ozone Concentration (ppb)	
													PM	WJ
2020-09-02	**105**	**91.00**	**353.56**	**0.28**	**1.21**	**12.79**	**0**	**6.96**	**5.06**	**568**	**0**	**5,888**	**73**	**75**
2014-08-28	104	89.54	175.78	0.53	2.00	19.46	0	7.22	4.87	565	0	5,857	67	70
2017-08-18	107	93.79	145.74	1.35	2.21	16.92	0	7.61	6.42	589	83	5,853	48	53
2017-09-01	108	96.00	347.8	2.78	3.45	17.46	0	6.78	6.89	597	119	5,870	64	63
2018-09-26	100	84.17	337.8	0.89	1.62	15.38	0	6.1	3.86	566	0	5,828	52	53
2018-09-27	102	83.50	341.47	0.05	1.15	15.29	0	6.12	3.64	544	0	5,854	54	53
2020-09-12	100	82.96	267.45	0.82	1.29	16.17	0	6.68	3.25	541	0	5,809	66	62
Average MDA8 Ozone Concentration of Meteorologically Similar Days													**58** ± 8	**59** ± 7

Our analysis expanded on methods shown in the EPA guidance and a previously concurred exceptional event demonstration to identify six days that are meteorologically similar to September 2, 2020 (Arizona Department of Environmental Quality, 2018). In addition to ground measurements of temperature, winds, humidity, boundary layer thickness, and CAPE, regional synoptic patterns and spatial correlation of meteorology at two atmospheric levels were examined to identify meteorologically similar days. Results show that at each exceedance-affected site, the expected MDA8 ozone concentration is over 10 ppb below the concentrations measured on September 2, 2020. This validates the existence of an extrinsic ozone source on September 2, 2020.

3.3.3 GAM Statistical Modeling

Generalized additive models (GAM) are a type of statistical model that allows the user to predict a response based on linear and non-linear effects from multiple variables (Wood, 2017). These models tend to provide a more robust prediction than Eulerian photochemical models or simple comparisons of similar events (Simon et al., 2012; Jaffe et al., 2013; U.S. Environmental Protection Agency, 2016). Camalier et al. (2007) successfully used GAM modeling to predict ozone concentrations across the eastern United States using meteorological variables with r^2 values of up to 0.8. Additionally, previous concurred exceptional event demonstrations and associated literature, i.e., Sacramento Metropolitan Air Quality Management District (2011), Alvarado et al. (2015), Louisiana Department of Environmental Quality (2018), Arizona Department of Environmental Quality (2016), and Pernak et al. (2019) used GAM modeling to predict ozone events that exceed the NAAQS standards, some in EE cases. By comparing the GAM-predicted ozone values to the actual measured ozone concentrations (i.e., residuals), we can determine the effect of outside influences, such as wildfires or stratospheric intrusions, on ozone concentrations each day (Jaffe et al., 2004). High, positive residuals suggest a non-typical source of ozone in the area but cannot specifically identify a source. Gong et al. (2017) and McClure and Jaffe (2018) used GAM modeling, in addition to ground and satellite measurements of wildfire pollutants, to estimate the enhancement of ozone during wildfire smoke events. Similar to other concurred EE demonstrations, we used GAM modeling of meteorological and transport variables to estimate the MDA8 ozone concentrations at multiple sites across Clark County for 2014-2020. To estimate the effect of wildfire smoke on ozone concentrations, we can couple the GAM residual results (observed MDA8 ozone–GAM-predicted MDA8 ozone) with the other analyses to confirm that the non-typical enhancement of ozone is due to wildfires on September 2, 2020.

Using the same GAM methodology as prior concurred EE demonstrations and the studies mentioned above, we examined more than 30 meteorological and transport predictor variables, and through testing, compiled the 16 most important variables to estimate MDA8 ozone each day at eight monitoring sites across Clark County, Nevada (Paul Meyer, Walter Johnson, Joe Neal, Green Valley, Boulder City, Jean, Indian Springs, and Jerome Mack). As suggested by EPA guidance (U.S. Environmental Protection Agency, 2016), we used meteorological variables measured at each station (the previous day's MDA8 ozone, daily min/max temperature, average temperature, temperature range, wind speed, wind direction, or pressure), if available (see Table 2-1). If meteorological variables

were not available at a specific site, we supplemented the data with National Centers for Environmental Prediction (NCEP) reanalysis meteorological data to fill any data gaps. We also tested filling data gaps with Jerome Mack meteorological data and found results had no statistical difference. We used sounding data from KVEF (Las Vegas Airport) to provide vertical meteorological components; soundings are released at 00:00 and 12:00 UTC daily. Variables such as temperature, relative humidity, wind speed, and wind direction were averaged over the first 1000 m above the surface to provide near-surface, vertical meteorological parameters. Other sounding variables, such as Convective Available Potential Energy (CAPE), Lifting Condensation Level (LCL) pressure, mixing layer potential temperature, mixed layer mixing ratio, and 500-1,000 hPa thickness provided additional meteorological information about the vertical column above Clark County. We also initiated HYSPLIT GDAS 1°x1° 24-hour back trajectories from downtown Las Vegas (36.173° N, -115.155° W, 500 m agl) at 18:00 and 22:00 UTC (10:00 a.m. and 2:00 p.m. local standard time) each day to provide information on morning and afternoon transport during critical ozone production hours. We clustered the twice-per-day back trajectories from 2014-2020 into seven clusters. **Figure 3-54** shows the clusters, percentage of trajectories per cluster, and heights of each trajectory cluster. We identified a general source region for each cluster: (1) Northwest U.S., (2) Stagnant Las Vegas, (3) Central California, (4) Long-Range Transport, (5) Northern California, (6) Southern California, and (7) Baja Mexico. Within the GAM, we use the cluster value to provide a factor for the distance traveled by each back trajectory. Additionally, day of year (DOY) was used in the GAM to provide information on season and weekly processes. The year (2014, 2015, etc.) was used a factor for the DOY parameter to distinguish interannual variability.

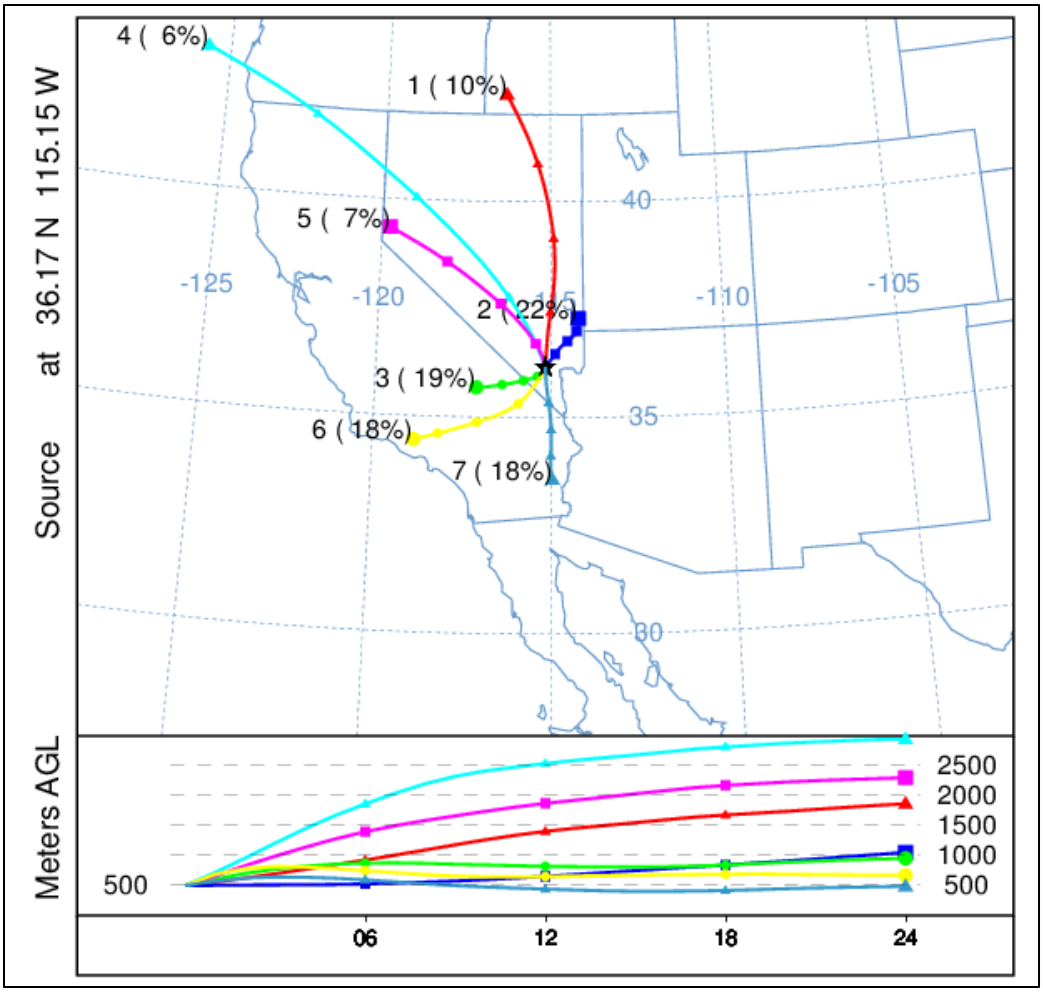

Figure 3-54. Clusters for 2014-2020 back trajectories. Seven unique clusters were identified for the twice daily (18:00 and 22:00 UTC) back-trajectories for 2014-2020 initiated in the middle of the Las Vegas Valley. The percentage of trajectories per cluster is shown next to the cluster number, and the height of each cluster is shown below the map.

Once all the meteorological and transport variables were compiled, we inserted them into the GAM equation to predict MDA8 ozone:

$$g(MDA8\ O_{3,i}) = f_1(V1_i) + f_2(V2_i) + f_3(V3_i) + \cdots + residual_i$$

where f_i are fit functions calculated from penalized cubic regression splines of observations (allowing non-linearity in the fit), Vi are the variables, and i is the daily observation. All variables were given a cubic spline basis except for wind direction, which used a cyclic cubic regression spline basis. For DOY and back trajectory distances, we used year factors (i.e., 2014-2020) and cluster factors (i.e., 1-7) to distinguish interannual variability and source region differences. The factors provide a different smooth function for each category (Wood, 2017). For example, the GAM smooth of DOY for 2014 can

be different than 2015, 2016, etc. In order to optimize the GAM, we first must adjust knots or remove any variables that are over-fitting or under-performing. We used the "mgcv" R package to summarize and check each variable for each monitoring site (Wood, 2020). A single GAM equation (using the same variables) was used for each monitoring site for consistency. During the initial optimization process, we removed the proposed 2018 and 2020 EE days from the dataset. We also ran 10 cross-validation tests by randomly splitting data 80/20 between training/testing for each monitoring site to ensure consistent results. All cross-validation tests showed statistically similar results with no large deviations for different data splits. We used data from each site during the April -September ozone seasons for 2014 through 2020, which is consistent with other papers modeling urban ozone (e.g., Pernak et al., 2019; McClure and Jaffe, 2018; Solberg et al., 2019; Solberg et al., 2018) and ozone concentrations during the periods with exceptional events are within the representative range of ozone in the GAM model.

Table 3-15 shows the variables used in the GAM and their F-value. The F-value suggests how important each variable is (higher value = more important) when predicting MDA8 ozone. Any bolded F-values had a statistically significant correlation ($p < 0.05$). R^2, the positive 95th quantile of residuals, and normalized mean square residual values for each monitoring site are listed at the bottom of the table.

Table 3-15. GAM variable results. F-values per parameter used in the GAM model are shown for each site. Units and data sources for each parameter in the GAM model are shown on the right of the table. The 95th quantile, R^2, and normalized mean square residual information are shown at the bottom of the table.

Parameters	Paul Meyer	Walter Johnson	Joe Neal	Green Valley	Jerome Mack	Boulder City	Jean	Indian Springs	Unit	Source
Day of Year (DOY) factored by Year (2014-2020)	**8.11**	**7.09**	**7.65**	**11.8**	**7.94**	**7.11**	**8.68**	**7.53**	--	--
Previous Day MDA8 Ozone	**37.9**	**22.7**	**41.5**	**18.1**	**27.9**	**31.3**	**105.5**	**123.8**	ppb	Monitor Data
Average Daily Temperature	1.92	**2.90**	**4.80**	0.05	1.83	2.13	0.12	1.83	K	Monitor Data/NCEP Reanalysis
Maximum Daily Temperature	1.37	**2.74**	**2.48**	0.16	0.38	0.02	1.30	1.52	K	
Temperature Range (TMax - TMin)	**4.12**	2.13	1.38	1.74	1.77	1.51	0.50	0.54	K	
Average Daily Pressure	**5.54**	**6.42**	**6.74**	**4.64**	**2.94**	0.22	2.17	0.24	hPa	
Average Daily Wind Speed	**11.1**	**5.03**	**7.49**	**5.02**	**15.3**	0.07	0.49	2.19	knots	
Average Daily Wind Direction	0.47	**1.04**	0.24	**1.35**	**2.43**	0.69	0.11	**2.48**	deg	
18 UTC HYSPLIT Distance factored by Cluster	1.70	1.82	1.69	0.92	2.52	2.97	1.66	1.03	km	HYSPLIT Back-Trajectories
22 UTC HYSPLIT Distance factored by Cluster	1.03	0.74	1.47	1.47	1.20	1.26	1.19	0.50	km	
00 UTC Convective Available Potential Energy	3.50	0.13	0.37	1.17	1.16	0.57	**5.71**	**6.49**	J/kg	Sounding Data
00 UTC Lifting Condensation Level Pressure	1.36	**2.78**	2.29	2.41	**3.76**	0.38	1.43	0.38	hPa	
00 UTC Mixing Layer Potential Temperature	0.65	0.79	1.72	0.10	1.23	0.97	1.09	2.53	K	
00 UTC Mixed Layer Mixing Ratio	**2.10**	**2.76**	**2.85**	**3.09**	**3.07**	**2.42**	0.69	1.04	g/kg	
00 UTC 500-1000 hPa Thickness	**2.91**	0.43	1.70	1.60	1.69	**4.11**	**2.18**	1.83	m	
12 UTC 1km Average Relative Humidity	**12.4**	**14.6**	**17.8**	**21.3**	**37.5**	**26.0**	**11.1**	2.18	%	
95th Quantile of Positive Residuals (ppb)	10	10	10	10	9	9	9	10		
R^2	0.55	0.58	0.60	0.58	0.61	0.58	0.57	0.55		
Normalized Mean Square Residual	3.6E-06	7.3E-04	6.1E-05	1.3E-04	3.1E-05	1.3E-04	1.2E-04	1.5E-04		

Table 3-16 provides GAM residual and fit results for all sites for the ozone seasons of 2014 through 2020. Overall, the residuals are low for all data points, and similarly low for all non-EE days. However, the 2018 and 2020 EE day residuals are significantly higher than the non-EE day results, meaning there are large, atypical influences on these days. Figure 3-55 shows non-EE vs EE median residuals with the 95th confidence intervals denoted as notches in the boxplots. We show the data in both ways to provide specific values, as well as illustrate the difference in non-EE vs EE residuals. Since the 95th confidence intervals for median EE residuals are above and do not overlap with those for non-EE residuals at any site in Clark County, we can state that the median residuals are higher and statistically different ($p<0.025$). The R^2 for each site ranged between 0.55 and 0.61, suggesting a good fit for each monitoring site, and similar to the results in prior studies and EE demonstrations mentioned previously (r^2 range of 0.4-0.8). We also provide the positive 95th quantile MDA8 ozone concentration, which is used to estimate a "No Fire" MDA8 ozone value based on the EPA guidance (U.S. Environmental Protection Agency, 2016). We also provide the median residuals (and confidence interval) for all non-EE days with observed MDA8 at or above 60 ppb; this threshold was needed to build a sufficient sample size with a representative distribution, and derive the median and 95% confidence interval. It should be noted that four out of the seven years modeled by the GAM were high wildfire years, and these values likely include a significant amount of wildfire days. We were not able to systematically remove wildfire influence by subsetting the Clark County ozone data based on HMS smoke, HMS smoke and $PM_{2.5}$ concentrations, and low wildfire years. These methods produced a significant number of false positives and negatives, and yielded datasets that were still affected by wildfire smoke. Therefore, these values should be considered an upper estimate of residuals for high ozone days. We see that the median residuals for 2018 and 2020 EE days are significantly higher than those on non-EE high observed ozone days since their confidence intervals do not overlap (or are comparable for the Jerome Mack station). The non-EE day residuals on days where observed MDA8 was at or above 60 ppb were determined to be normally distributed with a slight positive skew (median skewness = 0.39).

Table 3-16. Overall 2014-2020 GAM median residuals and 95% confidence interval range in square brackets for each site modeled. Sample size is shown in parentheses below the residual statistics. For sample sizes of less than ten, we include a range of residuals in square brackets instead of the 95% confidence interval. Residual results are split by non-EE days and the 2018 and 2020 EE days. R^2 for each site is also shown along with the positive 95th quantile result.

Site Name	All Residuals (ppb)	Non-EE Day Residuals (ppb)	2018 & 2020 EE Day Residuals (ppb)	R^2	Positive 95th Quantile (ppb)	Non-EE Day Residuals when MDA8 ≥ 60 ppb (ppb)
Boulder City	0.22 [-0.04, 0.48] (1,132)	0.22 [-0.04, 0.48] (1,130)	12.05 [10.38-13.72] (2)	0.58	9	4.05 [3.55, 4.55] (200)
Green Valley	0.17 [-0.15, 0.48] (948)	0.10 [-0.21, 0.41] (934)	7.38 [5.40, 9.36] (14)	0.58	10	3.76 [3.28, 4.23] (271)
Indian Springs	0.13 [-0.18, 0.44] (1,014)	0.08 [-0.22, 0.38] (1,010)	12.30 [9.37-17.19] (4)	0.55	10	4.79 [4.26, 5.32] (201)
Jean	0.21 [-0.06, 0.48] (1,149)	0.20 [-0.07, 0.47] (1,146)	12.57 [9.59-13.90] (3)	0.57	9	3.40 [2.94, 3.85] (290)
Jerome Mack	0.09 [-0.19, 0.36] (1,152)	0.05 [-0.22, 0.32] (1,141)	6.83 [4.21, 9.45] (11)	0.61	9	3.83 [3.32, 4.33] (242)
Joe Neal	0.23 [-0.08, 0.54] (1,113)	0.17 [-0.13, 0.47] (1,097)	7.77 [5.79, 9.75] (16)	0.60	10	3.32 [2.92, 3.71] (377)
Paul Meyer	0.21 [-0.08, 0.50] (1,159)	0.10 [-0.19, 0.39] (1,137)	8.11 [6.34, 9.88] (22)	0.55	10	3.58 [3.19, 3.97] (388)
Walter Johnson	0.27 [-0.03, 0.57] (1,163)	0.19 [-0.10, 0.48] (1,141)	7.16 [5.11, 9.21] (22)	0.58	10	3.53 [3.13, 3.93] (379)

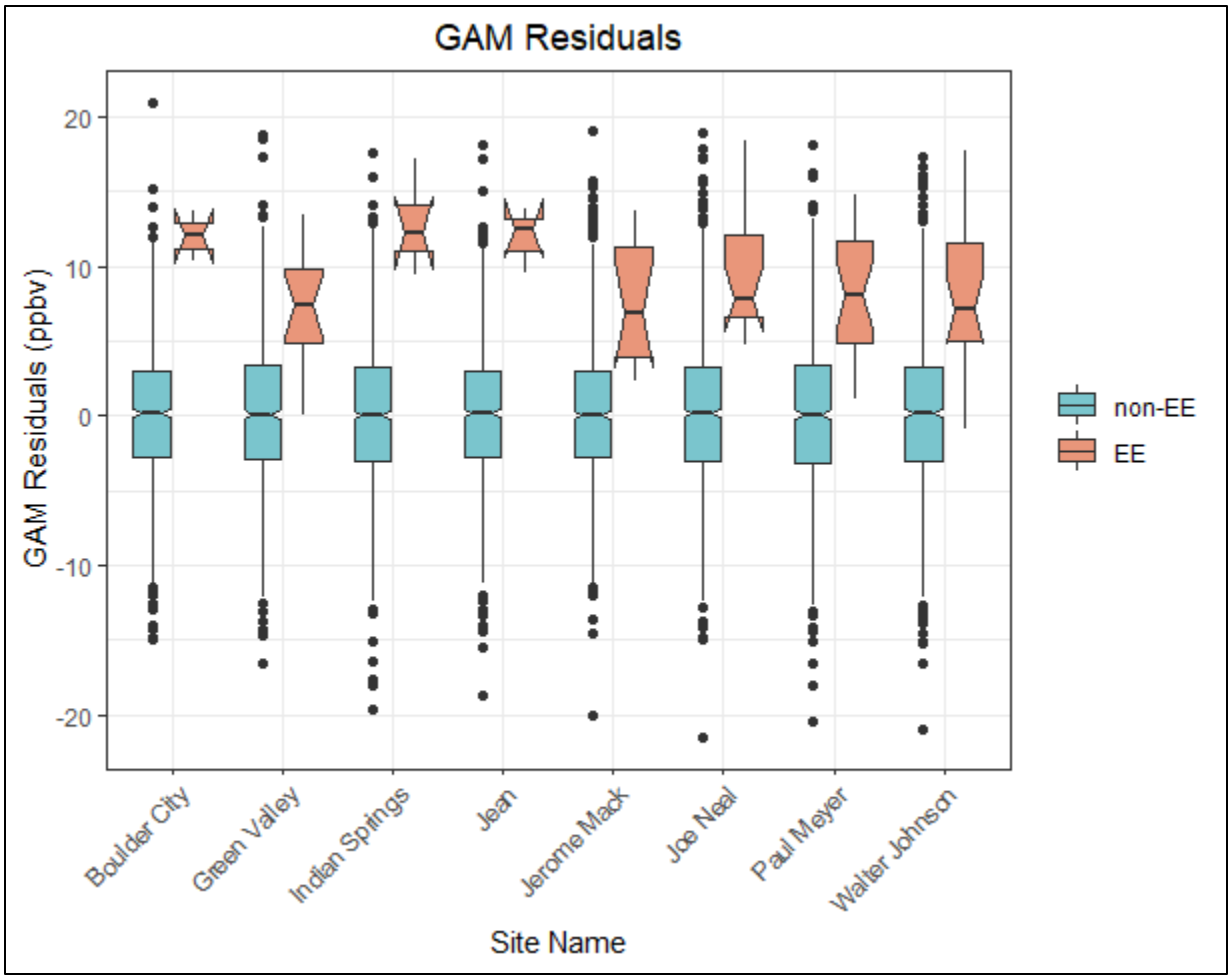

Figure 3-55. Exceptional event vs. non-exceptional event residuals. Non-exceptional events (non-EE in blue) and exceptional events (EE in orange) residuals are shown for each site modeled in Clark County. The notches for each box represent the 95th confidence interval. This figure illustrates the information in Table 3-16.

Overall, the GAM results show low bias and consistently significantly higher residuals on EE days compared with non-EE days. We also evaluated the GAM performance on verified high ozone, non-smoke days by looking at specific case studies. This was done to assess whether high-ozone days, such as the EE days, have a consistent bias that is not evident in the overall or high ozone day GAM performance. Out of the seven years used in the GAM model, four were high wildfire years in California (2015, 2017, 2018, and 2020). Since summer winds in Clark County are typically out of California (44% of trajectories originate in California according to the cluster analysis [not including transport through California in the Baja Mexico cluster]), wildfire smoke is likely to affect a large portion of summer days and influence ozone concentrations in Clark County. We identified specific case studies where most monitoring sites in Clark County had an MDA8 ozone concentration greater than or equal to 60 ppb and had no wildfire influence; "no wildfire influence" was determined by

inspecting HMS smoke plumes and HYSPLIT back trajectories for each day and confirming no smoke was over, near, or transported to Clark County. We found one to two examples from each year used in the GAM modeling, and required that at least half of the case study days needed to include an exceedance of the ozone NAAQS. **Table 3-17** shows the results of these case studies. Most case study days, including NAAQS exceedance days, show positive and negative residuals even when median ozone is greater than or equal to 65 ppb in Clark County, similar to the results for the entire multi-year dataset. GAM residuals on non-EE days when MDA8 is at or above 60 ppb have a median of 3.69 [95% confidence interval: 3.47, 3.88] (see Table 3-16). The high ozone, non-smoke case study days all show median residuals within or below the confidence interval of the high ozone residuals (from Table 3-16), meaning that the GAM model is able to accurately predict high ozone, non-smoke days within a reasonable range of error. Two additional factors indicate the GAM has good performance on normal, high ozone days: (1) the median residuals for the case studies are mostly lower than the 95% confidence interval of high ozone residuals (i.e., includes non-EE wildfire days), and (2) the case study days were verified as non-smoke days, Thus, residuals above the 95th confidence interval of the median residuals, such as those on the EE days, are statistically higher than on days with comparable high ozone concentrations, and not biased high because of the high ozone concentrations on these days.

Table 3-17. GAM high ozone, non-smoke case study results. Median GAM residuals for ten days in 2014-2020 are shown where most monitoring sites had MDA8 ozone concentrations of 60 ppb or greater. Sites used to calculate the MDA8 and GAM residual median/range are listed in the Clark County AQS Site Number column by site number.

Date	Clark County AQS Site Number	Median (Range) of Observed MDA8 Ozone (ppb)	Median (Range) GAM Residual (ppb)
5/17/2014	0601, 0075, 1019, 0540, 0043, 0071	66 (64-71)	1.66 (-0.53-4.28)
6/4/2014	0601, 0075, 0540, 1019, 0043, 0071	69 (66-72)	3.46 (1.70-4.80)
6/3/2015	1019, 0043, 0075, 0540, 7772, 0601, 0071	71 (65-72)	3.01 (-0.34-5.77)
6/20/2015	0601, 0298, 7772, 1019, 0540, 0075, 0043, 0071	65 (63-70)	1.40 (-6.20-5.28)
6/3/2016	0298, 1019, 0075, 0540, 0043, 0071	65 (63-71)	3.89 (1.89-5.26)
7/28/2016	0075, 0071, 0298, 0540, 0043	70 (63-72)	0.24 (-5.95-3.67)
6/17/2017	0601, 0075, 0071, 1019, 0540, 0298, 0043	66 (63-72)	1.85 (-1.94-7.01)
6/4/2018	0601, 0298, 7772, 1019, 0540, 0075, 0043, 0071	65 (60-67)	3.06 (-0.91-3.60)
5/5/2019	0601, 0298, 7772, 1019, 0540, 0075, 0043, 0071	65 (62-67)	1.28 (-2.00-3.42)
5/15/2020	0298, 0043, 0075, 0071	63 (63-65)	1.52 (1.09-3.49)

We also evaluate the bias of GAM residuals versus predicted MDA8 ozone concentrations in Figure 3-56. Residuals (i.e., observed ozone minus GAM-predicted MDA8 ozone) should be independent of the GAM-predicted ozone value, meaning that the difference between the actual ozone concentration on a given day and the GAM output should be due to outside influences and not well described by meteorological or seasonal values (i.e., variables used in the GAM prediction). Therefore, in a well-fit model, positive and negative residuals should be evenly distributed across all

GAM-predicted ozone concentrations and on average zero. In Figure 3-56, we see daily GAM residuals at all eight monitoring sites in Clark County from 2014-2020, the residuals are evenly distributed across all GAM-predicted ozone concentrations, with no pattern or bias at high or low MDA8 fit concentrations. This evaluation of bias in the model is consistent with established literature and other EE demonstrations (Gong et al., 2018; McVey et al., 2018; Texas Commission on Environmental Quality, 2021; Pernak et al., 2019), and indicate a well-fit model. In **Figure 3-57**, we also provide a histogram of the residuals at each monitoring site modeled in Clark County. This analysis shows that residuals at each site are distributed normally around a median near zero, and none of the distributions shows significant tails at high or low residuals (median skew = 0.05 with 95% confidence interval [-0.03, 0.12]). This analysis of error in the model and our results are consistent with previously concurred EE demonstrations (Arizona Department of Environmental Quality, 2016) and previous literature (Jaffe et al., 2013; Alvarado et al., 2015; Gong et al., 2017; McClure and Jaffe, 2018; Pernak et al., 2019). **Appendix D** provides GAM residual analysis from the concurred ADEQ and submitted TCEQ demonstrations that compare well with our GAM residual results. Based on these analysis methods, bias in the model is low throughout the range of MDA8 prediction values and confirms that the GAM can be used to predict MDA8 ozone concentrations in Clark County.

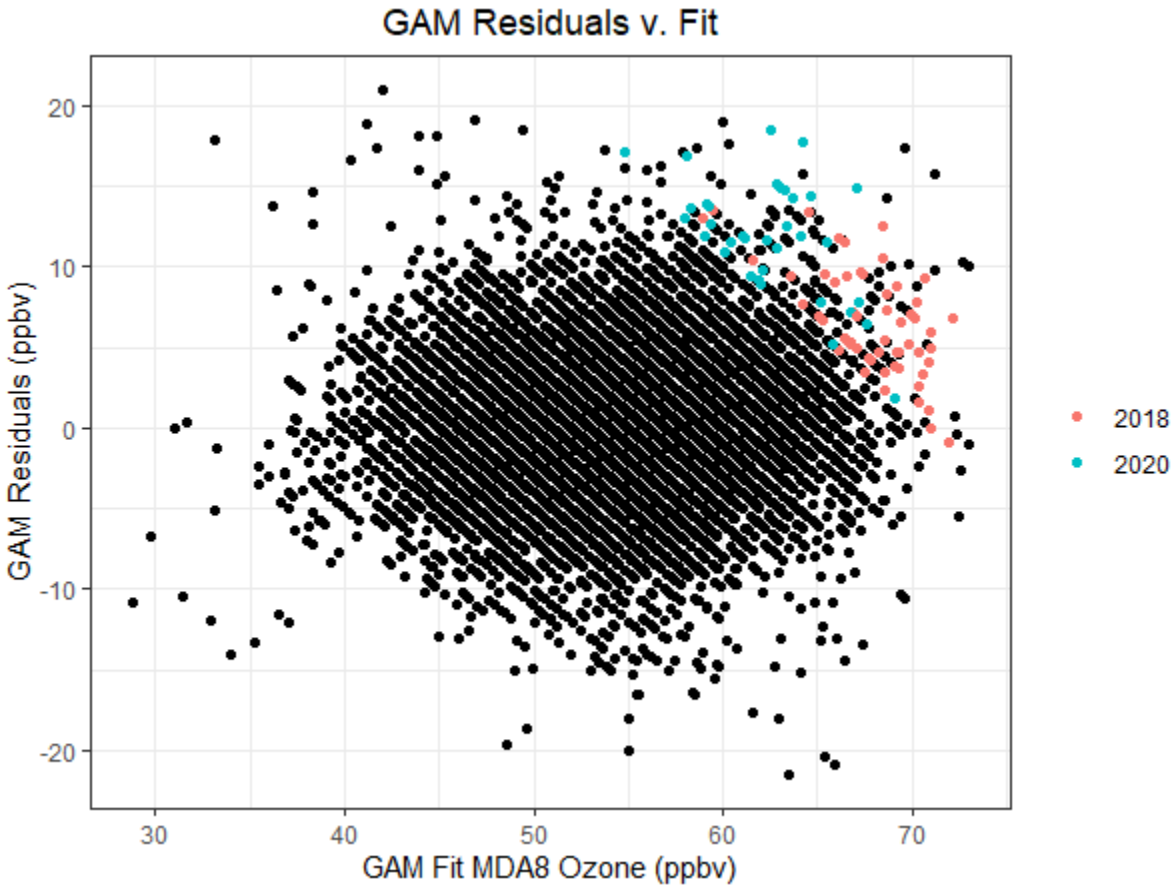

Figure 3-56. Daily GAM residuals for 2014-2020 vs GAM Fit (Predicted) MDA8 Ozone values. 2018 and 2020 exceptional events residuals are shown in red and blue.

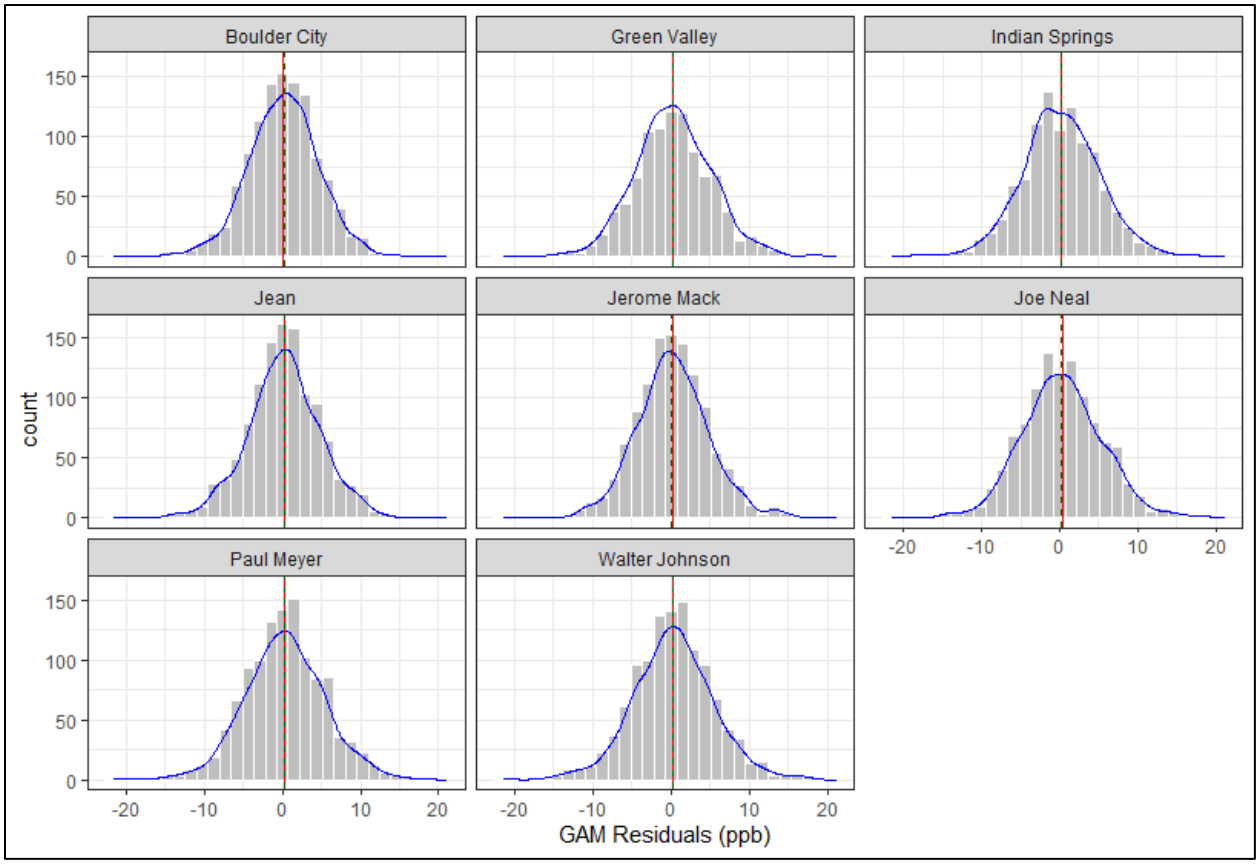

Figure 3-57. Histogram of GAM residuals at all modeled Clark County monitoring sites. The red line indicates the mean and the green dashed line indicates the median. The blue line provides the density distribution.

Within the GAM model, we include HYSPLIT 24-hour distance values, which are factored by cluster, to provide source region and stagnation information into the algorithm. A major upwind pollution source for Las Vegas is the Los Angeles Basin (see the Southern California cluster), which is around 400 km away. Since the GAM model uses source region and distance traveled information to help predict daily MDA8 ozone concentrations, contributions from LA should be accounted for in the algorithm. Based on this, we can assess whether GAM residuals on LA-source region days were significantly different from other source regions. In **Figures 3-58 and 3-59**, we subset the GAM results by removing any potential EE days. From these results, we find that both morning (18:00 UTC) and afternoon (22:00 UTC) trajectory data have similar distributions for all clusters. The notches in the box plots (representing the 95th confidence interval) provide an estimate of statistical difference, and show that the median of residuals is near zero for all clusters. The Northwest U.S. cluster at 18:00 UTC shows slightly negative residuals, while the Long-Range Transport cluster shows slightly positive residuals for both 18:00 and 22:00 UTC. The Southern California cluster shows a median residual of around zero for both 18:00 and 22:00 UTC trajectories, with significant overlap between the 95th confidence intervals of most other clusters (not statistically different). Additionally, the number of data points per cluster (bottom of each figure) corresponds well with transport from California being

dominant for the April through September time frame. Overall, this analysis provides evidence that even when the Los Angeles Basin (Southern California cluster) is upwind of Las Vegas, the GAM model performs well (low median residuals), and the results are statistically similar to most of the other clusters. This implies that when residuals are large, the Los Angeles Basin's influence is unlikely to be the only contributor to enhancements in MDA8 ozone.

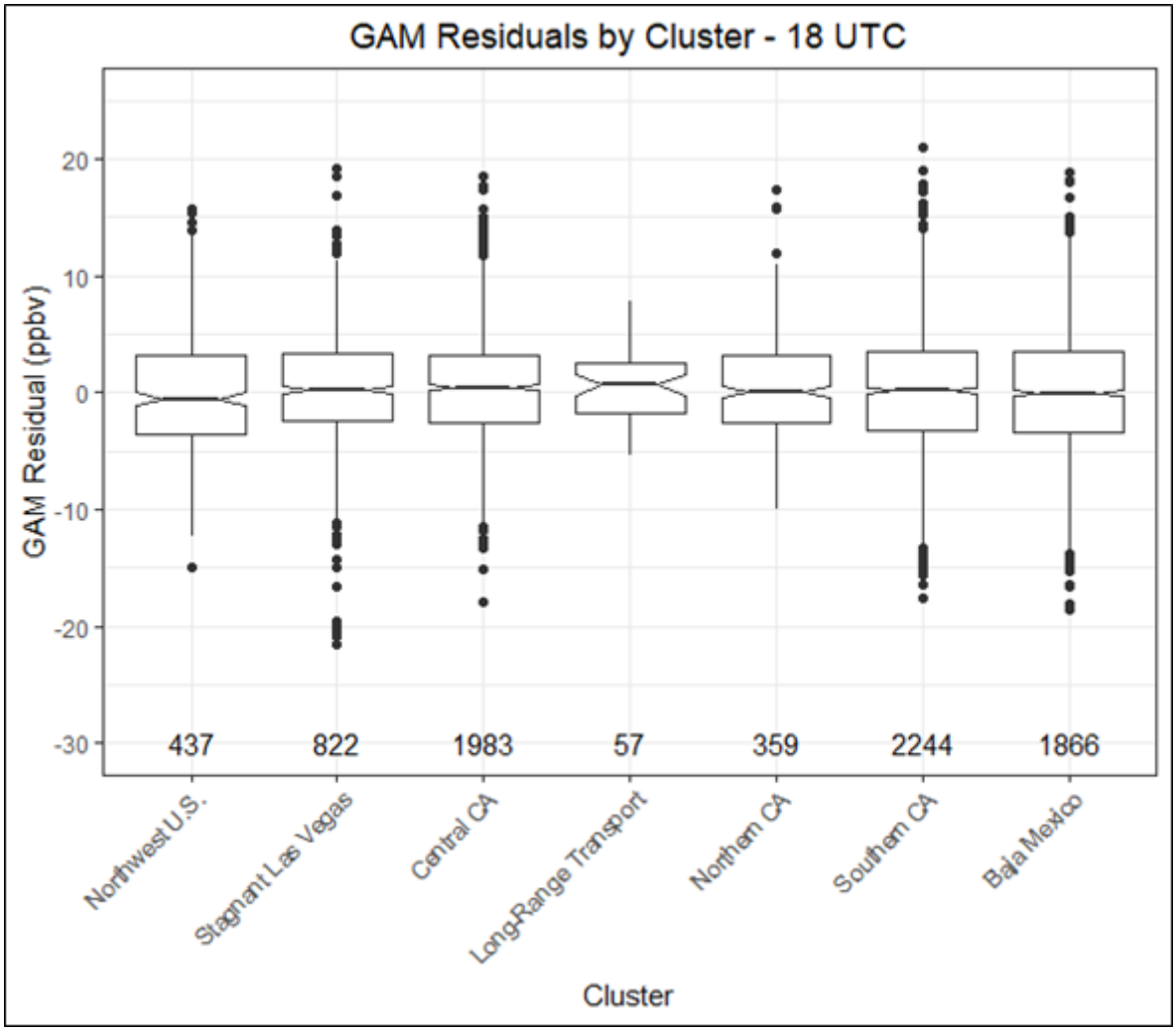

Figure 3-58. GAM cluster residual results for 18:00 UTC. The cluster is determined by grouping 24-hour back trajectories from Las Vegas based on their path. Clusters were created by using back trajectory results from Clark County between 2014 and 2020 (EE days were removed).

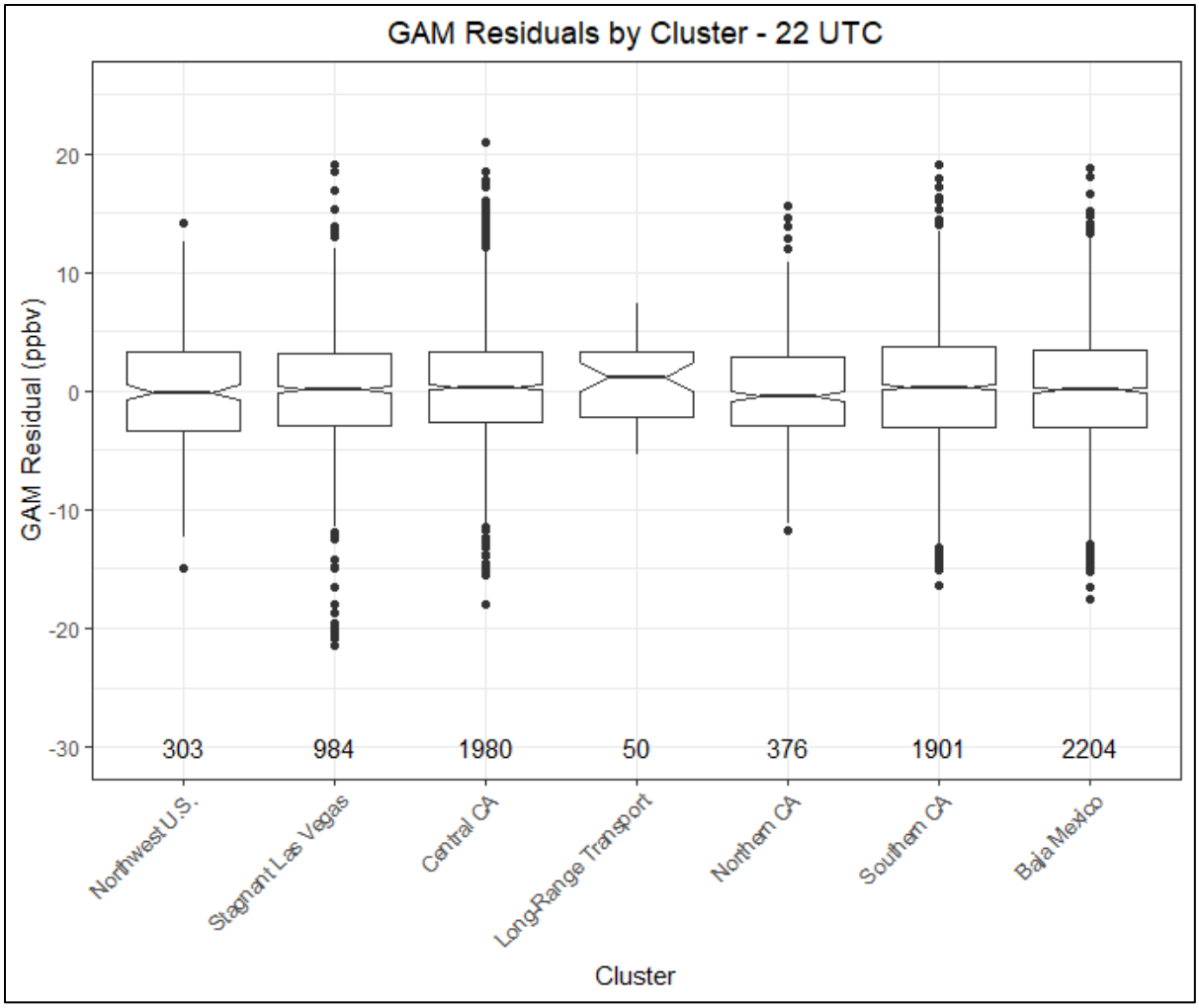

Figure 3-59. GAM cluster residual results for 22:00 UTC. The cluster is determined by grouping 24-hour back trajectories from Las Vegas based on their path. Clusters were created by using back trajectory results from Clark County between 2014 and 2020 (EE days were removed).

Mobile emissions sources decreased throughout the U.S. after COVID restrictions went into place in March 2020. Based on emission inventories from Las Vegas, on-road emissions make up a significant portion of the NO_x emissions inventory (see Section 2.3 for more details). Based on traffic data from the Nevada Department of Transportation, on-road traffic in Clark County in 2020 was significantly different than 2019 through early to mid-June (depending on the area where traffic volume was measured; see **Appendix E** for more details). **Figure 3-60** provides a scatter plot of MDA8 ozone observed versus GAM fit for all eight monitoring sites, separated by year. The linear regression fit, slope, and intercept do not show large difference between 2020 and other modeled years. **Figure 3-61** provides a more in-depth look at the most heavily affected months due to COVID restrictions and traffic changes (April – May 2020). The 95th confidence interval (shown as a notch in the box plots) show overlap between 2020 and most other years (except 2015 and 2016). The May 6, 9, and 28 EE days are included in the 2020 box. This analysis shows that there was not a statistically

different GAM response in 2020 compared with other years; this is confirmed in the COVID analysis section (Appendix E), where we show that MDA8 ozone during April – May 2020 in Las Vegas was not statistically different from previous years. While the reduction in traffic emissions due to COVID restrictions did not affect the September 2 event, we thought it was important to address the effects of COVID restrictions on the 2020 GAM results. Overall, ozone in Clark County did not change significantly and, similarly, GAM results were not significantly affected.

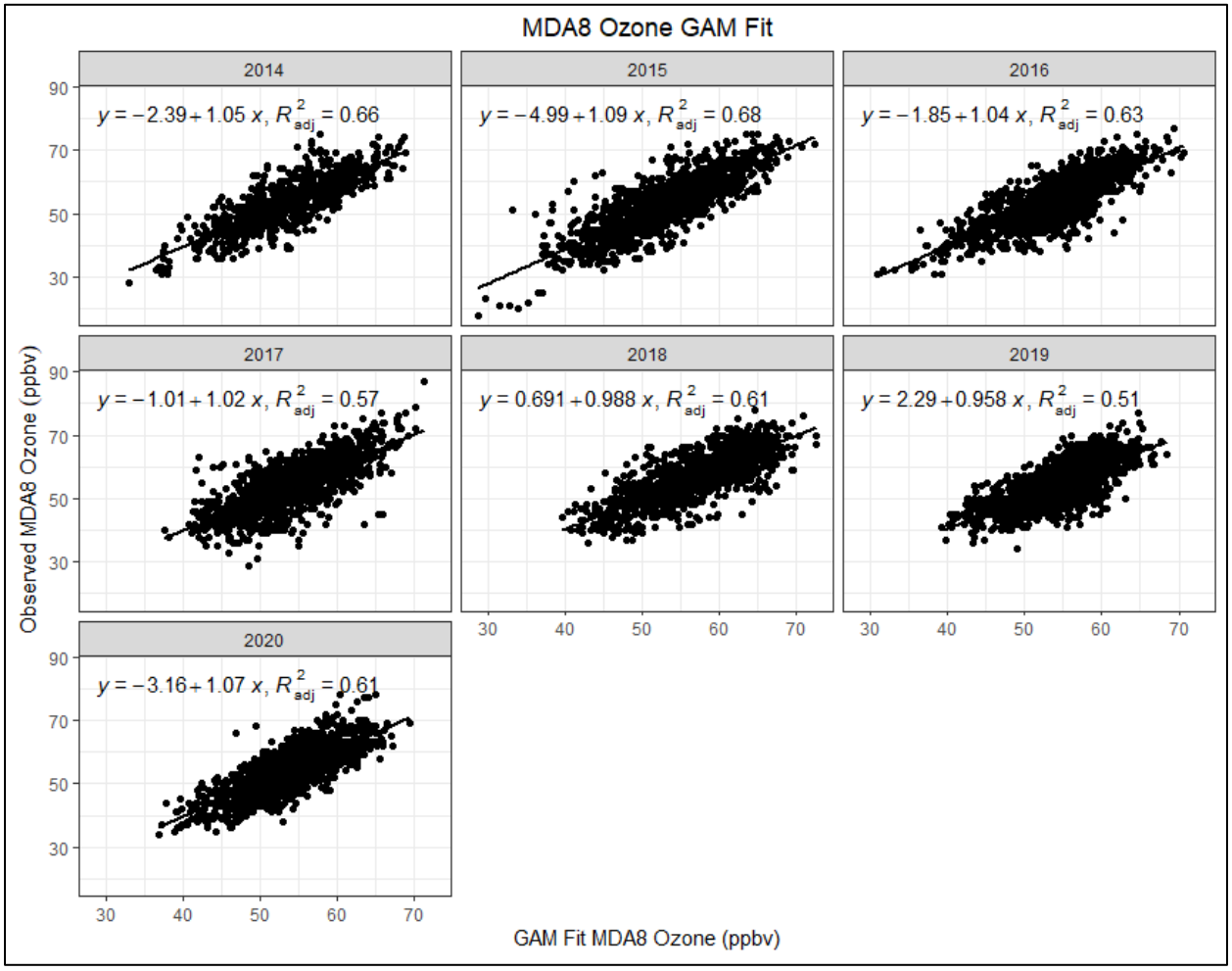

Figure 3-60. Observed MDA8 ozone vs. GAM fit ozone by year. The relationship between observed MDA8 ozone and GAM fit ozone at all eight modeled monitoring sites in Clark County is broken out by year, with linear regression and fit statistics shown (slope, intercept, and r^2). EE days are not included in the regression equations.

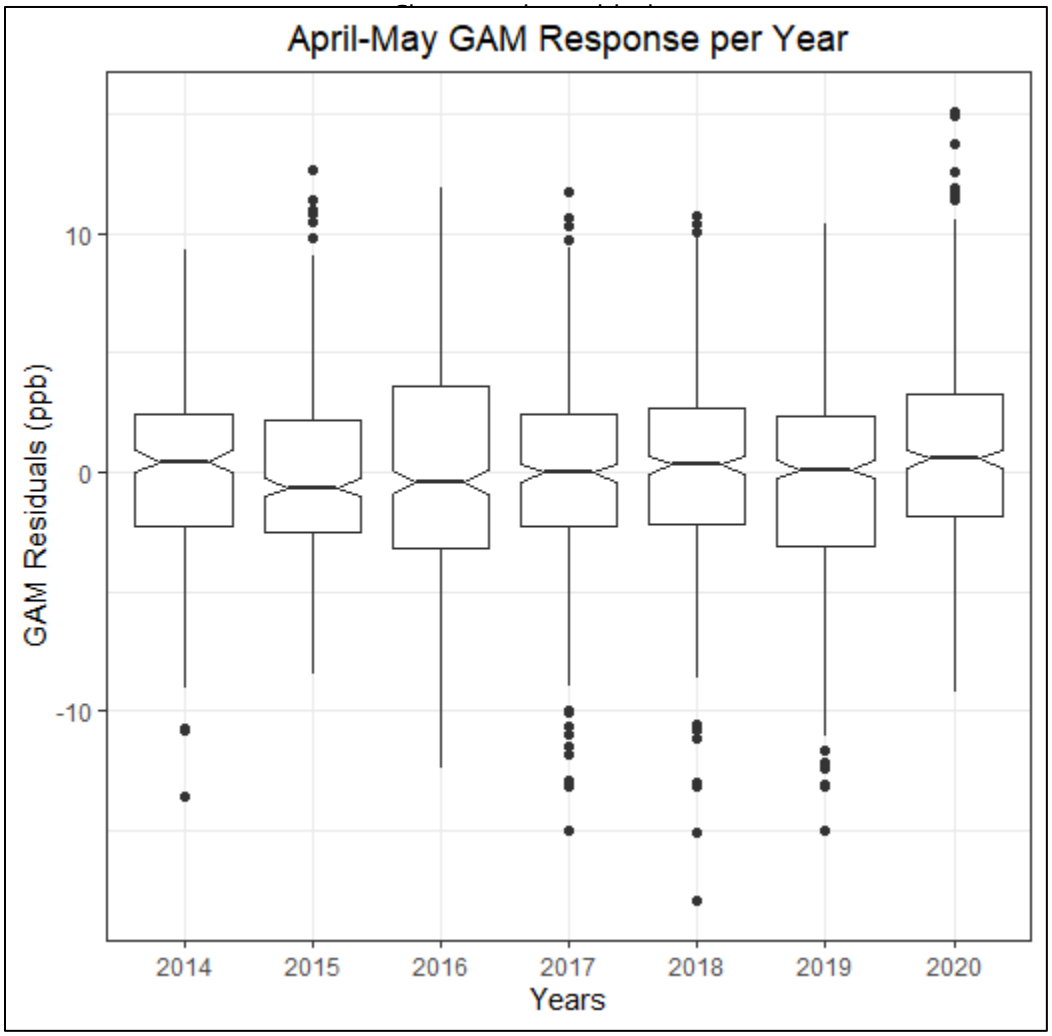

Figure 3-61. April–May Interannual GAM Response. April–May residuals per year from 2014–2020 are plotted for all eight modeled monitoring sites in Clark County. The potential EE days of May 6, 9, and 28 are included.

Figure 3-62 provides the observed MDA8 ozone versus GAM Fit MDA8 from 2014 through 2020 for the sites affected on September 2 (Paul Meyer and Walter Johnson). We marked the possible 2020 (red), 2018 (blue), and other (purple) EE days to show that observed MDA8 ozone on these days is higher than those predicted by the GAM. The other (purple) points are from 2014–2016 and are suspected wildfire events, as indicated in EPA AQS record. We also highlight the September 2, 2020, EE day as a large red triangle in each figure. Linear regression statistics (slope, intercept, and r^2) are also provided for context. Both linear regressions show a slope near unity, and a low intercept value (around 4 ppb) with a good fit r^2 value.

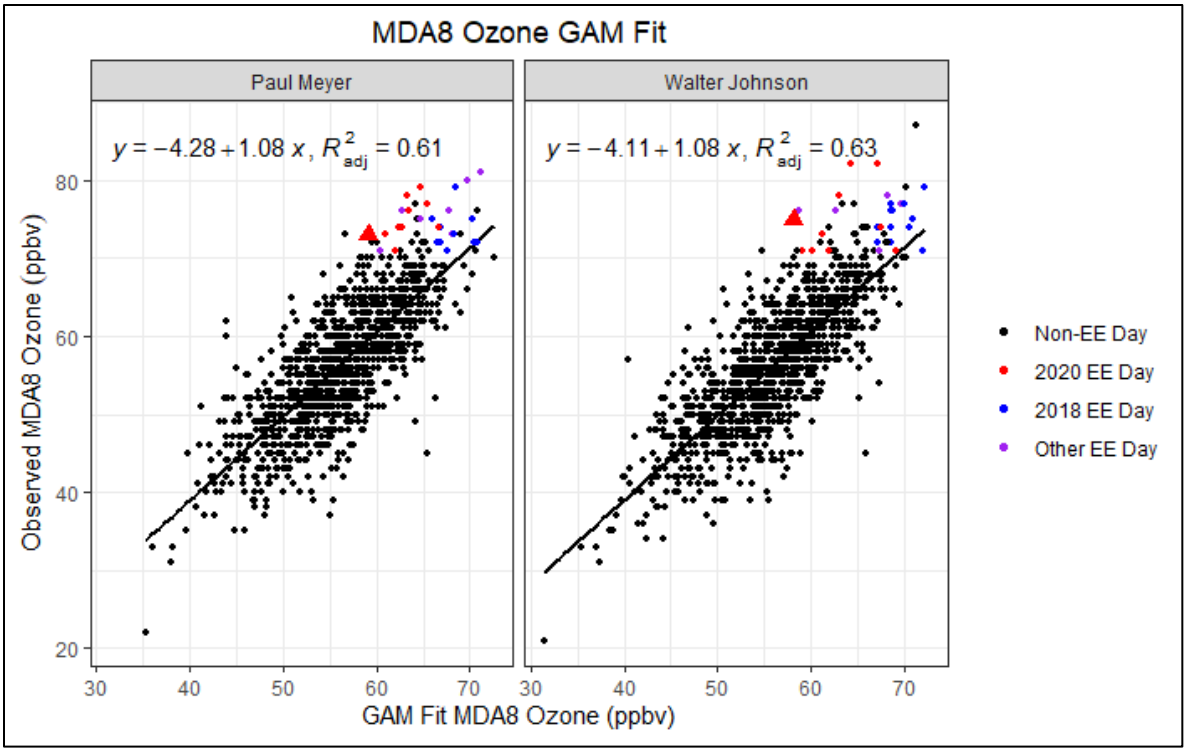

Figure 3-62. GAM MDA8 Fit versus Observed MDA8 ozone data from 2014 through 2020 for the EE affected sites on September 2, 2020. Black circles indicate data not associated with the 2018 or 2020 EE days, red circles indicate 2020 EE days, blue circles indicate 2018 EE days, and purple circles indicate 2014-2016 EE days. September 2 is shown as a red triangle. The black line is the linear regression of the data, and statistics (equation and r^2 value) are shown in the top of each sub-figure.

Table 3-18 provides the GAM results for September 2, 2020, at each monitoring site affected by the EE. GAM residuals show a modeled wildfire impact between 14 and 17 ppb for all monitoring sites, with MDA8 GAM prediction values well below the 0.070 ppm standard. EPA guidance requires a further level of investigation; by adding the GAM MDA8 Prediction value and the Positive 95th quantile of residuals, we calculated the "No Fire" MDA8 ozone value. The difference between the observed and "No Fire" MDA8 ozone value (6 to 7 ppb) is a conservative estimate of the influence of wildfire smoke at each site. Due to the large number of wildfires affecting Clark County during the seven-year modeling period, we also calculate the "No Fire" and minimum predicted fire influence given the 75th percentile (9 to 12 ppb). This provides a range of minimum smoke enhancement (4 to 12 ppb). The actual enhancement due to wildfire smoke likely lies between the minimum smoke enhancement estimate and the GAM residual. Previous studies and concurred EE demonstrations show and discuss the limitations of the 95th positive percentile evaluation (Miller et al., 2014; Arizona Department of Environmental Quality, 2016). Additionally, production of ozone is an extremely complex process that can only be predicted by meteorological variables in a GAM model with a 50-80% correlation based on previously cited papers (our GAM model shows a 55-61% correlation). In our case, this leaves exceptional events, wildfire influence during high wildfires years, stratospheric

intrusions, non-normal emissions, non-normal meteorology, etc., which make up the other 39-45%. Due to the large number of high wildfires years used in the GAM model, we assert that the minimum predicted fire influence value (as determined by the positive 95^{th} quantile) should not be used as strict guideline for actual fire influence. Based on the values from the GAM model, we see a significant, non-typical enhancement in MDA8 ozone concentrations at the affected Clark County monitoring sites on September 2, 2020.

Table 3-18. September 2 GAM results and residuals for each site. The GAM residual is the difference between observed MDA8 ozone and the GAM Prediction. We also estimate the minimum predicted fire influence based on the positive 95th quantile and GAM prediction value.

Site Name	MDA8 O_3 Concentration[a] (ppm)	MDA8 GAM Prediction[b] (ppm)	GAM Residual (ppm)	Positive 75th-95th Quantile[c] (ppm)	"No Fire" MDA8[b+c] (ppm)	Minimum Predicted Fire Influence[a-(b+c)] (ppm)
Paul Meyer	0.073	0.059	0.014	0.005-0.010	0.064-0.069	0.004-0.009
Walter Johnson	0.075	0.058	0.017	0.005-0.010	0.063-0.068	0.007-0.012

Finally, Figure 3-63 shows a two-week time series of observed MDA8 ozone values across Clark County and the GAM prediction values at those sites. September 2, 2020, shows the large gap between observed MDA8 ozone and the GAM-predicted values. Outside of the possible EE day, the GAM prediction values are very close to the observed values, suggesting that immediately before and after the event, we are able to accurately predict typical fluctuations in ozone on non-event days.

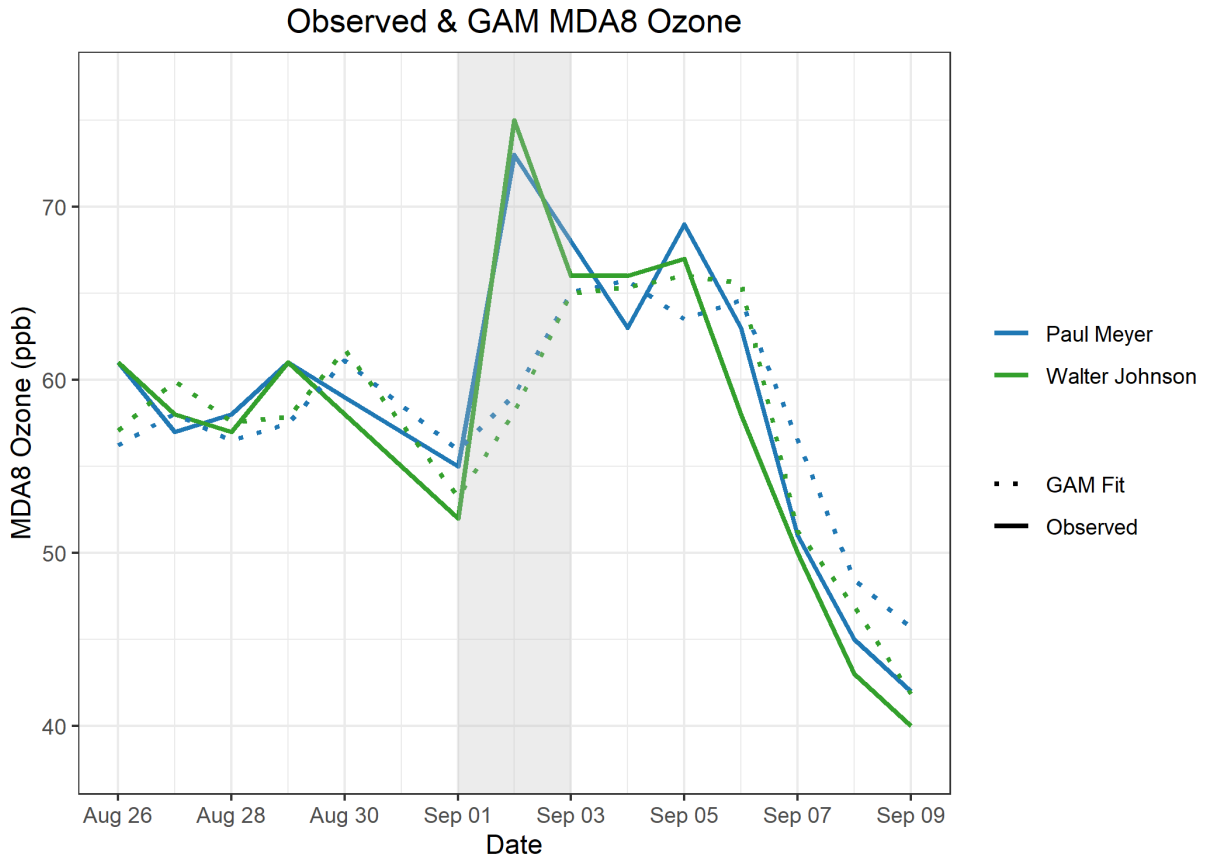

Figure 3-63. GAM time series showing observed MDA8 ozone for two weeks before and after the September 2 EE (solid lines). The GAM MDA8 ozone fit value is also shown for two weeks before and after September 2 (dotted line).

Overall, the GAM evidence clearly demonstrates that a non-typical source of ozone significantly impacted concentrations at both EE-affected Clark County sites on September 2, 2020. Coupled with wildfire smoke evidence from all other tiers of analyses, we can conclude by weight of evidence that the enhancement in ozone concentration was due to smoke from the wildfires in California and Oregon that was transported to Clark County, Nevada.

3.4 Clear Causal Relationship Conclusions

The analyses conducted in this report support the impact of smoke from the large, naturally caused wildfires in California and Oregon on ozone concentrations in Clark County, Nevada, on September 2, 2020. We find that:

1. Visible satellite imagery, news articles, and trajectories support the conclusion of smoke transport from California and Oregon to Clark County.
2. A large mixing layer, aerosols in the vertical profile, back trajectories starting aloft near the fire and ending at the surface in Clark County, and surface enhancements of wildfire-related pollutants (e.g., $PM_{2.5}$, NO_x, and Levoglucosan) in Clark County support the conclusion that smoke was mixed down to the surface in Clark County.
3. Comparisons with non-event concentrations, meteorologically similar matching day analysis, and GAM statistical modeling support the conclusion that the ozone concentrations seen in Clark County were significantly above typical summer concentrations for the meteorological conditions on the day.

The analyses presented in this report fulfill the requirements for a Tier 3 EE demonstration, and all conclusions for each type of analysis are summarized in Table 3-19. The effect of these large fire complexes in California and Oregon on Clark County caused ozone exceedances at the Paul Meyer and Walter Johnson monitoring stations. Based on evidence that the west coast fires were natural events and unlikely to recur, as well as the clear causal relationship between the wildfire events and the monitored exceedances, we conclude that the ozone exceedance event on September 2, 2020, in Clark County was not reasonably controllable or preventable.

Table 3-19. Results for each tier analysis for the September 2 EE.

Tier	Requirements	Finding
1	• Comparison of fire-influenced exceedance with historical concentrations • Key factor: Evidence that fire and monitor meet one of the following criteria: — Seasonality differs from typical season, or — Ozone concentrations are 5-10 ppb higher than non-event related concentrations • Evidence of transport of fire emissions to monitor: — Trajectories of fire emissions (reaching ground level), or — Satellite Images and supporting evidence from surface measurements — Media coverage and photographic evidence of smoke	• The September 2, 2020, ozone exceedance occurred during a typical ozone season, but event concentrations were significantly higher than non-event concentrations. • Trajectories, satellite images, media coverage, and ground images support smoke transport from the California and Oregon fires into Clark County.
2	• All Tier 1 requirements • Key Factor #1: Fire emissions and distance of fires • Key Factor #2: Comparison of the event-related ozone concentration with non-event-related high ozone concentrations (high percentile rank over five years/seasons) — Annual and seasonal comparison • Evidence that fire emissions affected the monitor (at least one of the following): — Visibility impacts — Changes in supporting measurements — Satellite enhancements of fire-related species (i.e., NOx, CO, AOD, etc.) — Fire-related enhancement ratios and/or tracer species — Differences in spatial/temporal patterns	• Q/D values for the Lionshead, White River, and California fires were well below 100. • Ozone concentrations at all sites showed high percentile rank over the past six years and ozone seasons. • Surface concentrations of supporting pollutants (e.g., $PM_{2.5}$, NO_x, CO) show enhanced concentrations and changes in typical diurnal profiles, consistent with smoke. • Satellite measurements also show enhanced levels of fire-related species near the source regions. • Levoglucosan, a wildfire tracer, showed a positive detection during this event.
3	• All Tier 2 requirements • Evidence of fire emissions effects on monitor: — Multiple analyses from those listed for Tier 2 • Evidence of fire emissions transport to the monitor: — Trajectory or satellite plume analysis, and — Additional discussion of meteorological conditions • Additional evidence such as: — Comparison to ozone concentrations on matching (meteorologically similar) days — Statistical regression modeling — Photochemical modeling of smoke contributions to ozone concentrations	• Meteorology patterns during this event show transport from the Pacific Northwest and California to Clark County. • Vertical profiles show vertical mixing and transport to the surface as well as increased aerosol in the column. • Meteorologically similar day analysis shows that average MDA8 ozone across similar days was well below the ozone NAAQS and 10 ppb lower than the September 2 exceedance at both sites. • GAM statistical modeling predicts ozone concentrations lower than observed, suggesting an impact from non-typical sources on ozone concentrations in Clark County during this event.

4. Natural Event Unlikely to Recur

A wildfire is defined in 40 CFR 50.1(n) as "any fire started by an unplanned ignition caused by lightning; volcanoes; other acts of nature; unauthorized activity; or accidental, human-caused actions, or a prescribed fire that has developed into a wildfire. A wildfire that predominantly occurs on wildland is a natural event." Furthermore, a "wildland" is "an area in which human activity and development are essentially non-existent, except for roads, railroads, power lines, and similar transportation facilities. Structures, if any, are widely scattered." 40 CFR 50.1(o). As shown in Table 3-3, each fire that contributed to this event was cause by either lightning, or accidental, human-caused actions, and therefore meets the definition of wildfire. Based on the documentation provided in Section 3.2.1 of this submittal, the collection of large fires throughout California and Oregon that contributed to wildfire smoke in Clark County predominately took place on wildlands designated as National Forests, as seen in Figure 3-26. Therefore, under 40 CFR §50.1, each wildfire listed in Table 3-3 can be classified as natural event that is unlikely to recur. Accordingly, the Clark County Department of Environment and Sustainability has shown in this submittal that smoke from California and Oregon wildfires, which led to an ozone exceedance in Clark County of September 2, 2020, may be considered for treatment as an EE.

5. Not Reasonably Controllable or Preventable

As shown by the documentation provided in Section 3.2.1 of this submittal, each wildfire listed in Table 3-3 burned predominantly on wildland. The Exceptional Events rule stated in 40 CFR 50.1(j) indicates that a wildfire that occurs on wildland is not reasonably controllable or preventable. Previous sections of this report have shown that each fire referenced in this report was a wildfire that occurred on wildland. The InciWeb report for each incident indicates that these wildfires burned across vast areas in generally inaccessible land, limiting firefighting efforts in each event (https://inciweb.nwcg.gov/). The Clark County Department of Environment and Sustainability is not aware of any evidence clearly demonstrating that prevention or control efforts beyond those made would have been reasonable. Therefore, the emissions that caused exceedances at monitors in Clark County on September 2 are neither reasonably controllable or preventable.

6. Public Comment

This exceptional event demonstration will undergo a 30-day public comment period concurrent with EPA's review beginning July 1, 2021. A copy of the public notice, along with any comments received and responses to those comments, will be submitted to EPA after the comment period has closed, consistent with the requirements of 40 CFR 50.14(c)(3)(v). **Appendix F** contains documentation of the public comment process.

7. Conclusions and Recommendations

The analyses conducted in this report support the conclusion that smoke from large complex wildfires in California and Oregon impacted ozone concentrations in Clark County, Nevada, on September 2, 2020. This EE demonstration has provided the following elements required by the EPA guidance for wildfire EEs (U.S. Environmental Protection Agency, 2016):

1. A narrative conceptual model that describes the wildfires in California and Oregon and how the emissions from these wildfires led to ozone exceedances downwind in Clark County (Sections 1 and 2).
2. A clear causal relationship between the California and Oregon wildfires and the September 2 exceedance through ground and satellite-based measurements, air mass trajectories, emission modeling, comparison with non-event concentrations, vertical profile analysis, meteorologically similar day analyses, and statistical modeling (Section 3).
3. Event ozone concentrations at or above the 99th percentile when compared with the last six years of observations at each site and among the four highest ozone days at each site (excluding other 2018 and 2020 EE events – Section 3).
4. All of the wildfires in California and Oregon were determined to be caused by lighting (except for two whose causes were unknown) and began in wildland area where they grew rapidly and quickly beyond firefighting controls, classifying this event as natural and unlikely to recur (Section 4).
5. Demonstration that the California and Oregon wildfires that transported emissions to Clark County were neither reasonably controllable or preventable (Section 5).
6. This demonstration went through the public comment process via Clark County's Department of Environment and Sustainability (Section 6).

The major conclusions and supporting analyses found in this report are:

1. Visible satellite imagery, news articles, and trajectories support the conclusion of smoke transport from the California and Oregon wildfires to Clark County.
2. A large mixing layer, aerosols in the vertical profile, back trajectories starting aloft near the fire and ending at the surface in Clark County, and surface enhancements of wildfire-related pollutants in Clark County support the conclusion that smoke was mixed down to the surface in Clark County.
3. Comparisons with non-event concentrations, meteorologically similar matching day analysis, and GAM statistical modeling support the conclusion that the ozone concentrations seen in Clark County were well above typical summer concentrations.

The analyses presented in this report fulfill the requirements for a Tier 3 EE demonstration, and all conclusions for each type of analysis are summarized in Table 3-19. The effect of the California and Oregon wildfires on Clark County caused ozone exceedances at the Paul Meyer and Walter Johnson monitoring stations. Based on evidence that the California and Oregon wildfires were natural events and unlikely to recur, as well as the clear causal relationship between the wildfire events and the monitored exceedances, we conclude that the ozone exceedance event on September 2, 2020, in Clark County was not reasonably controllable or preventable.

8. References

Alvarado M., Lonsdale C., Mountain M., and Hegarty J. (2015) Investigating the impact of meteorology on O_3 and $PM_{2.5}$ trends, background levels, and NAAQS exceedances. Final report prepared for the Texas Commission on Environmental Quality, Austin, TX, by Atmospheric and Environmental Research, Inc., Lexington, MA, August 31.

Arizona Department of Environmental Quality (2016) State of Arizona exceptional event documentation for wildfire-caused ozone exceedances on June 20, 2015 in the Maricopa nonattainment area. Final report, September. Available at https://static.azdeq.gov/pn/1609_ee_report.pdf.

Arizona Department of Environmental Quality (2018) State of Arizona exceptional event documentation for wildfire-caused ozone exceedances on July 7, 2017 in the Maricopa Nonattainment Area. Final report, May. Available at https://static.azdeq.gov/pn/Ozone_2017ExceptionalEvent.pdf.

Bhattarai H., Saikawa E., Wan X., Zhu H., Ram K., Gao S., Kang S., Zhang Q., Zhang Y., Wu G., Wang X., Kawamura K., Fu P., and Cong Z. (2019) Levoglucosan as a tracer of biomass burning: recent progress and perspectives. *Atmospheric Research*, 220, 20-33, doi: 10.1016/j.atmosres.2019.01.004. Available at http://www.sciencedirect.com/science/article/pii/S0169809518311098.

Brey S.J. and Fischer E.V. (2016) Smoke in the city: how often and where does smoke impact summertime ozone in the United States? *Environ. Sci. Technol.*, 50(3), 1288-1294, doi: 10.1021/acs.est.5b05218, 2016/02/02.

Bytnerowicz A., Cayan D., Riggan P., Schilling S., Dawson P., Tyree M., Wolden L., Tissell R., and Preisler H. (2010) Analysis of the effects of combustion emissions and Santa Ana winds on ambient ozone during the October 2007 southern California wildfires. *Atmospheric Environment*, 44, 678-687, doi: 10.1016/j.atmosenv.2009.11.014.

Camalier L., Cox W., and Dolwick P. (2007) The effects of meteorology on ozone in urban areas and their use in assessing ozone trends. *Atmospheric Environment*, 41, 7127-7137, doi: 10.1016/j.atmosenv.2007.04.061.

Clark County Department of Air Quality (2019) Ozone Advance program progress report update. August.

Clark County Department of Environment and Sustainability (2020) Revision to the Nevada state implementation plan for the 2015 Ozone NAAQS: emissions inventory and emissions statement requirements. September. Available at https://files.clarkcountynv.gov/clarknv/Environmental%20Sustainability/SIP%20Related%20Documents/O3/20200901_2015_O3%20EI-ES_SIP_FINAL.pdf?t=1617690564073&t=1617690564073.

Draxler R.R. (1991) The accuracy of rrajectories during ANATEX calculated using dynamic model analyses versus rawinsonde observations. *Journal of Applied Meteorology*, 30, 1446-1467, doi: 10.1175/1520-0450(1991)030<1446:TAOTDA>2.0.CO;2, February 25. Available at https://journals.ametsoc.org/doi/abs/10.1175/1520-0450%281991%29030%3C1446%3ATAOTDA%3E2.0.CO%3B2.

Finlayson-Pitts B.J. and Pitts Jr J.N. (1997) Tropospheric air pollution: Ozone, airborne toxics, polycyclic aromatic hydrocarbons, and particles. *Science*, 276, 1045-1051, (5315).

Gong X., Kaulfus A., Nair U., and Jaffe D.A. (2017) Quantifying O_3 impacts in urban areas due to wildfires using a generalized additive model. *Environ. Sci. Technol.*, 51(22), 13216-13223, doi: 10.1021/acs.est.7b03130.

Gong X., Hong S., and Jaffe D.A. (2018) Ozone in China: spatial distribution and leading meteorological factors controlling O_3 in 16 Chinese cities. *Aerosol and Air Quality Research*, 18(9), 2287-2300. Available at http://dx.doi.org/10.4209/aaqr.2017.10.0368.

Hennigan C.J., Sullivan A.P., Collett J.L., Jr., and Robinson A.L. (2010) Levoglucosan stability in biomass burning particles exposed to hydroxyl radicals. *Geophysical Research Letters*, 37(L09806), doi: 10.1029/2010GL043088. Available at https://www.firescience.gov/projects/09-1-03-1/project/09-1-03-1_hennigan_etal_grl_2010.pdf.

Hoffmann D., Tilgner A., Iinuma Y., and Herrmann H. (2009) Atmospheric stability of levoglucosan: a detailed laboratory and modeling study. *Environ. Sci. Technol.*, 44, 694–699.

Jaffe D., Chand D., Hafner W., Westerling A., and Spracklen D. (2008) Influence of fires on O_3 concentrations in the western U.S. *Environ. Sci. Technol.*, 42(16), 5885-5891, doi: 10.1021/es800084k.

Jaffe D.A., Bertschi I., Jaegle L., Novelli P., Reid J.S., Tanimoto H., Vingarzan R., and Westphal D.L. (2004) Long-range transport of Siberian biomass burning emissions and impact on surface ozone in western North America. *Geophys. Res. Let.*, 31(L16106).

Jaffe D.A. and Wigder N.L. (2012) Ozone production from wildfires: A critical review. *Atmospheric Environment*, 51, 1-10, doi: https://doi.org/10.1016/j.atmosenv.2011.11.063.

Jaffe D.A., Wigder N., Downey N., Pfister G., Boynard A., and Reid S.B. (2013) Impact of wildfires on ozone exceptional events in the western U.S. *Environ. Sci. Technol.*, 47(19), 11065-11072, doi: 10.1021/es402164f, October 1. Available at http://pubs.acs.org/doi/abs/10.1021/es402164f.

Kimbrough S., Hays M., Preston B., Vallero D.A., and Hagler G.S.W. (2016) Episodic impacts from California wildfires identified in Las Vegas near-road air quality monitoring. *Environ. Sci. Technol.*, 50(1), 18-24. Available at https://doi.org/10.1021/acs.est.5b05038.

Lai C., Liu Y., Ma J., Ma Q., and He H. (2014) Degradation kinetics of levoglucosan initiated by hydroxyl radical under different environmental conditions. *Atmospheric Environment*, 91, 32-39, doi: 10.1016/j.atmosenv.2014.03.054, 2014/07/01/. Available at http://www.sciencedirect.com/science/article/pii/S1352231014002398.

Langford A.O., Senff C.J., Alvarez R.J., Brioude J., Cooper O.R., Holloway J.S., Lin M.Y., Marchbanks R.D., Pierce R.B., Sandberg S.P., Weickmann A.M., and Williams E.J. (2015) An overview of the 2013 Las Vegas Ozone Study (LVOS): impact of stratospheric intrusions and long-range transport on surface air quality. *Atmospheric Environment*, 109, 305-322, doi: 10.1016/j.atmosenv.2014.08.040, 2015/05/01/. Available at http://www.sciencedirect.com/science/article/pii/S1352231014006426.

Louisiana Department of Environmental Quality (2018) Louisiana exceptional event of September 14, 2017: analysis of atmospheric processes associated with the ozone exceedance and supporting data. Report submitted to the U.S. EPA Region 6, Dallas, TX, March. Available at https://www.epa.gov/sites/production/files/2018-08/documents/ldeq_ee_demonstration_final_w_appendices.pdf.

Lu X., Zhang L., Yue X., Zhang J., Jaffe D., Stohl A., Zhao Y., and Shao J. (2016) Wildfire influences on the variability and trend of summer surface ozone in the mountainous western United States. *Atmospheric Chemistry & Physics*, 16, 14687-14702, doi: 10.5194/acp-16-14687-2016.

McClure C.D. and Jaffe D.A. (2018) Investigation of high ozone events due to wildfire smoke in an urban area. *Atmospheric Environment*, 194, 146-157, doi: 10.1016/j.atmosenv.2018.09.021, 2018/12/01/. Available at http://www.sciencedirect.com/science/article/pii/S1352231018306137.

McVey A., Pernak R., Hegarty J., and Alvarado M. (2018) El Paso ozone and $PM_{2.5}$ background and totals trend analysis. Final report prepared for the Texas Commission on Environmental Quality, Austin, Texas, by Atmospheric and Environmental Research, Inc., Lexington, MA, June. Available at https://www.tceq.texas.gov/assets/public/implementation/air/am/contracts/reports/da/582188176307-20180629-aer-ElPasoOzonePMBackgroundTotalsTrends.pdf.

Miller D., DeWinter J., and Reid S. (2014) Documentation of data portal and case study to support analysis of fire impacts on ground-level ozone concentrations. Technical memorandum prepared for the

U.S. Environmental Protection Agency, Research Triangle Park, NC by Sonoma Technology, Inc., Petaluma, CA, STI-910507-6062, September 5.

National Weather Service Forecast Office (2020) Las Vegas, NV: general climatic summary. Available at https://www.wrh.noaa.gov/vef/lassum.php.

Pernak R., Alvarado M., Lonsdale C., Mountain M., Hegarty J., and Nehrkorn T. (2019) Forecasting surface O_3 in Texas urban areas using random forest and generalized additive models. *Aerosol and Air Quality Research*, 19, 2815-2826, doi: 10.4209/aaqr.2018.12.0464.

Sacramento Metropolitan Air Quality Management District (2011) Exceptional events demonstration for 1-hour ozone exceedances in the Sacramento regional nonattainment area due to 2008 wildfires. Report to the U.S. Environmental Protection Agency, March 30.

Simon H., Baker K.R., and Phillips S. (2012) Compilation and interpretation of photochemical model performance statistics published between 2006 and 2012. *Atmospheric Environment*, 61, 124-139, doi: 10.1016/j.atmosenv.2012.07.012.

Simoneit B.R.T., Schauer J.J., Nolte C.G., Oros D.R., Elias V.O., Fraser M.P., Rogge W.F., and Cass G.R. (1999) Levoglucosan, a tracer for cellulose in biomass burning and atmospheric particles. *Atmospheric Environment*, 33, 173-182.

Simoneit B.R.T. (2002) Biomass burning - a review of organic tracers for smoke from incomplete combustion. *Applied Geochemistry*, 17, 129-162.

Solberg S., Walker S.-E., Schneider P., Guerreiro C., and Colette A. (2018) Discounting the effect of meteorology on trends in surface ozone: development of statistical tools. Technical paper by the European Topic Centre on Air Pollution and Climate Change Mitigation, Bilthoven, the Netherlands, ETC/ACM Technical Paper 2017/15, August. Available at https://www.eionet.europa.eu/etcs/etc-atni/products/etc-atni-reports/etcacm_tp_2017_15_discount_meteo_on_o3_trends.

Solberg S., Walker S.-E., Guerreiro C., and Colette A. (2019) Statistical modelling for long-term trends of pollutants: use of a GAM model for the assessment of measurements of O_3, NO_2 and PM. Report by the European Topic Centre on Air pollution, transport, noise and industrial pollution, Kjeller, Norway, ETC/ATNI 2019/14, December. Available at https://www.eionet.europa.eu/etcs/etc-atni/products/etc-atni-reports/etc-atni-report-14-2019-statistical-modelling-for-long-term-trends-of-pollutants-use-of-a-gam-model-for-the-assessment-of-measurements-of-o3-no2-and-pm-1.

Texas Commission on Environmental Quality (2021) Dallas-Fort Worth area exceptional event demonstration for ozone on August 16, 17, and 21, 2020. April. Available at https://www.tceq.texas.gov/assets/public/airquality/airmod/docs/ozoneExceptionalEvent/2020-DFW-EE-Ozone.pdf.

U.S. Census Bureau (2010) State & County QuickFacts. Available at http://quickfacts.census.gov/qfd/states/.html.

U.S. Environmental Protection Agency (2008) Network design criteria for ambient air quality monitoring, 40 CFR Part 58, Appendix D.

U.S. Environmental Protection Agency (2015) 40 CFR Part 50, Appendix U: interpretation of the primary and secondary National Ambient Air Quality Standards for ozone. Available at https://www.ecfr.gov/cgi-bin/text-idx?SID=43eb095cc6751633290941788ab4f3bd&mc=true&node=ap40.2.50_119.u.

U.S. Environmental Protection Agency (2016) Guidance on the preparation of exceptional events demonstrations for wildfire events that may influence ozone concentrations. Final report, September. Available at www.epa.gov/sites/production/files/2016-09/documents/exceptional_events_guidance_9-16-16_final.pdf.

U.S. Environmental Protection Agency (2020) Green Book: 8-hour ozone (2015) area information. Available at https://www.epa.gov/green-book/green-book-8-hour-ozone-2015-area-information.

Wigder N.L., Jaffe D.A., and Saketa F.A. (2013) Ozone and particulate matter enhancements from regional wildfires observed at Mount Bachelor during 2004–2011. *Atmospheric Environment*, 75, 24-31, doi: 10.1016/j.atmosenv.2013.04.026, August. Available at http://www.sciencedirect.com/science/article/pii/S1352231013002719.

Wood S. (2020) Mixed GAM computation vehicle with automatic smoothness estimation. Available at https://cran.r-project.org/web/packages/mgcv/mgcv.pdf.

Wood S.N. (2017) *Generalized additive models: an introduction with R*, 2nd edition, CRC Press, Boca Raton, FL.

Zhang L., Lin M., Langford A.O., Horowitz L.W., Senff C.J., Klovenski E., Wang Y., Alvarez R.J., II, Petropavlovskikh I., Cullis P., Sterling C.W., Peischl J., Ryerson T.B., Brown S.S., Decker Z.C.J., Kirgis G., and Conley S. (2020) Characterizing sources of high surface ozone events in the southwestern US with intensive field measurements and two global models. *Atmospheric Chemistry & Physics*, 20, 10379-10400, doi: 10.5194/acp-20-10379-2020. Available at https://acp.copernicus.org/articles/20/10379/2020/acp-20-10379-2020.pdf.